

For New Technology Network

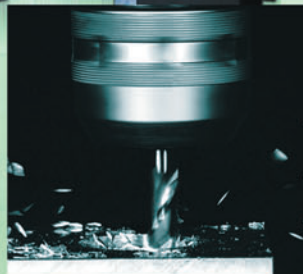
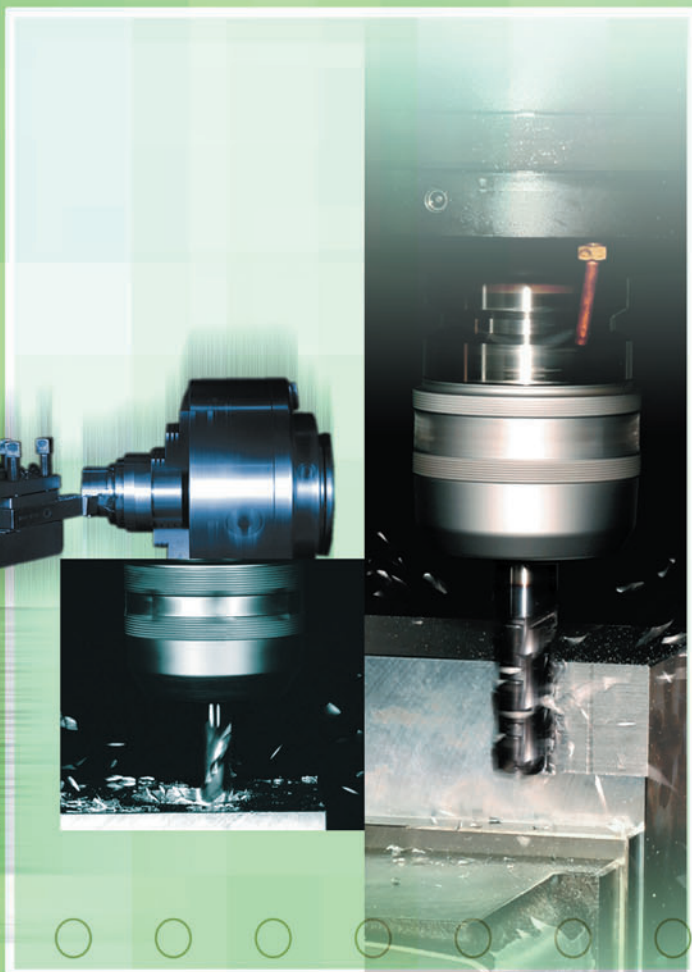
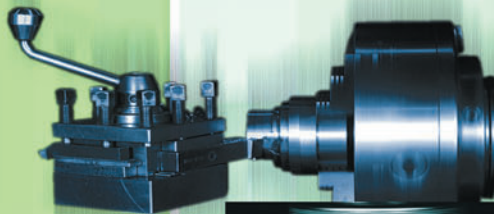
**NTN**®

# TECHNICAL REVIEW

No.  
**72**

Special Issue; Machine Tool Bearings and  
Precision Apparatus Products

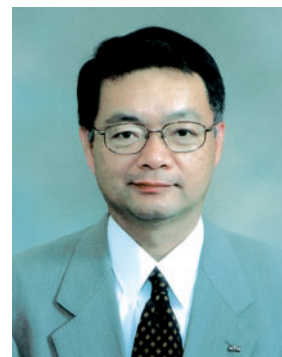
October 2004



# CONTENTS

<b>Preface</b>	Osamu KATO	1
<b>Contribution</b>	<b>Latest Trend of Main Spindle for NC Machine Tool</b> Yoshiaki KAKINO	2
<b>Bearings for Machine Tools</b>	Development of Eco - friendly Oil Jet Lubricated Angular Contact Ball Bearings for Machine Tool Yoshinobu AKAMATSU and Masatsugu MORI	6
	Minimizing Lubricant Supply in an Air-Oil Lubrication System Yoshinobu AKAMATSU and Masatsugu MORI	12
	Development of Long Life Grease for High Speed Application "ME-1" Grease for Motor Bearings Hidenobu MIKAMI	20
	"ULTAGE" Series Precision Bearings for Machine Tools Hiroshi TAKIUCHI and Futoshi KOSUGI	26
	ULTAGE Standard Angular Contact Ball Bearings, 79U/70U type Keiichi UEDA	30
	HTA U Type ULTAGE Angular Contact Ball Bearings for Axial Loads Yasuyuki HIROTA	36
	High Speed and Long Life Double-Row Cylindrical Roller Bearings Naota YAMAMOTO and Mamoru MIZUTANI	42
	Next Generation Deep Groove Ball Bearing for High-Speed Servomotor Chikara KATAGIRI and Kenichiro NAITO	46
<b>Precision Apparatus Products</b>	Multi-Repair System for Color Filters Masahiro SARUTA	52
	Repair System for Sixth and Seventh Generation LCD Color Filters Akihiro YAMANAKA and Akira MATSUSHIMA	56
	PDP Rib Repair System Shizuka YAMAZAKI and Yuji YADA	64
	Improvement of the Accuracy of an Air Spindle of the Nano-meter Order - Improvement of Rotational Accuracy by Optimization of Feed Hole Positioning - Yoshio FUJIKAWA, Takashi HARAGUCHI, Kazuyuki AONO and Teruyoshi HORIUCHI	70
	Nanometer accuracy positioning system Akio NAKAJIMA	78
<b>Our Line of New Products</b>		84

## Special Issue

*Machine Tool Bearings and Apparatus Products*

**Osamu KATO**  
Director

We are in the fourth year of the 21st century or the century of the environment. Safety and humanity must be carefully planned and designed into industrial products, too. At NTN CORPORATION, 'Coexisting in Harmony with the Environment' is our underlying philosophy as we undertake programs to improve our environmental management. In the automobile and industrial machinery fields, NTN is offering to our customers environmentally friendly products that are designed for longer life, low torque, light weight, and energy conservation.

The 22nd Japan International Machine Tools Fair (JIMTOF2004) will open on November 1, 2004 through the 8th. The theme for this year is "MONO-ZUKURI" innovation. NTN will present our own solution to the needs of the machine tool market under a theme of 'Proposals for "MONO-ZUKURI New Age". Our ULTAGE series new bearings were developed with a basic concept of 'Realizing ultra high speed, high precision, and high reliability while maintaining harmony with the environment.' We now have Grease-lubricated Sealed bearings and Eco-conscious Air-Oil Lubricated bearings available on the market. Every one of these products has been highly accepted as 'being people-friendly and ecologically sound.'

In the coming JIMTOF2004, NTN will present our unique user-friendly, highly functional, and ecologically sound technologies that are designed for machine tools of today and tomorrow. We plan to exhibit products that will add more functionality to machine tools and, at the same time, provide improvement in the customer's work environment and reduce the environmental burden.

In this special issue, we will review the development of new technologies and introduce some of our brand new technologies to you.

Since the founding of our company in 1918, NTN has been engaged in the manufacture and sales of rolling bearings. In 1963, we began and have since been producing and supplying constant velocity joints to automobile and various equipment manufacturers. We entered the field of precision apparatus products in 1985 with our mechatronics technology, which is a combination of mechanical and electronic technologies. NTN now manufactures and sells component products such as hydrostatic bearings, magnetic bearings, and positioning tables, and system products based on these components such as FPD (Flat display) repair units for liquid crystal, PDP, organic EL, etc. that are equipped with image processing function and laser. Growth in this field has been remarkable. Some of the leading component products meet the accuracy requirements of nanometers and sub nanometers, while the system products must accommodate even larger manufacturing devices and provide finer fabrication technology. In addition to the traditional engineering issues of 'faster', 'more precise', and 'more functional,' NTN will strive to find solutions to 'challenge of "ultra" in the advanced fields.' This special issue also carries an introduction to the related new type repair units and the nanometer control technology.

Under the concept of '**For New Technology Network,**' NTN is committed to make all out effort in expanding our business as a full-line manufacturer of bearings, constant velocity joints, and precision apparatus products.

## Latest Trend of Main Spindle for NC Machine Tool



Yoshiaki KAKINO

KAKINO Technical Laboratory, Chief  
Professor of Kyoto University

This paper overviews today's technologies and future trends in high-speed spindles for machine tools. High-speed machine tools have been popularized in order to meet the progress of machining technologies led by the technical progress in tools and in workpiece materials. We consider that such progress will continue for a while, and that spindle systems will get faster. The  $d_{min}$  value may reach as high as 4 million in the near future.

### 1. Introduction

The machine tool manufacturers today are excited about good business for the first time in several years and are loaded with an unprecedented amount of orders. The order amount for this year appears to surpass that of the previous year by more than 160%. The orders include not only compound machine tools, 5-axis control machining centers, or other multi-axis control, complex, and high-end machine tools, but also such popular equipment as common 2-axis NC lathes and vertical machining centers. The primary reason for this huge order volume is that the domestic manufacturers have finally rebounded from the recent spell of low market demands and begun their full capital investment drives.

When business is good, manufacturers tend to tone down technology development and place priority on the production of easy-to-manufacture equipment. Nevertheless, the technological innovation in the NC machine tools was staggering up until a year ago. It all began with the pursuit for high-speed main spindles, and then came the high-speed feeding systems. Soon, the high-speed feeding systems caught up with and passed the high-speed main spindles, creating a situation where they are pushing the main spindles to even higher speeds.

In the following sections, we will review the changes that have taken place in the machining technology, which are the true cause for this pursuit of high speeds. We will then look at the today's status of the high-speed trend in the main spindle and feed systems.

### 2. Changes in machining technology

Progress in machining technology is generally triggered by development of new cutting tool material (lately including new coating technologies) and, indirectly, by the changes in the workpiece materials and profiles at the end users. The fabrication method for hardened dies, for example, has suddenly changed to the past 10 years. In the past, the raw material of about HRC25 was machined and hardened by heat treatment. Since the material was too hard to machine, it was finished with electrical discharge machining.

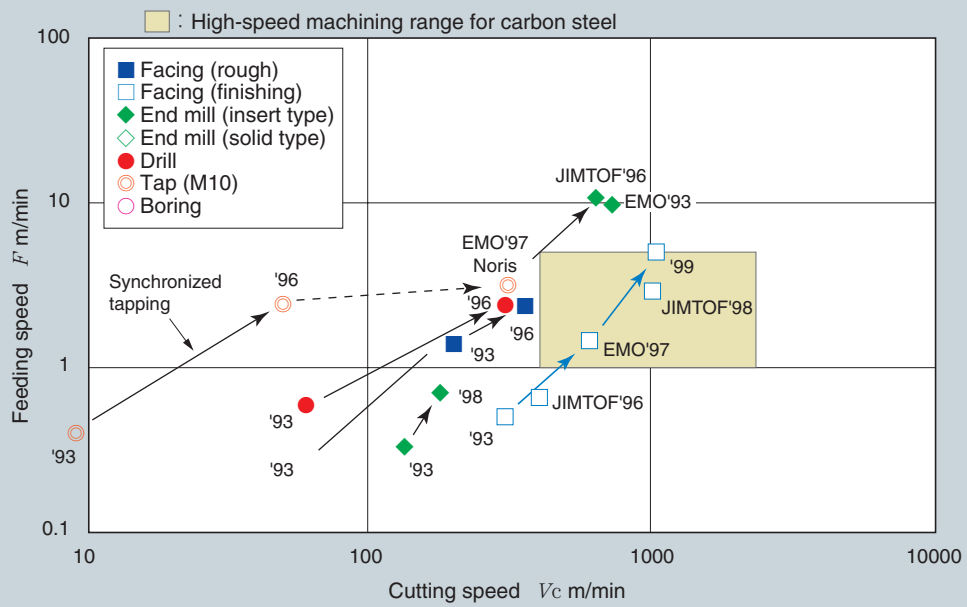
With the advent of (Al, Ti) N-coated ultra hard end mill cutting tools, machining of the hardened materials was made possible. High-speed machining technology that cuts hardened SKD61 die steel of about HRC53 at an amazing 200m/min was developed, which brought a big change in the configuration of the die machining processes and machine tools. Furthermore, there has been a rapid transition in the complex, free-form finishing process from the use of electrical discharge machining to small bore ball end mill cutting tools. This change accelerated a shift towards high-speed main spindles in the machining centers for die fabrication.

In the parts fabrication works, a major change took place in the workpiece material for energy conservation from steel to aluminum, which could be machined at high speeds. These two developments brought significantly fast main spindles and high-speed, high-acceleration feeding system to medium and small size machining centers.

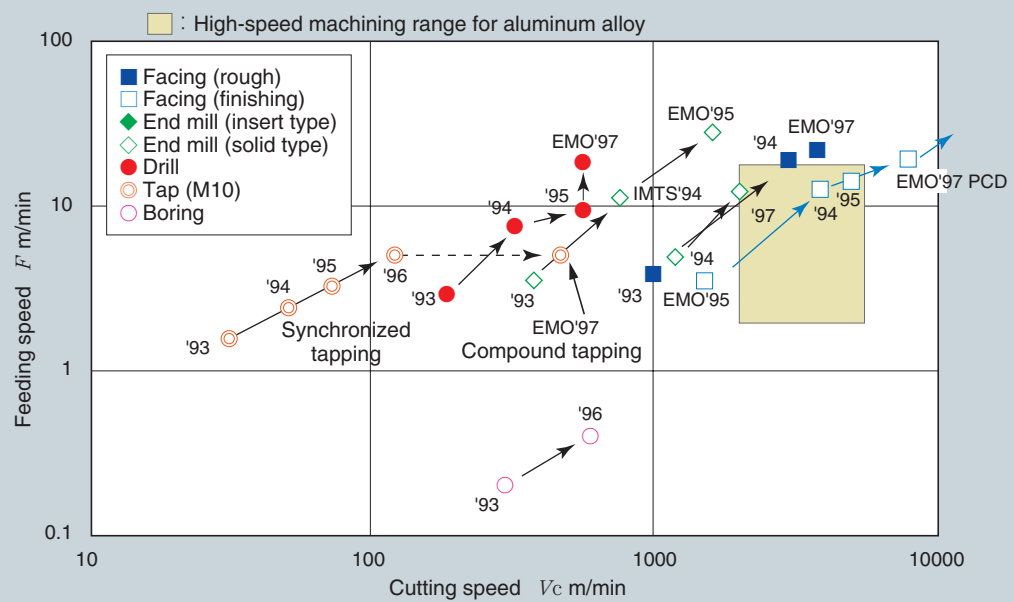
These changes may be described as changes "from low-speed, heavy cutting to high-speed, light cutting."

speeds of various materials, which depicts the compound effects of the above developments.

Fig. 1 shows the historical transition in the machining



(a) Carbon steel



(b) Aluminum alloy

Fig.1 Improvement of cutting speed

### 3. Evolution of main spindle speed

The  $d_{m1n}$  values are often used as an index to indicate high-speed performance of the main spindle. " $d_m$ " represents the ball pitch circle diameter of the bearing rollers in millimeters, and " $n$ " is a product of a realizable maximum revolution of the main spindle represented by /min. The limit of the  $d_{m1n}$  value naturally varies with the methods of lubrication and the types of bearings.

Fig. 2 shows the history of the bearing speeds for NTN's main spindle bearings in the past 20 years. Around 1990, the maximum  $d_{m1n}$  value of the air-oil lubricated bearings was about 2 million. Today, with advancement in optimization of the bearings internal specifications, the  $d_{m1n}$  value has reached 3 million. Since, as mentioned above, heavy cutting has declined, demands for rolling bearings of high rigidity, which can be used at low-speeds only, have not increased much. Instead, more and more ball bearings, especially those using  $\text{Si}_3\text{N}_4$  ceramic balls of smaller specific gravity, are used very frequently. In the past, the ceramic balls were considered more expensive and less accurate as compared to the steel

balls. Now, with increased production, the quality of the ceramic balls has stabilized and the price has come down. As a result, more bearings with the ceramic balls are being used. It is not an overstatement when they say that almost all the rolling bearings rated for 1.5 million in the  $d_{m1n}$  value use the ceramic balls.

Another recent trend is the customer's preference for environmentally friendly lubrication methods. The environmentally friendly lubrication methods are often low-cost lubrication methods, too. For this reason, this trend appears to proliferate faster. NTN re-evaluated grease lubrication in preference to the relatively popular air-oil lubrication method and successfully made the grease-lubricated sealed angular contact ball bearings available for service at up to 1.4 million in the  $d_{m1n}$  value. This speed is often sufficient for use in steel parts fabrication, and bearings of this type are increasing their applications.

Leading the race for faster bearing speed, the air-oil lubrication method has been improved by NTN for low noise and less consumption of air and oil. Eco-conscious type bearings are contributing to reduction in environmental burdens.

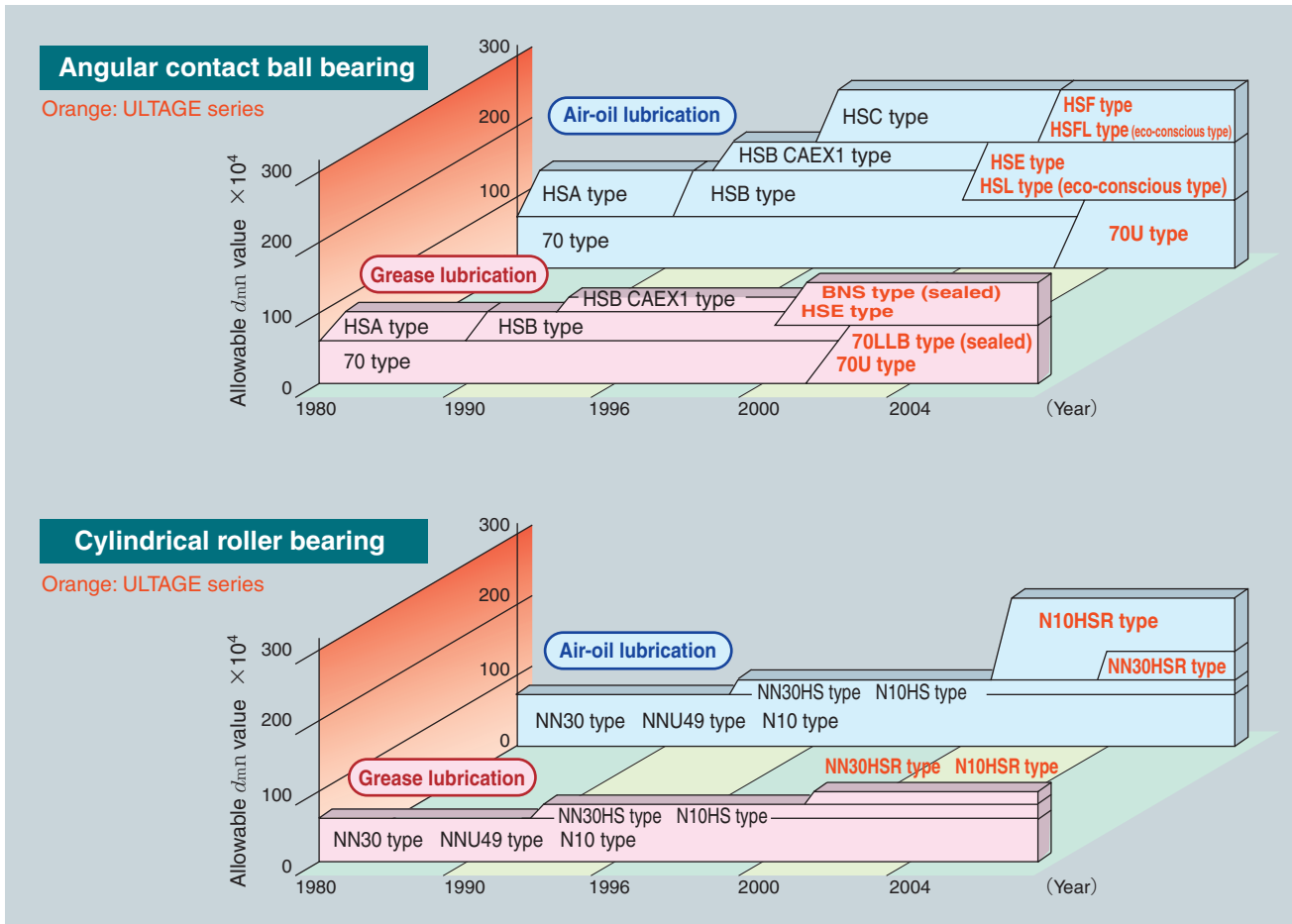


Fig.2 Improvement of NTN bearing speed for main spindle

#### 4. Faster feeding speed

As mentioned above, it is desirable for the main spindles and the feeding systems to advance hand-in-hand in the race for faster speeds in view of fabrication technology. However, they do not always progress in synchronization subject to the status of the technological development. Recently, more significant advancement is visible in high-speed, high-acceleration feeding systems. This progress was led by the introduction of linear motors into machine tools, and then followed by the use of high-lead ball screws.

**Fig. 3** shows the status of development. There are machining centers in the market that utilize the parallel mechanisms without the use of guides.

Thanks to these technologies, the maximum feeding speed of 60m/min and the maximum acceleration of 1G in the machining centers no longer draw special attention. (Nevertheless, in many actual applications, this performance is sufficient.) The maximum speed of over 100m/min and acceleration reaching 2G have already been achieved on actual equipment. Considering that 24m/min and 0.1G were the standards some 10 years ago, there has been great progress. On the other hand, the speed of the corresponding main spindle for BT40 is 40,000/min, though is still in the testing stage and has not proven to be service worthy.

#### 5. Conclusion

As mentioned above, it is desirable for the main spindles and the feeding systems to advance hand-in-hand in the race for faster speeds. Lately, achievement in making faster main spindles is somewhat behind that of the feeding systems. I hope that **NTN** will develop a high-speed technology for main spindles to break this cycle, and become the leader of the world's machine tool industry.

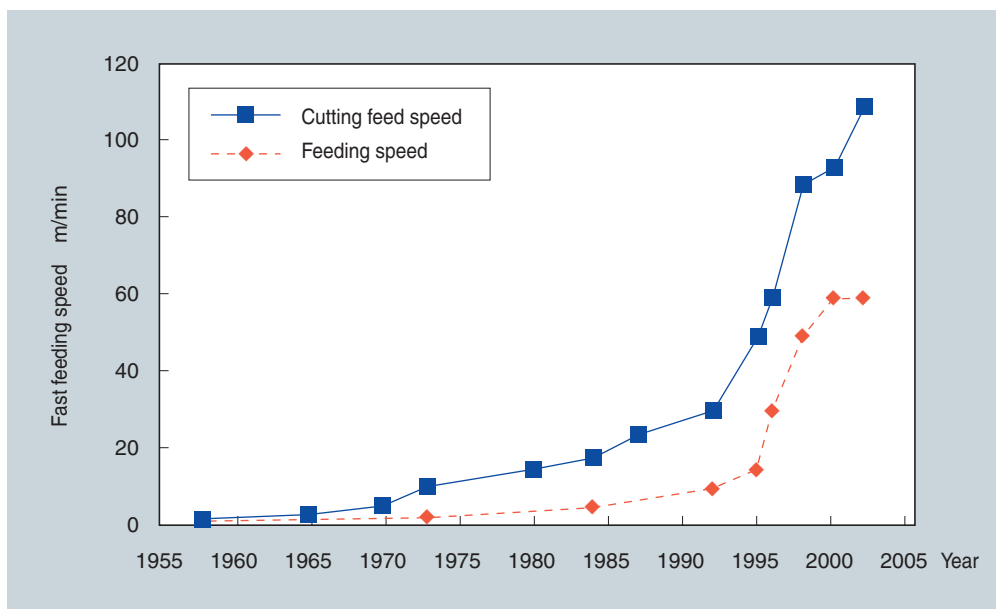
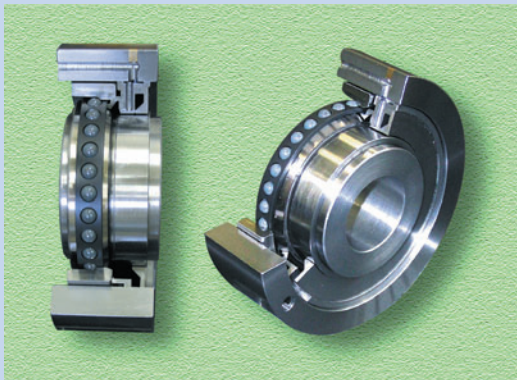


**Fig.3** Improvement of feeding speed for machining center

## Development of Eco - friendly Oil Jet Lubricated Angular Contact Ball Bearings for Machine Tool



Yoshinobu AKAMATSU\*  
Masatsugu MORI\*

The lubrication system is critical for the high-speed operation of a machine tool. In 1992, NTN developed a complex lubrication system with oil jet lubrication and an under-race lubrication system for angular contact ball bearings with  $d_{m\dot{n}} \leq 390$  million ( $d_m =$  ball pitch circle diameter,  $\dot{n} =$  speed). In order to increase the speed limit of angular contact ball bearings, the “Eco-friendly Oil Jet Lubrication System” was developed. In this paper, the eco-friendly jet lubricated bearing and the lubrication system are introduced. This paper summarizes a test that measured the power loss and temperature of bearings (70mm bore,  $d_{m\dot{n}}$  value = 500 million) using this new lubrication system.

### 1. Introduction

Faster rotation of machine tool main spindles is needed to improve the surface quality and machining efficiency of machine tools. The key technologies to accomplish this will increase the speed and accuracy of the rolling bearings that support main spindles. NTN has already established a technology that analyzes the relationship between the accuracy of the bearing components and the bearing vibration under preload <sup>1), 2), 3)</sup>. This technology makes it possible to study how to reduce bearing vibration. The speed of rolling bearings for machine tool main spindles depends on lubrication methods which include, in the ascending order of the limiting speed, grease lubrication, air-oil lubrication, oil jet lubrication, and under-race lubrication. In 1992, NTN combined oil jet lubrication and under-race lubrication mechanisms into an angular contact ball bearing of 100mm bore and achieved a  $d_{m\dot{n}}$  value of 3.9 million <sup>4), 5), 6)</sup>. The oil jet lubrication system supplied a jet of lubricant through a nozzle that was facing the inner ring raceway from the outer ring spacer. The under-race

lubrication mechanism supplied a lubricant jet from the outer ring spacer to the cylindrical surface of the scoop, which was formed by enlarging the ID of the inner ring end surface. This scoop is connected to the lubricant supply hole leading to the inner ring raceway through the axial through-hole in the inner ring, thus accomplishing supply of the lubricant. Both lubrication mechanisms lubricate the bearing. At the same time, the oil jet lubrication contributes to the cooling effect of the outer ring and the under-race lubrication to the cooling of the inner ring.

As mentioned above, adoption of oil jet lubrication and under-race lubrication increased the speed of the bearings. However, if even faster bearings are desired, these lubrication mechanisms require a driving unit of larger capacity to compensate for the power loss on the bearings caused by a large amount of lubricant that passes through the bearings. This paper describes a new eco-conscious oil jet lubrication mechanism that has reduced the power loss of the bearing and achieved ultra high-speed rotation.

\*Research & Development Center Technical Research Dept.



## 2. Eco-friendly oil jet lubrication mechanism

The technical issue to be resolved in achieving higher speeds with rolling bearings is reduction in power loss and preload fluctuation. In the oil jet lubrication mechanism, reduction in power loss would require a reduction in the drag against the rotation of the rolling elements aside from the friction torque of the rolling elements at their contact surfaces. To do this, the technology that controls the amount of lubricant inside the bearing is important. Additionally, high-speed operation of a bearing causes the bearing to produce heat, which leads to thermal expansion of the outer ring and inner ring raceways. Furthermore, centrifugal force causes the inner ring raceway to expand and increases preload. Oil jet lubrication cools the outer ring, but its cooling effect on the inner ring is low. Therefore, the oil jet lubrication requires a cooling mechanism for the inner ring.

To resolve these issues, the eco-conscious oil jet lubrication mechanism shown in **Figs 1 and 2** was developed. Lubricant supplied to the outer ring spacer is injected towards the scoop formed at the inner ring end surface through the nozzle. Inside the scoop, centrifugal force of the rotating inner ring causes the lubricant to stick to the inner diameter of the scoop. Then the lubricant, moves from the inner ring end surface to the conical surface by centrifugal force and surface tension. At the conical surface of the inner ring, a portion of the outer ring spacer has a ring that creates clearance to allow oil passage. A portion of the lubricant on the inner ring passes through this clearance into the internal structure of the bearing, while the remaining lubricant cools the inner ring. If

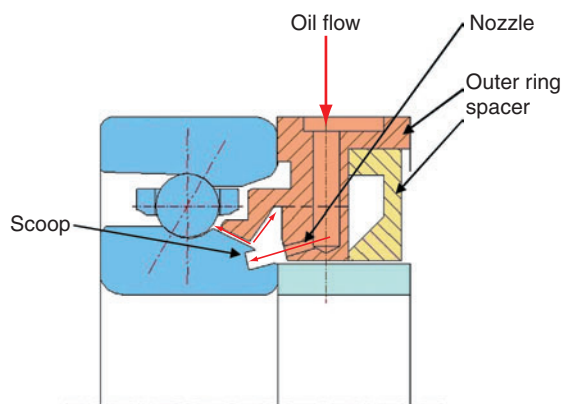


**Fig.1** Bearing design

then flows along the inner diameter, shown on the right side in the figure, of the ring that establishes the clearance. The outer ring spacer consists of a bearing side spacer with a nozzle and a counter bearing side spacer. As shown in **Fig. 2**, only the nozzle portion of the bearing side spacer protrudes towards the inner diameter and the remainder forms an annulus ring of a larger diameter than the inner diameter of the nozzle. Consequently, the lubricant moving along the inner diameter of the smaller annulus ring moves towards the counter bearing side spacer as shown in **Fig. 2**.

A special lubrication device is typically installed for the bearings of machine tool main spindles. **Fig. 2** shows the lubrication system used for this study where a jacket-cooling device for the machine tool was used as a lubrication device. Here, the oil from the cooling oil delivery device is filtered and fed to the outer ring spacer for lubrication. Oil that has cooled the inner ring is pumped out from the outer ring spacer, and oil that has lubricated the bearing, cooled the outer ring, and then come out of the bearing is returned to the oil recovery tank by the discharge oil pump. The discharged oil is returned from the oil recovery tank back to the cooling oil delivery device for circulation. The lubrication system shown in **Fig. 2** does not require any special lubrication devices other than the filter and the discharge oil pump. Thus, this lubrication system incurs less power loss as compared to the traditional oil jet lubrication system, and it requires no cost for the peripheral equipment. That is why this system is called an eco-friendly oil jet lubrication mechanism.

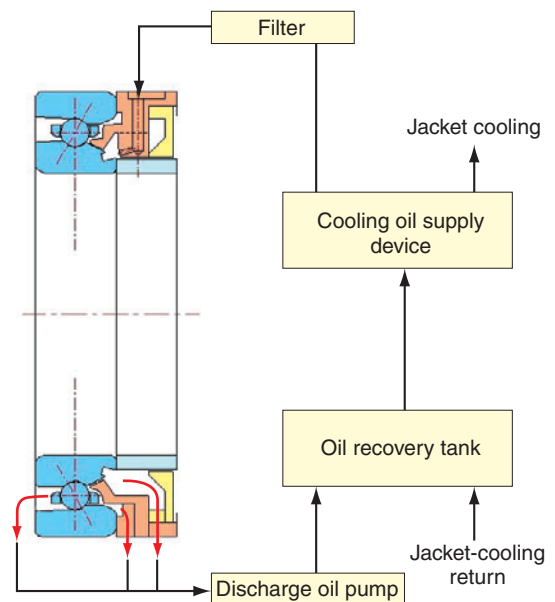


**Fig.2** Eco-friendly oil jet lubrication system

### 3. Test results

#### 3.1 Test conditions and test equipment

The outer ring temperature of a bearing and power loss of a motor were measured at different bearing speeds using a 70mm bore angular contact ball bearing equipped with the eco-friendly oil jet lubrication mechanism. **Fig. 3** shows the structure of the test spindle and **Photo 1** shows the appearance of the test equipment. A built-in motor powered the spindle. The spindle was supported by two test bearings and two support bearings. The inner diameter of the support bearings was 35mm. Lubricant was supplied to the test bearings through the orange oil hole at the top indicated in **Fig. 3**, and it was discharged through the orange discharge hole at the bottom. The test equipment also supplied jacket-cooling oil to the test bearings, motor, and the support bearings. For lubrication of the support bearings, eco-friendly air-oil lubrication was used. A constant

preload was used. To compare the test lubrication mechanism to the air-oil lubrication mechanism, the same performance test was conducted on the air-oil lubrication mechanism. The air-oil lubrication was established by 0.03cc/3min of oil and 30NL/min of air.

The primary test conditions are shown in **Table 1**.

**Table 1** Test conditions

Test bearing	$\phi 70 \times \phi 110 \times 20$
Contact angle	30°
Lubricant	Lubricating oil for machine tools ISO VG2
Initial preload	1kN
Jacket-cooling rate	3L/min
Jacket-cooling oil temperature	Room temperature $\pm 1^\circ\text{C}$
Race material	Carburized steel, High-speed tool steel
Ball material	Si3N4
Cage material	PEEK

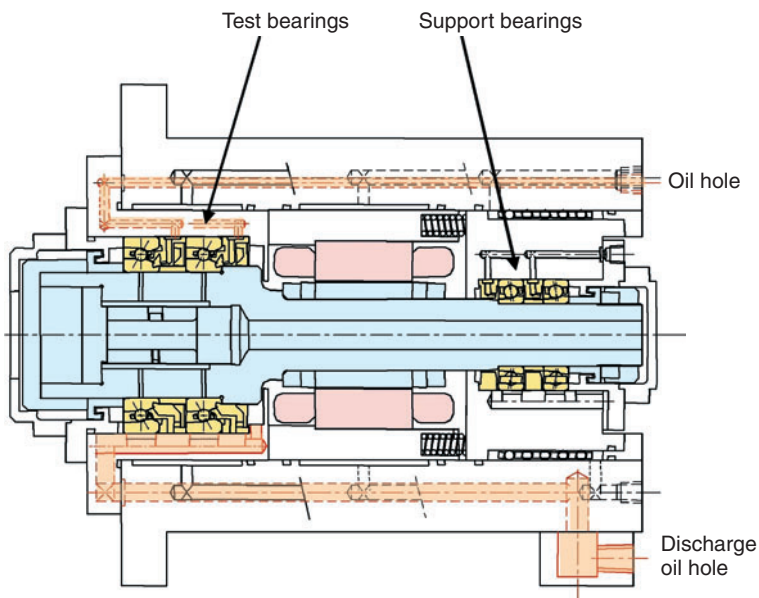


**Fig.3** Schematic construction of test spindle

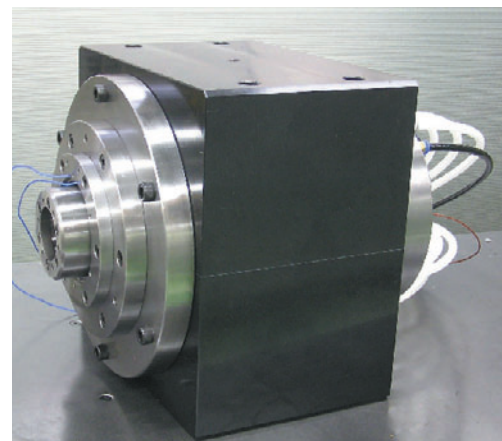


**Photo 1** Test spindle

### 3.2 Test results

The test spindle was set at predetermined rotational speeds starting with the lowest speed using an inverter controlled built-in motor. When the bearing speed stabilized, the motor's power loss and the outer ring temperature were measured. After the measurement, the rotational speed was raised to a pre-determined speed and the test continued until a  $d_{m\Omega}$  value of 5 million was reached. For the air-oil lubrication mechanism, the test was terminated when a maximum speed of 2.5 million in the  $d_{m\Omega}$  value was reached.

Fig. 4 shows a comparison of the motor's power loss between eco-friendly oil jet lubrication and air-oil lubrication. The delivery rate of the oil jet lubrication was 3L/min. The measured power loss values included friction torque of the support bearing. However, when comparing the eco-friendly oil jet lubrication to the air oil lubrication mechanisms, the differential between the two is simply the differential between the two lubrication methods for the test bearing. In the same figure, the power loss of eco-friendly oil jet lubrication is about the same as that of air-oil lubrication. The test for the air-oil lubrication mechanism finished at the  $d_{m\Omega}$  value of 2.5 million, but even if the measured value is extended up to 5 million in the  $d_{m\Omega}$  value, the power loss in the eco-conscious oil jet lubrication is about the same as that of the air-oil lubrication. The support bearings were smaller in size as compared to the test bearings. If the power loss in the support bearings is zero, the power loss in the eco-conscious oil jet lubrication at the  $d_{m\Omega}$  value of 5 million was below 8kW.

A quantitative discussion of the preload changes associated with the rising rotational speed would require measurements of the outer ring and the inner ring temperatures as well as calculations of the centrifugal expansion of the inner ring. In this test, however, the outer ring temperature in the eco-conscious oil jet lubrication method was verified to be

within the operating temperature range.

Fig. 5 shows a comparison of the temperature rise of the outer ring between the eco-friendly oil jet lubrication and the air-oil lubrication methods. The delivery rate of the eco-friendly oil jet lubrication mechanism was 3L/min. In this figure, it is clear that the eco-friendly oil jet lubrication method is superior to the air-oil lubrication method in terms of the temperature rise in the outer ring. Also confirmed was the fact that the temperature rise in the outer ring for the eco-friendly oil jet lubrication mechanism at a  $d_{m\Omega}$  value of 5 million was below 60°C.

For the eco-friendly oil jet lubrication method, the amount of the lubricant delivered inside the bearing seems to determine the friction torque of the bearing as well as the cooling capability of the outer ring. Fig. 6 shows the measurements of power loss for the eco-friendly oil jet lubrication method with different oil delivery. In this figure, the delivery rate of the eco-friendly oil jet lubrication mechanism was measured at the nozzle, and it was not the amount of the lubricant that passed through the bearing. The discussion of the measurement results, however, assumed that the oil flow through the bearing is proportional to the delivery rate at the nozzle. Fig. 6 shows that the more oil was delivered inside the bearing, the larger the

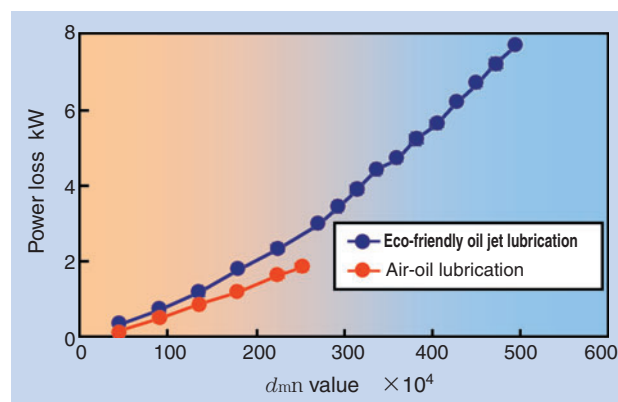


Fig.4 Effect of lubrication type on power loss

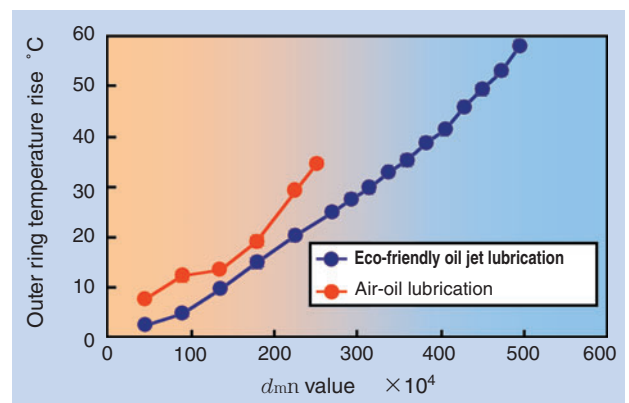


Fig.5 Effect of lubrication type on outer race temperature

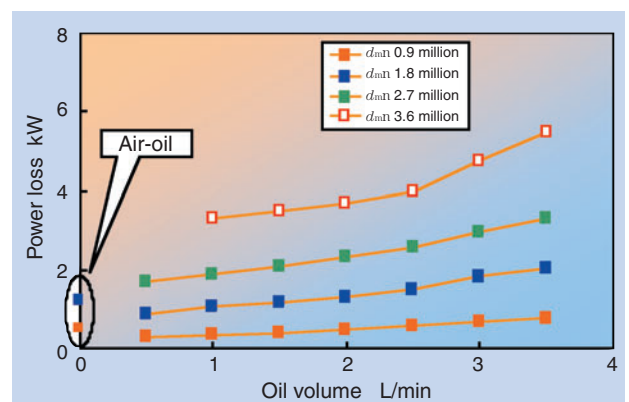


Fig.6 Effect of amount of lubricant on power loss

power loss. It also shows that, at higher revolutions, the rate of power loss became greater as the oil delivery increased.

Fig. 7 shows the temperature rise of the outer ring at different lubricant delivery rates using the eco-friendly oil jet lubrication method. The outer ring temperature dropped as the lubricant delivery increased. At low revolution rates, increase in the lubricant delivery rate did not significantly cool the outer ring, but as the revolution rate became higher, the cooling effect on the outer ring increased. In the figure, the delivery rates in the air-oil lubrication at  $d_{m\Omega}$  0.9 million and  $d_{m\Omega}$  1.8 million were plotted as being close to zero. However, since these points are almost on the extension lines of the measurements of oil jet lubrication, we can say that the amount of lubricant delivered into the bearing determines the cooling efficiency of the outer ring.

Since the relationship of the lubricant delivery rate for oil jet lubrication and friction torque on the bearing is opposite that of the lubricant delivery rate for oil jet lubrication and cooling efficiency, the optimal lubrication conditions for machine tool main spindle bearings can be determined by selecting a proper lubricant delivery rate for the eco-friendly oil jet lubrication mechanism.

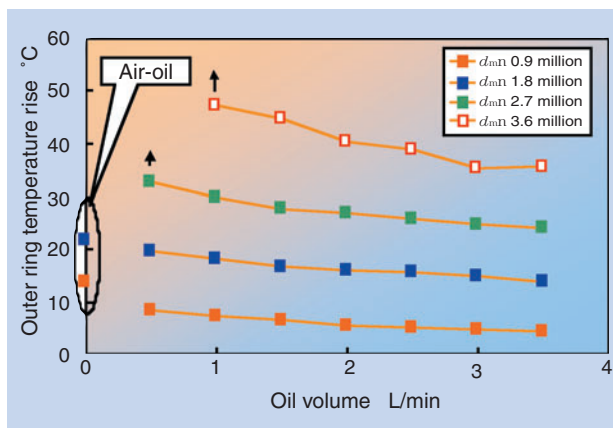


Fig.7 Effect of amount of lubricant on outer race temperature

Photos of authors



Yoshinobu AKAMATSU

Technical Research Dept.  
Research & Development Center



Masatsugu MORI

Technical Research Dept.  
Research & Development Center

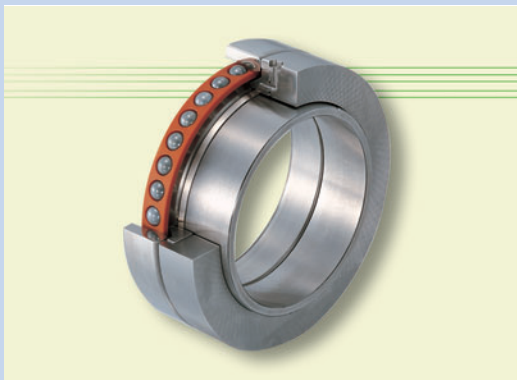
## 4. Conclusion

To meet the needs for increased speeds in main spindle bearings for machine tools, we have developed an eco-friendly oil jet lubrication mechanism with less power loss and fewer changes in bearing temperatures. This lubrication mechanism was successfully applied to a 70mm bore angular contact ball bearing at an operating speed of  $d_{m\Omega}$  5 million. It is our hope that this lubrication mechanism will contribute to the development of faster machine tools.

## References

- 1) T. Sakaguchi and Y. Akamatsu, Proc. Int. Trib. Conf. Nagasaki (2000)1795.
- 2) T. Sakaguchi and Y. Akamatsu, NTN TECHNICAL REVIEW No.69(2001)69, (in Japanese)
- 3) Y. Akamatsu and T. Sakaguchi, Proc. JAST Trib Conf.(Tokyo 2004-5) 383, (in Japanese)
- 4) M. Mori and M. Niina, NTN TECHNICAL REVIEW No.60(1992)41, (in Japanese)
- 5) K. Hibi, M. Mori and M. Niina, Proc. JAST Trib Conf.(Tokyo 1992-5) 633, (in Japanese)
- 6) K. Fujii, Proc. JAST Trib Forum '98 (1998) 95, (in Japanese)

# Minimizing Lubricant Supply in an Air-Oil Lubrication System



**Yoshinobu AKAMATSU\***  
**Masatsugu MORI\***

Rolling bearings for machine tool main spindles must have low vibration, low friction, and ability to operate at high speed. NTN's environment-friendly ULTAGE series HSL-type air-oil lubricated angular ball bearing meets all of these requirements. The HSL-type bearing supplies lubricant via the inner ring surface by delivering an air-oil mixture to the cone-shaped counter bore of the inner ring. The traditional lubrication method of supplying the air-oil mixture to the inner ring/roller

contact surface produces an air-piercing sound as the rollers cut through the flow of the air-oil mixture, and this new structure successfully eliminates the air-piercing sound. It also successfully reduces the required amounts of oil and air.

This paper describes the technology for minimizing the lubricant supply used in the HSL-type angular ball bearing, and more specifically, evaluates the limit of the counter bore tilt angle, swash clearance, lubricant viscosity, effects of air flow rate, uniformity of oil, and the factors for the minimum required oil amount. It then concludes that the swash angle is determined by the  $d_{m1}$  value and that smaller wettability of the tube results in more uniform lubricant supply.

## 1. Introduction

Faster rotation of the machine tool main spindles is needed to improve the surface quality and the machining efficiency of works. The key technologies to accomplish them are those that increase the speed and accuracy of the rolling bearings that support the main spindles. The speed of the rolling bearings for machine tool main spindles depends on lubrication methods which include grease lubrication, air-oil lubrication, oil jet lubrication, and under-race lubrication. Presently, the revolving spiral limit of a grease-lubricated angular contact ball bearing with the shaft diameter of 100mm is 1.4 million in the  $d_{m1}$  value, and this bearing has reached its service life of 20,000 hours or longer <sup>1)</sup>. The oil consumption in the air-oil lubrication method is a low 1/100,000 that of oil jet lubrication or under-race lubrication, and this lubrication method does not lose power due to the agitation resistance of the lubricant. Nevertheless, the market demands reduction in the oil and air consumption in the air-oil lubrication method. In 2000, NTN developed high-performance air-oil lubrication mechanism <sup>2), 3), 4)</sup> that increases the counter bore

diameter of the inner ring from the end surface to the raceway to make it a conical shape and supplies air-oil mixture to this counter bore surface. This lubrication method eliminated the air-piercing noise caused by passage of the rolling elements in the traditional structures <sup>2)</sup> and successfully reduced such noise by about 10dBA between the  $d_{m1}$  1.3 million and 2.65 million. This high-performance air-oil lubrication mechanism also reduced oil consumption down to 1/10 and air consumption to 1/4 at  $d_{m1}$  2.65 million <sup>1), 4)</sup>. NTN is offering this new bearing as an eco-conscious air-oil lubricated bearing <sup>1)</sup>.

Rolling bearings for machine tool main spindles demand minimal heat generation. In this respect, it is necessary to determine the minimum necessary amount of oil to hold the bearing torque at a minimum and to establish lubricant delivery technology. This paper describes our studies on the technology for minimizing the lubricant delivery, and more specifically, evaluates the inner ring swash angle that delivers the lubricant, swash clearance, viscosity of lubricant, effects of air flow rate, and leveling of pulsation of the lubricant.

\*Research & Development Center Technical Research Dept.

## 2. Structure of air-oil lubricated angular contact ball bearing

A traditional air-oil lubricated angular contact ball bearing, shown in Fig. 1 (a), is so structured to inject air-oil mixture from the nozzle to the rolling elements. Fig. 1 (b) is a low-noise bearing developed to reduce the air-piercing sound of air-oil mixture. The low-noise bearing injects air-oil mixture onto the tilted surface of the inner ring counter bore and delivers lubricant to the rolling elements by centrifugal force<sup>2)</sup>. This structure reduced noise, improved the delivery capability of the lubricant, and reduced the necessary amount of oil and the minimum delivery air flow<sup>3)</sup>.

Fig. 1 (c) shows the structure of an eco-conscious type bearing that was developed for further energy conservation. The low noise bearing has a circumferential groove at the exit of the nozzle to release pressure. It was confirmed that, when air supply is reduced, lubricant in this circumferential groove entered the inner section of the bearing, causing temperature rise. With the eco-conscious type bearing, the pressure release space at the exit of the nozzle was formed on the rotating inner ring to avoid collection of lubricant in the circumferential groove, thus improving the lubricant delivery to the rolling elements<sup>4)</sup>.

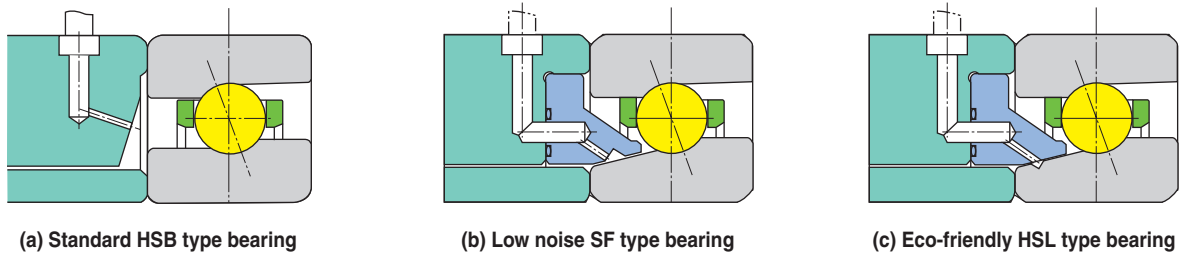


Fig.1 Air-oil lubrication angular contact ball bearings

## 3. Designing inner ring swash angle

In the air-oil lubrication mechanism for the low-noise and the eco-conscious bearings, lubricant moves towards the rolling elements by the component force of centrifugal force along the slope of the inner ring counter bore. Therefore, the swash angle is a key design factor. For this reason, a test was conducted to determine factors that impact the lubricant flow along this swash surface. The test used bearings with an inner diameter  $\phi$  100mm and inner diameter  $\phi$  70mm with different swash angles and clearances, lubricant viscosity, and rotating speeds.

### 3.1 Test method

To confirm the flow of lubricant on the swash surface, a model test was carried out by installing an inner ring on the rotating shaft and an oil absorbing paper (filter) on the outside of the inner ring, Fig. 2. The oil absorbing paper was held against the housing by way of an acrylic plate. This allowed an observation of the oil splash during the bearing operation. Fig. 2 shows an oil absorbing paper after the test, indicating oil collection at the inner ring. When oil collects on the inner ring, it moves to the edge of the swash surface and splashes by centrifugal force. Some oil was observed to have splashed off the outer face of the inner ring by centrifugal force.

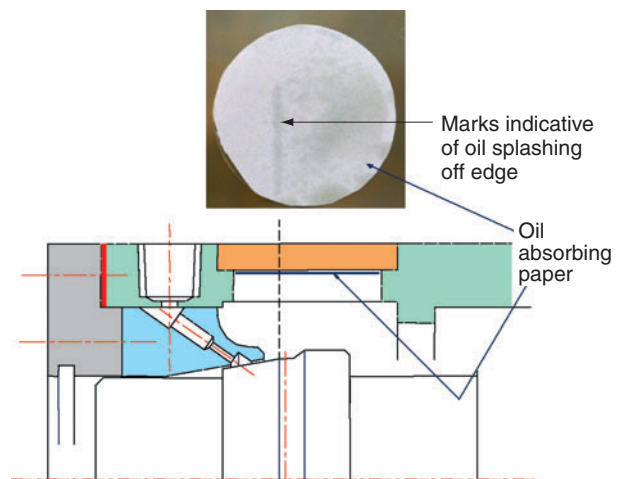
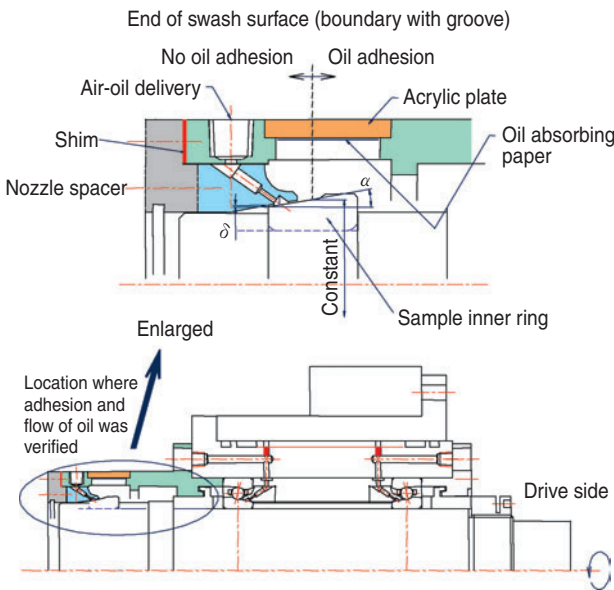


Fig.2 Test for oil flow on swash surface of inner ring

**Fig. 3** shows the structure of the test equipment. The components with which to observe oil adhesion and flow were installed at the end of the spindle that was supported by an air-oil lubricated bearing. To study impacts of the swash angle  $\alpha$ , the shoulder dimension of the swash surface at the inner ring groove was kept consistent and the swash angle was changed. Impacts of the swash surface clearance  $\delta$  (radial clearance) between the nozzle spacer and the swash surface were also studied. The swash surface clearance was adjusted by changing the shim thickness, thereby moving the nozzle spacer in the axial direction.



**Fig.3** Test equipment for lubricant flow observation

**Table 1** shows the different bearing sizes, inner ring swash angles, swash surface clearances, lubricant names, and viscosity used in the test. The injection angle of the nozzle with respect to the center of the main spindle was 30°

**Table 1** Test conditions for lubricant flow observation

Bearing	Inner Diameter $\phi$ 100mm	Inner Diameter $\phi$ 70mm
Nozzle diameter (mm)	$\phi$ 1.2	$\phi$ 0.8
Swash angle $\alpha$ (°)	2~16	10, 12, 14
Swash surface clearance $\delta$ (mm)	0.16~1.0	0.1~0.3
Air supply rate (NL/min)	20	20
Oil supply rate (mL/shot interval min)	0.01/5	0.01/5
Viscosity of oil (mm <sup>2</sup> /s)	10, 32, 68	32
Rotating speed (min <sup>-1</sup> )	~21000	~30000

**3.2 Test results**

**3.2.1 Swash surface angle and oil adhesion and flow of lubricant**

**Figs.4** and **5** show the test results of the lubricant adhesion and flow using sample inner rings of  $\phi$ 100mm ID and  $\phi$ 70mm ID and different swash angles. Lubricant readily adheres and flows if the swash angle is large and the rotating speed is fast. These results indicate that a larger swash angle produces a larger component force of centrifugal force, making lubricant

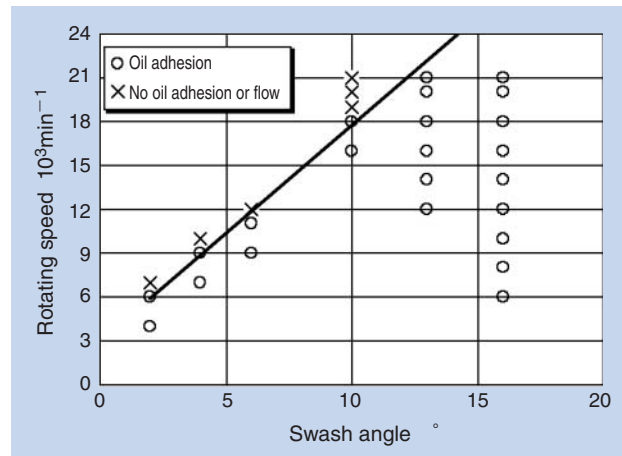


**Fig.4** Effect of swash angle and rotational speed on oil adhesion ( $d=100\text{mm}$ )

(Test conditions)

- Swash surface clearance  $\delta$  : 0.16 ~ 0.2mm
- Nozzle diameter :  $\phi$  1.2
- Air supply rate : 20NL/min
- Oil supply rate : 0.01mL/5min shot interval
- Oil used : Mobil Velocity No. 6 (VG10)

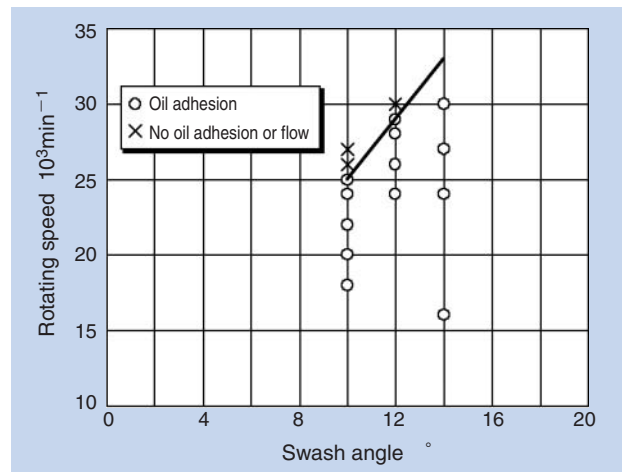


**Fig.5** Effect of swash angle and rotational speed on oil adhesion ( $d=70\text{mm}$ )

(Test conditions)

- Swash surface clearance  $\delta$  : 0.15mm
- Nozzle diameter :  $\phi$  0.8
- Air supply rate : 20NL/min
- Oil supply rate : 0.01mL/5min shot interval
- Oil used : Mobil DTE OilLight (VG32)

more readily adhere and flow and that faster rotating speeds cause swirling of air around the rotating shaft, preventing air-oil from adhering. Reading these figures, the adhesion limit swash angle at  $d_{m1}$  2.1 million ( $d_{m1}$  2.63 million) is about  $12.3^\circ$ . This indicates that the limit angle at which adhesion and flow can be established may be affected by the circumferential speed ( $d_{m1}$  value). Fig. 6 is a  $d_{m1}$  value conversion of the adhesion limit speeds at different swash angles shown in Figs. 4 and 5.

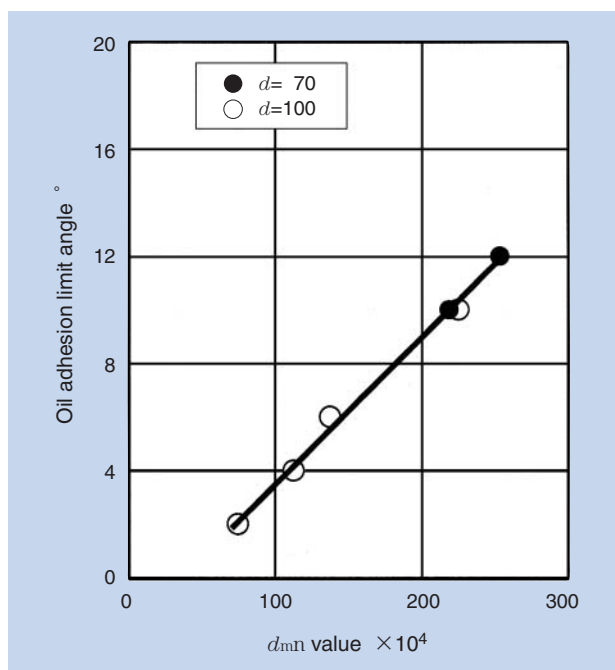


Fig.6 Relation between  $d_{m1}$  value and swash angle

### 3.2.2 Swash surface clearance and lubricant adhesion and flow

The study results of the impacts of the swash surface clearance ( $\delta$ ) on the lubricant adhesion and flow are shown in Fig. 7. The test used a sample with an inner diameter  $\phi$  100 and swash angles of 10, 13, and  $16^\circ$ . All other test conditions were identical. With the sample set at  $13^\circ$  and  $16^\circ$  swash angles, adhesion and flow of oil were verified when the swash surface clearance was increased up to 1mm. On the other hand, the sample that was set at  $10^\circ$  swash angle did not show adhesion or flow at rotating speeds at or above  $19000\text{min}^{-1}$  irrespective of the swash surface clearance ( $\delta = 0.19, 0.52\text{mm}$ ). Adhesion and flow were confirmed at  $18000\text{min}^{-1}$  or lower. These results concluded that the swash surface clearance did not affect the adhesion or the flow of lubricant.

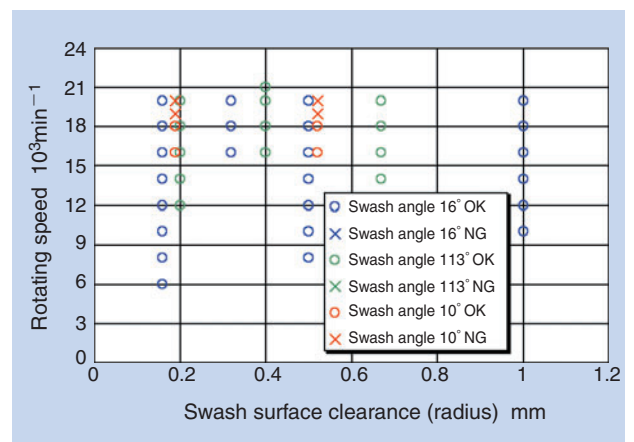


Fig.7 Effect of swash angle, rotational speed and clearance  $\delta$  on oil adhesion

(Test conditions)  
 ID :  $\phi$  100mm  
 Nozzle diameter:  $\phi$  1.2  
 Air supply rate: 20NL/min  
 Oil supply rate: 0.01mL/5 min shot interval  
 Oil used: Mobil Velocity No. 6 (VG10)



## 4. Leveling air-oil pulsation

To further reduce the usage of air and oil in the air-oil lubrication method, it is critical to have a technology that evenly distributes the amount of oil delivered to bearings. The following sections describe the results of the model test that was conducted to determine an optimal air-oil delivery system for air-oil reduction. The test evaluated the materials and sizes of the air-oil tubing and air-oil delivery methods (intermittent and continuous delivery) that affect the oil transfer characteristics in the air-oil lubrication method.

### 4.1 Test method

The test used a 2m tube one end of which was connected to an air-oil unit and the other to a nozzle. Time for lubricant to come out of the nozzle was measured and the delivery of the lubricant observed. Fig. 8 shows the set-up of the test equipment. The delivery status of the lubricant was recorded by a recorder, where a recording paper was moved at a constant speed for evaluation of the level of oil absorption. The nozzle profile used for this test is shown in Fig. 8. The recorder used was Rectigraph. Table 2 shows the test conditions.

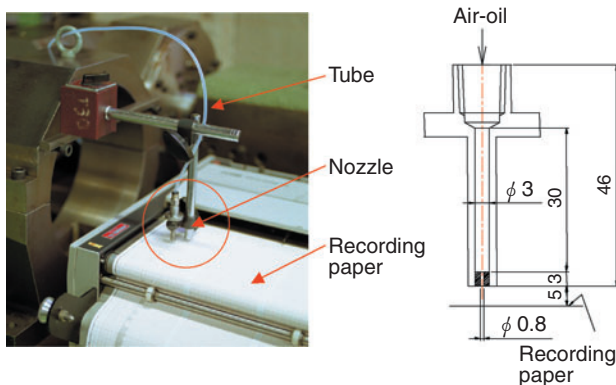


Fig.8 Equipment for oil flow observation

Table 2 Test conditions for oil flow observation

Material of Tubing	Polyurethane, Teflon
Tubing Inner Diameter × Outer Diameter (mm)	φ 1.5 × φ 3.5, φ 2.5 × φ 4, φ 4 × φ 6
Length of tubing (m)	2
Air supply rate (NL/min)	7.5~20
Oil shot interval (min)	Continuous ~ 20
Oil	Mobil DTE OilLight (VG32)

### 4.2 Test results

#### 4.2.1 Effects of tube diameter and material on oil flow

Fig. 9 compares the time from the start of air-oil supply to oil delivery by different sample tubing to the air supply rate in intermittent supply of 0.03mL oil per shot at 5min shot interval.

The larger the tube ID and the less air supply rate, the longer it took for the air-oil to come out of the nozzle and the harder the flow became. With a φ 4 × φ 6 polyurethane tube, the air supply rate was increased to 20NL/min and the oil took more than 40 minutes to come out (the test was terminated at 40 minutes). A Teflon tube of φ 2 × φ 4 delivered oil within the shortest period of time and offered easy flow because of its small surface tension and lipophobic characteristic.

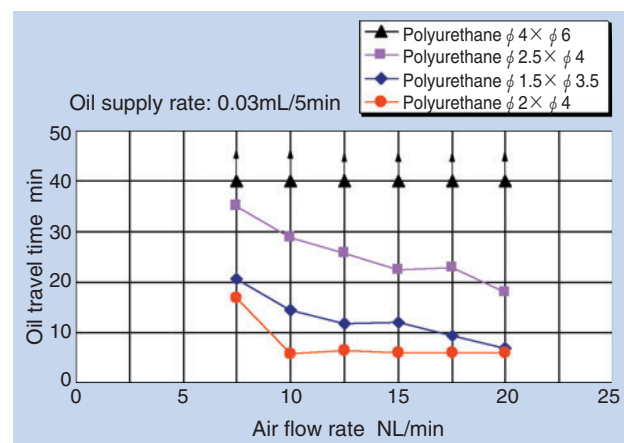
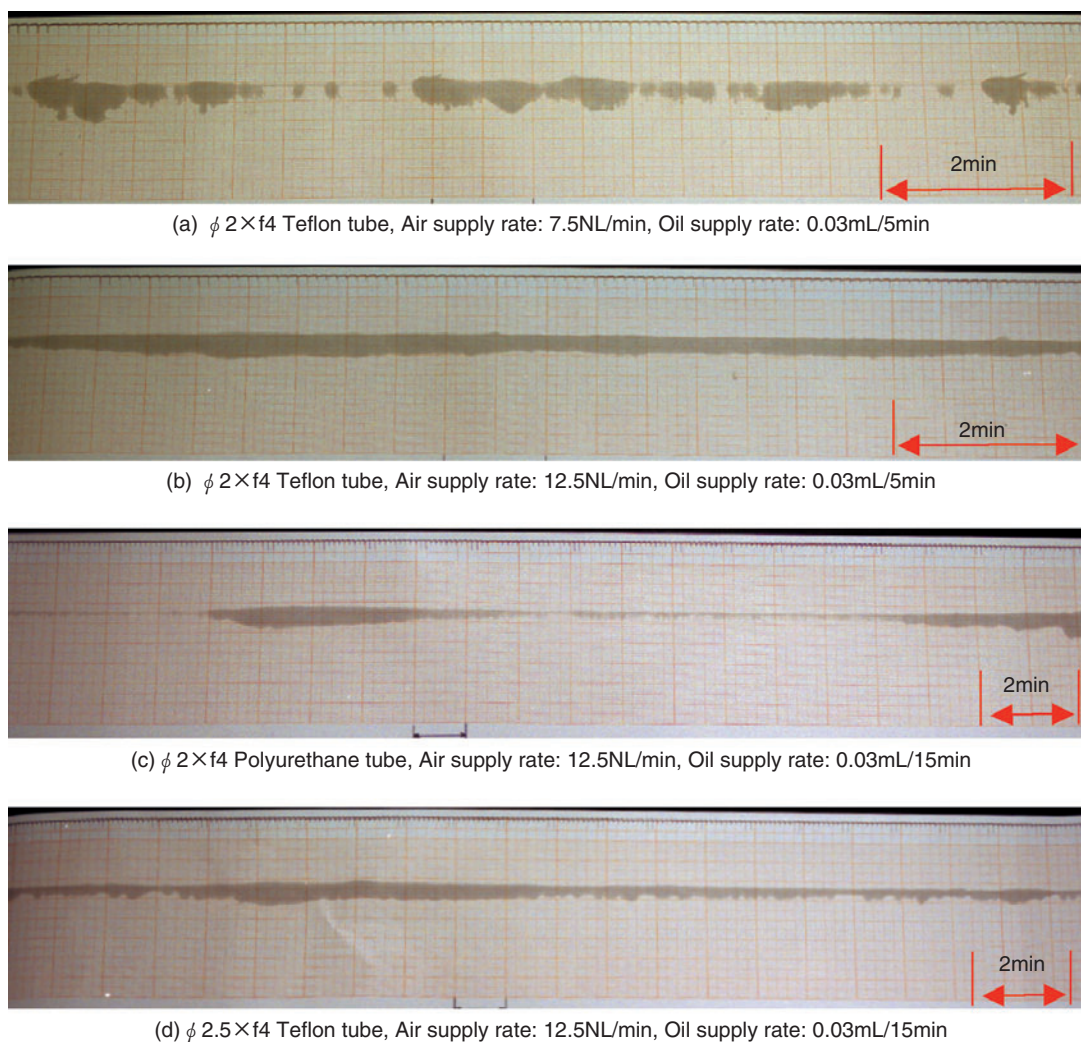


Fig.9 Air flow rate and oil travel time

#### 4.2.2 Fluctuation in oil delivery

A study was made to identify how the air-oil supply conditions and different sample tubes affected the consistency in oil delivery. The test used an intermittent oil supply unit and recorded chronological changes in the oil amount (fluctuation in oil delivery) delivered from the nozzle by way of oil absorption on the recording paper. Fig. 10 shows the recorded oil absorption. As shown in (a) and (b), with a Teflon tube, when air supply rate was small, its capability to transport oil decreased and the oil moved in lumps,

causing fluctuation in oil delivery. With the air supply rate kept constant, when the oil supply time was extended, oil was delivered in correspondence with the shot interval as shown in (b) and (c). If the interval is long, it causes fluctuation in oil delivery. On the other hand, polyurethane tubes showed less fluctuation in oil delivery even though the shot interval was extended, (c) and (d). It was because polyurethane tubes had large resistance on the internal walls that stopped the oil flow inside the tubes.



**Fig.10** Example of lubricant jet soak on recorder chart

### 4.2.3 Impacts of continuous and intermittent oil supply

Ease of air-oil flow was studied using a system that was capable of continuously supplying a very small amount of oil and a  $\phi 2 \times \phi 4$  Teflon tube. Fig. 11 shows the results. Like intermittent oil supply, continuous oil supply showed a tendency of losing air-oil flow as the air supply rate became smaller. Ease of air-oil flow was also compared between the continuous and the intermittent oil supply methods with the oil delivery rate per hour maintained the same. As a result, the continuous oil supply method took longer time than the intermittent oil supply method in delivering oil with poorer oil flow. This may have been caused by poor oil transport efficiency of air because the continuous oil supply method makes the oil grains that adhere to the tube wall smaller.

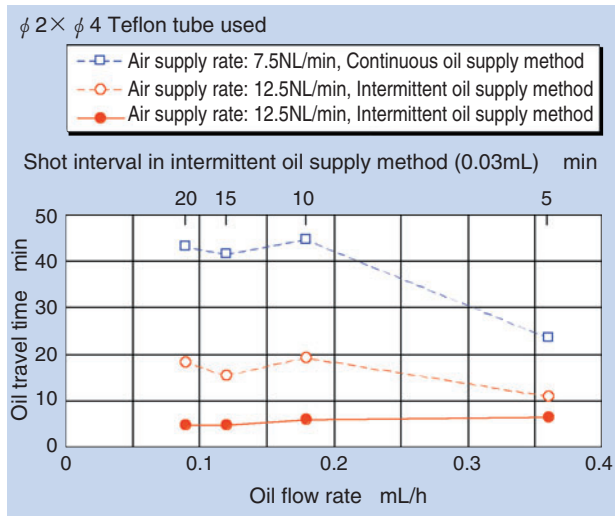


Fig.11 Oil flow rate and oil travel time

Figs. 12 and 13 show the fluctuation in oil delivery, defined as Variance  $\beta$  (mm) of the maximum and the minimum absorption marks, in the continuous oil supply method using a  $\phi 2 \times \phi 4$  Teflon tube. In the continuous oil supply method, oil delivery rate was less subject to air and oil supply rates. As compared to the intermittent oil supply method, the continuous oil supply method showed less fluctuation in oil delivery at air supply rate of 7.5NL/min.

The continuous oil supply method has less favorable oil transport efficiency within tubes than the intermittent oil supply method. However even if the air supply is small, it has less fluctuation in oil delivery and offers stability in the supply of lubricant.

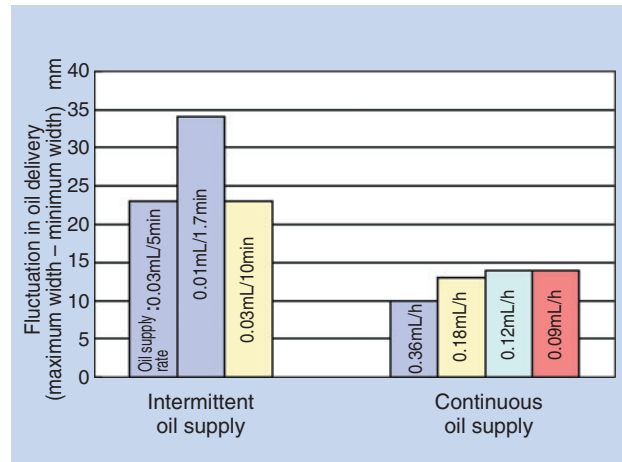


Fig.12 Variation  $\beta$  for intermittent and continuous oil supply (air 7.5NL/min)

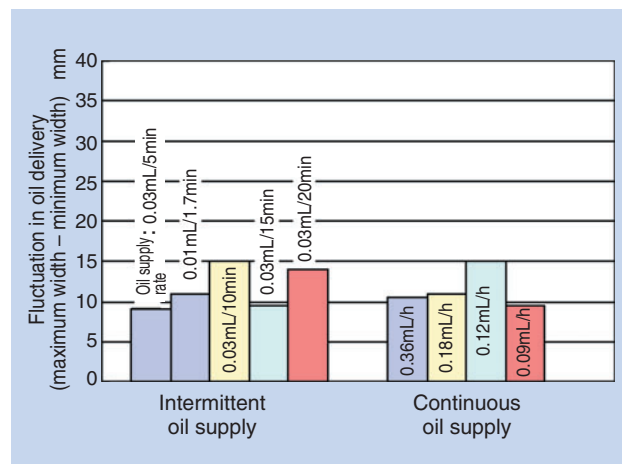


Fig.13 Variation  $\beta$  for intermittent and continuous oil supply (air 12.5NL/min)

## 6. Conclusion

Faster rotation of the rolling bearings for machine tools can be accomplished by optimization of the bearings internal components and the development of the lubrication technology. In order to minimize the oil supply rate to air-oil lubricated rolling bearings that support the machine tool main spindles, this report concludes that the oil supply swash angle of the inner ring is determined by the  $d_{m1}$  value and that minimizing oil wettability of tubes is effective to reduce the fluctuation of oil delivery into bearings at the oil nozzle.

### References

- 1) F. Kosugi, NTN TECHNICAL REVIEW, No.71 (2003) 18-27 (in Japanese).
- 2) K. Fujii, M. Mori and Y. Ohta, Proc. JSPE Autumn Conf, (2000) 449 (in Japanese).
- 3) K. Fujii, M. Mori and Y. Ohta, Proc. JSPE Spring Conf, (2001) 392 (in Japanese).
- 4) K. Fujii and M. Mori, Proc. JSPE Autumn Conf. (2001) 561 (in Japanese)

### Photos of authors

---



Yoshinobu AKAMATSU

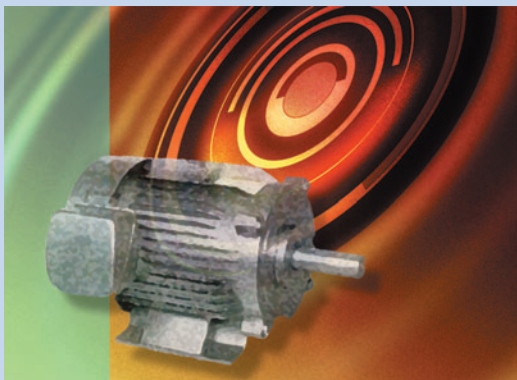
Technical Research Dept.  
Research & Development Center



Masatsugu MORI

Technical Research Dept.  
Research & Development Center

## Development of Long Life Grease for High Speed Application — “ME-1” Grease for Motor Bearings —



Hidenobu MIKAMI\*

Electric motors are used in many household and industrial applications. They are essential to our daily lives. Motors are expected to be quiet and highly efficient. The motor bearings, too, should have low noise and low torque. For these reasons, Li soap/ester greases are widely used in motor bearings. They exhibit low torque and excellent acoustic characteristics. Several years ago, greases having urea thickener and poly- $\alpha$ -olefin (PAO) or ester oils were developed to extend the life of motor bearings, and today they are seeing increasingly wide use. The market, on the other hand, still demands even longer bearing life. A new grease needs to be developed to meet this demand.

To extend the life of a grease, it is necessary to prevent oxidation of the base oil. Thermal oxidation stability of the base oil and oxidation inhibiting additives play a large role in extending the life of the grease, so it is necessary to use the proper inhibitor. In this paper, the effectiveness of oxidation inhibitors suitable for PAO and ester base greases is discussed. The paper also introduces NTN's “ME-1” long life electric motor grease that was recently developed based on this knowledge.

### 1. Introduction

Electric motors are used in many households and industrial applications. They are essential to our daily lives. Motors are expected to be quiet and highly efficient. The motor bearings, too, should have low noise and low torque. For these reasons, Li soap/ester greases are widely used in motor bearings. They exhibit low torque and excellent acoustic characteristics. Recently, greases having urea thickener and poly- $\alpha$ -olefin (PAO) or ester oils were developed to extend the life of motor bearings, and today they are seeing increasingly wide use<sup>1)</sup>. The market, on the other hand, still demands even longer bearing life. A new grease needs to be developed to meet this demand.

Electric motors are also used by machine tools for driving main spindles and feeding devices. In these applications, demands for longer life, higher speed, and higher precision are growing around greases.

To extend the life of grease, it is necessary to prevent oxidation of the base oil. Thermal oxidation stability<sup>2)</sup> and oxidation inhibiting additives in the base oil play a large role in extending the life of the grease, so it is necessary to use the proper inhibitor suitable for the base oil used. In this paper, the effectiveness of oxidation inhibitors suitable for PAO and ester base greases is discussed. The paper also introduces NTN's “ME-1” long life grease for electric motors that was recently developed based on this knowledge.

\*Research & Development Center Technical Research Dept.

## 2. Extending grease life

Greases are made of thickener, base oil (lubricant) and additives. When grease is used at high temperatures for an extended period of time, its base oil suffers from oxidation. To extend the life of grease, it is necessary to control deterioration of the base oil. Consequently, it is critical to select a suitable base oil and oxidation inhibitor.

Fig. 1 shows weight changes of lubricant exposed to high temperature. When lubricant is exposed to high temperature, it loses weight as time elapses. As soon as the time period needed for the lubricant to begin oxidation (induction time), the weight rapidly decreases. Oxidation of lubricant makes it volatile and quickly reduces its weight. Therefore, lubricants without antioxidants have a shorter induction period and those with antioxidants have a longer induction period. Even if antioxidant is added, less effective antioxidants can result in a shorter induction period.

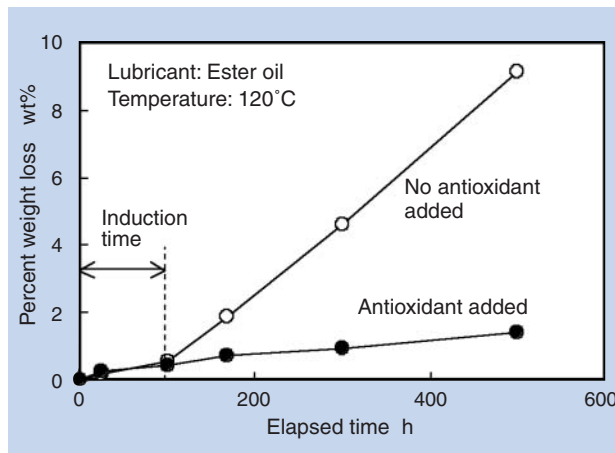


Fig.1 Oil loss at high temperature

Antioxidants are divided into two types based on their functionality; radical scavengers and peroxide decomposers<sup>3)</sup>. Effectiveness of antioxidants added to mineral oils<sup>4), 5)</sup> has been reported, but many unknown factors remain with respect to how effective they may be when added to synthetic oils such as PAO and ester oils. To verify their effectiveness, PAO and ester oils of different dynamic viscosity were selected and an antioxidant of 1 wt% was added. Then they were exposed to high temperature for measurement of any weight changes. For ester oils, traditional polyolester and a special ester oil that has excellent heat resistance were selected. Tables 1 and 2 show the selected lubricants and antioxidants.

Table 1 Test oils

	PAO-A	PAO-B	Ester A	Ester B
Type of oil	PAO	PAO	Polyol ester	Special ester
Dynamic viscosity mm <sup>2</sup> /s	40°C	31	46	33
	100°C	6	8	6
Viscosity index	135	138	128	125

Table 2 Test antioxidants

	Type	Name of chemical compound
A0-1	Radical scavengers	Alkyl diphenylamine
A0-2		Hindered phenol
A0-3	Peroxide decomposers	Zinc dithiophosphate
A0-4		Thioether

**Figs. 2 ~ 5** show the measurements. Lubricants without antioxidants began oxidation within a short period of time and the induction time for all the specimens was several tens of hours. In contrast, those with antioxidants reduced weight loss and prolonged the induction time. PAO oils (**Figs. 2 and 3**) extended the induction period with zinc dithiophosphate (AO-3) or thioether (AO-4) added to them. However, alkyl diphenylamine (AO-1) and hindered phenol (AO-2) showed little effect. Unlike the PAO oils, the ester oils (**Figs. 4 and 5**) exhibited

benefit when alkyl diphenylamine (AO-1) or hindered phenol (AO-2) was added.

In order to inhibit oxidation, an appropriate antioxidant must be added to suit the type of lubricant such as PAO and ester oils. Peroxide decomposers were found to have a greater effect in inhibiting oxidation of the PAO oils and radical scavengers for the ester oils. When radical scavenger was added to ester-B (special ester oil), the greatest improvement in oxidation deterioration resistance was observed.

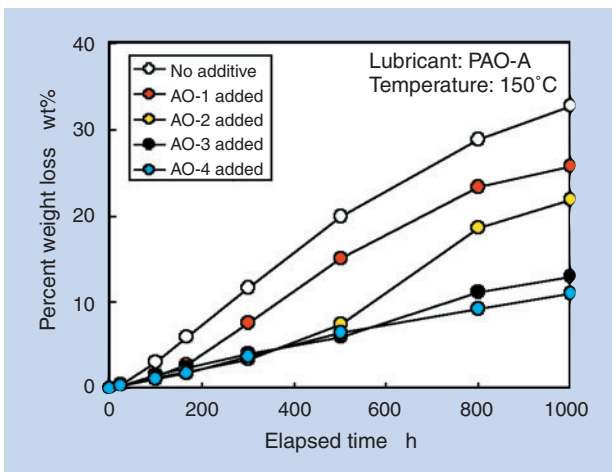


**Fig.2** Percent weight loss of PAO-A at high temperature

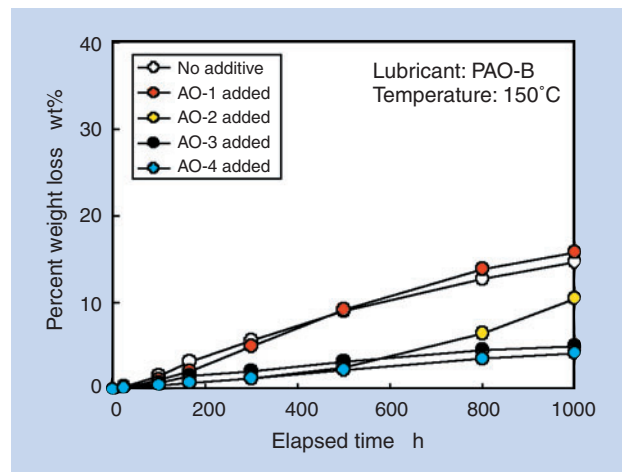


**Fig.3** Percent weight loss of PAO-B at high temperature

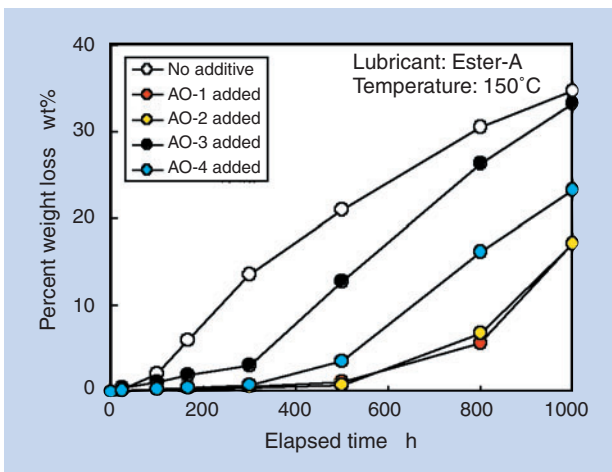


**Fig.4** Percent weight loss of Ester-A at high temperature

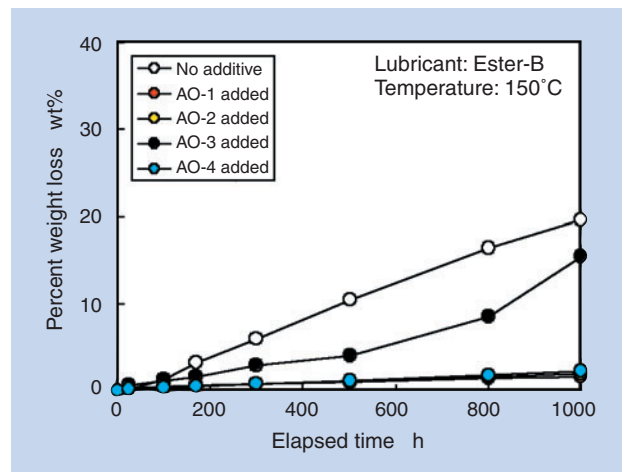


**Fig.5** Percent weight loss of Ester-B at high temperature

### 3. Grease for motor bearings

#### 3.1 Traditional greases

Greases for motor bearings must be low-noise, low torque and long life performance. Consequently, Li soap grease (commercially available Grease A) made of low-viscosity ester oil as the base oil is widely used, as shown in Table 3. For applications that require a broader temperature range, high-speed and long life urea grease (commercially available Grease B, MP-1) made of poly- $\alpha$ -olefin (PAO oil) or ester oil as the base oil is used.

#### 3.2 Composition and physical properties of ME-1 grease

"ME-1" grease uses urea compound as a thickener and a mixture of ester and PAO oils as the base oil. A suitable antioxidant is added to inhibit oxidation deterioration of the base oil, thus extending its life. Table 4 shows the representative physical properties of ME-1 grease.

**Table 3** Greases for motor bearings

	Commercially available grease A	Commercially available grease B	MP-1
Thickener	Li soap	Urea	Urea
Base oil	Ester	PAO	PAO+Ester
Viscosity of base oil mm <sup>2</sup> /s 40°C	25~30	46	40
Worked penetrateion 60W 25°C	250	220	250

**Table 4** Typical properties of ME-1 grease

	ME-1	Test method
Thickener	Urea	
Base oil	Ester + PAO	
Viscosity of base oil mm <sup>2</sup> /s 40°C	60	JIS K2220.23
Worked penetrateion 60W 25°C	250	JIS K2220. 7
Dropping point °C	250 or higher	JIS K2220. 8
Evaporation loss % 99°C, 22h	0.2	JIS K2220.10
Oil separation mass % 100°C, 24h	0.0	JIS K2220.11
Oxidation stability kPa 99°C, 100h	30	JIS K2220.12
Low temperature torque Starting	300	JIS K2220.18
mN·m -30°C Rotating	57	

#### 3.3 High temperature durability

A high temperature endurance test (per ASTM D3336) was conducted on ME-1 grease. Fig. 6 shows the test results of commercially available greases and ME-1 grease. Endurance of ME-1 grease is more than five times that of commercially available grease A and 1.5~2 times that of commercially available grease B, urea grease, and MP-1. ME-1 grease uses a special ester as the base oil and an appropriate antioxidant to inhibit oxidation for longer life.

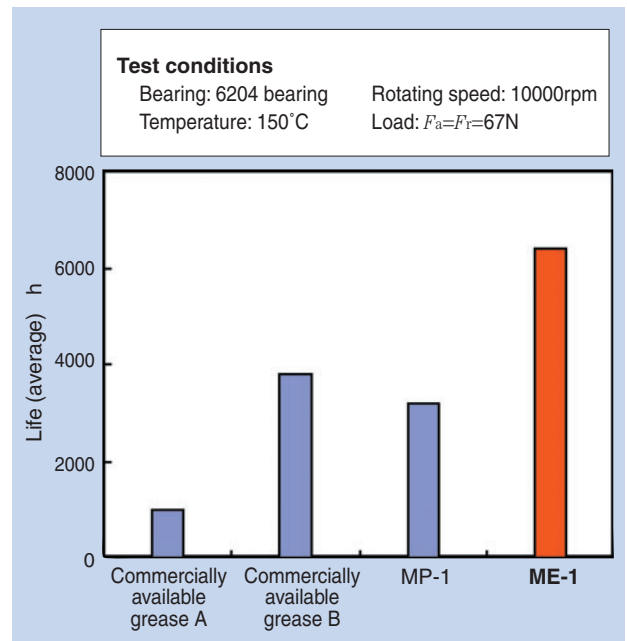


**Fig.6** Endurance test results



### 3.4 Acoustic characteristics

Since low noise is a requirement for motor bearing greases, the rotational acoustics of the grease sealed bearings were measured. Fig. 7 shows the measurements. The acoustic value of ME-1 grease measured the same as that of commercially available grease A and was better than that of commercially available grease B. Generally, urea grease is difficult to micro-disperse a thickener, and for this reason, it is considered poorer than Li soap grease in terms of the acoustic characteristics. However, both ME-1 and MP-1 greases have thickener micro-dispersed in the products, their acoustic characteristics are better than those of ordinary urea greases.

### 3.5 Rotational torque

Smaller rotational torque is also a requirement for motor bearings for reduction in energy consumption.

Fig. 8 compares the rotational torque of ME-1 grease to that of commercially available greases. Though the rotational torque of ME-1 grease was poorer than that of commercially available grease A, the performance was equal to those of commercially available grease B and MP-1. The smaller the viscosity of the base oil, the smaller becomes the rotational torque. ME-1 grease uses special ester of higher viscosity in its base oil, but it maintains low rotational torque to be equal in its performance to commercially available grease B and MP-1, both of which use the base oil of lower viscosity. For this reason, ME-1 possesses torque performance sufficient for field applications.

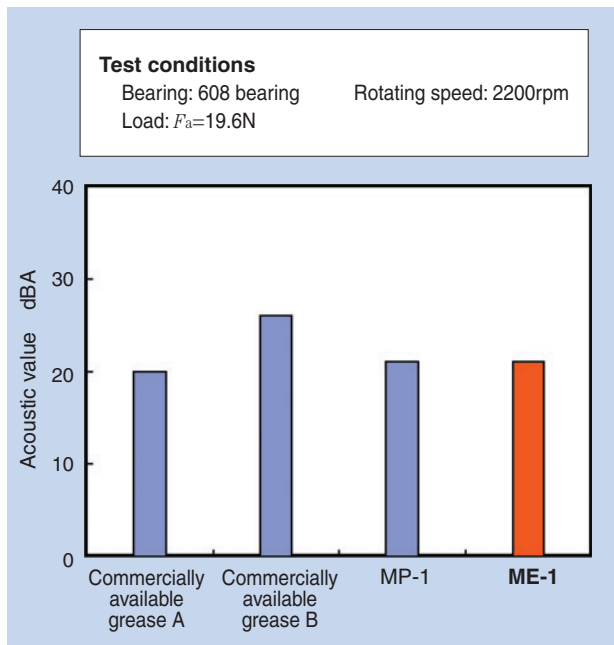


Fig.7 Noise levels of various greases

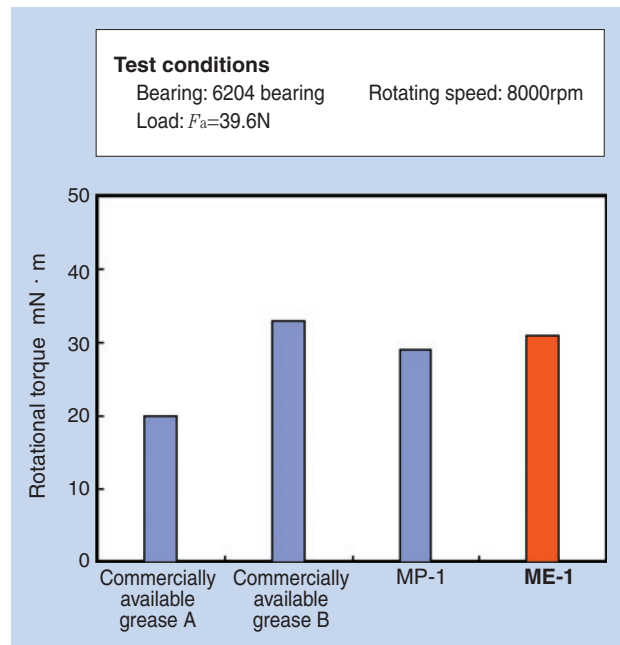


Fig.8 Rotational torque of various greases

## 4. Conclusion

ME-1 grease has excellent high-temperature endurance and acoustic characteristics and exhibits sufficient rotational torque for field applications. Motors are expected to become more compact, light-weight and efficient. Today's market will demand greases for motor bearings to last longer and perform at a higher level. We sincerely hope that "ME-1" grease will help machine tool and other various motors achieve an even higher level of performance.

### References

- 1) Seiji Okamura, THE TRIBOLOGY 9 (2001) 47.
- 2) Yuji Ohnuki, Hiroshi Kimura, TRIBOLOGY Kaigi Yokoshuu (Tokyo, 1998.5)
- 3) Yasukazu Ohkatsu, TRIBOLOGISTS 40.4 (1995) 60.
- 4) Jinichi Igarashi, The Nisseki review 32,3 (1990) 5.
- 5) Jinichi Igarashi, The Nisseki review 32,3 (1990) 17.

### Photos of author

---



Hidenobu MIKAMI

Technical Research Dept.  
Research & Development Center

## "ULTAGE" Series Precision Bearings for Machine Tools



Hiroshi TAKIUCHI\*  
Futoshi KOSUGI\*

To meet the market needs for faster, more efficient, and more precise machine tool main spindles, NTN has created new bearing designs and recently reorganized our product line into "**ULTAGE Series**" bearings.

The paper explains various bearing types and their applications in plain terms. The paper also describes the configurations of "**ULTAGE Series**" bearings.

### 1. Introduction

To meet the market needs for faster, more efficient, and more precise machine tool main spindles, NTN has been involved with the development and improvement of various bearings. Recently NTN adopted an approach of "What are the bearing specifications that are truly desired of precision bearings" and reviewed the bearing designs of traditional product series. As a result, the traditional product line has been reorganized into "**ULTAGE Series**" bearings.

In the last Technical Review, Issue No. 71, NTN introduced the "**ULTAGE Series**" bearings. Since then, NTN added four new types, changed the names of some of those products, and reorganized the product line for the customers to readily understand the characteristics of different types. In this issue, we have re-defined the configuration of the "**ULTAGE Series**" bearings.

ULTAGE is a term created by NTN combining "ULTIMATE" and "STAGE" to represent NTN's pursuit for the highest level of precision in machine tool bearings.

### 2. Development history of precision bearings for machine tools

The applications for the machine tool precision bearings are divided largely into those for main spindles and those for feeding systems. For the main spindle application, there are angular contact ball bearings (for radial loads and axial loads) and cylindrical roller bearings. For the feeding system application, there are ball screw support bearings.

**Table 1** shows the chronological development of precision bearings for machine tools. (Y-axis is the scale of high-speed/high functionality.) Also added is a brief history of the development of the above-mentioned three types of bearings.

\*Industrial Engineering Department Industrial Sales Headquarters

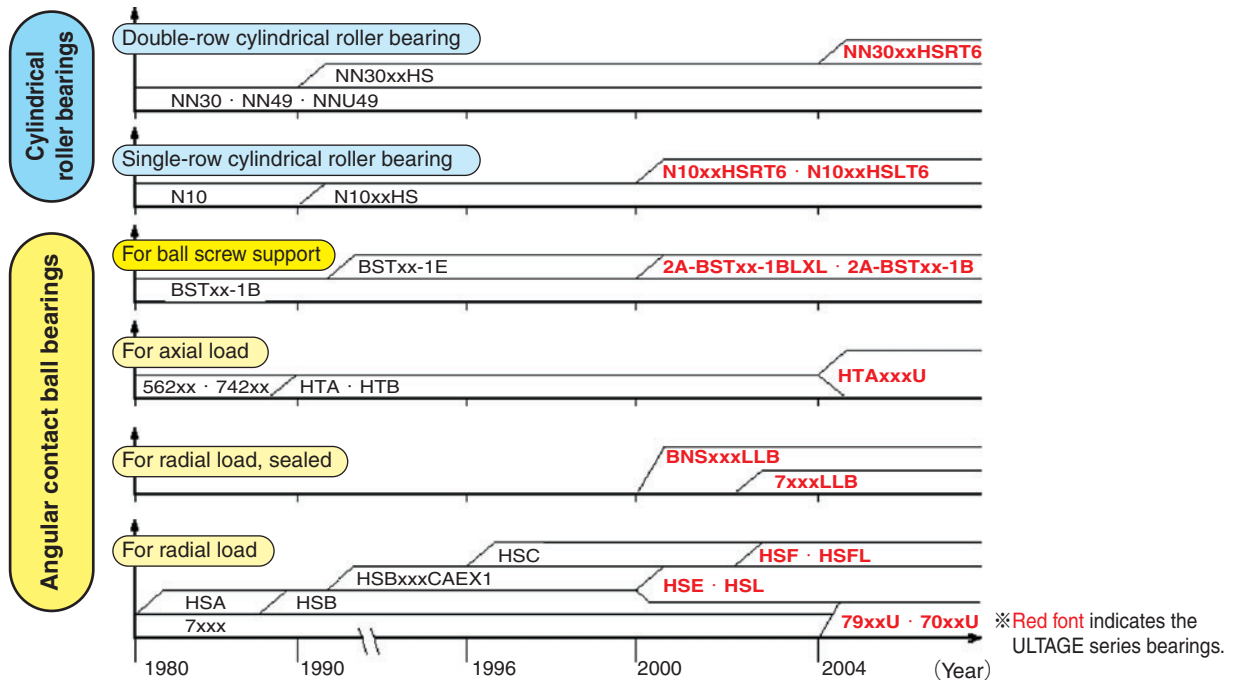


Table 1 Development history of precision bearings for machine tools

## 2.1 Angular contact ball bearing

### 2.1.1 Angular contact ball bearing for radial load

The standard angular contact ball bearing (7xxx type) is the base for the angular contact ball bearing for radial load. In the middle of the 1980's, the rolling elements were made smaller in diameter to produce the HSA type, and in the late 1980's, the HSA type was improved to reduce heat generation and the HSB type was announced. In the early to mid 1990's as demands increased for faster and more rigid machine tool main spindles, NTN added to this product line, the HSBxxxCAEX1 type and the HSC type, which uses even smaller rolling element diameter than the HSB type.

In 2000 JIMTOF, NTN announced the HSE type with improved wear and seizure resistance and a low-noise type (predecessor to the HSL type).

Again, in 2002 JIMTOF, NTN announced, in addition to the HSE type bearings, sealed angular contact ball bearings (BNSxxxLLB type, 7xxxLLB type) for longer life and eco-conscious angular contact ball bearings (HSL type) for low-noise, low air-oil consumption purposes, both of which are called the "ULTAGE Series" bearings.

NTN has added yet another type bearing based on the standard angular contact ball bearing. The standard 7xxx type was improved in its speed and functionality to build the new 70xxU/79xxU types, which were added to the "ULTAGE" Series.

### 2.1.2 Angular contact ball bearing for axial load

For a long time, duplex thrust angular contact ball bearings (562xxx, 742xxx types) have been the main stream of angular contact ball bearings for axial load. In the late 1980's, when applications began to demand faster operation, NTN announced the HTA and the HTB types of bearings that combined two single-row angular contact ball bearings. Since then, the HTA type has replaced almost all the traditional bearings for this use in Japan. However, recent requirements for even faster operation prompted NTN to review the specifications of the HTA type bearing. A new HTAxxxU type bearing was created to meet this need and added to the "ULTAGE" Series.

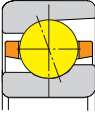
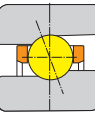
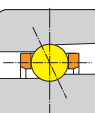
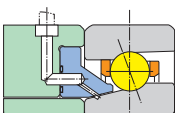
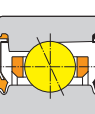
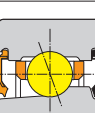
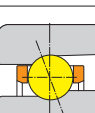
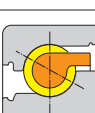
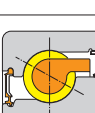
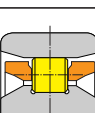
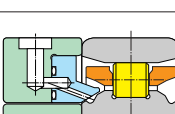
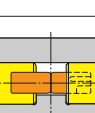
## 2.2 Cylindrical roller bearing

Cylindrical roller bearings come in double-row cylindrical roller bearings (NN30, NN49, NNU49 types) and single-row cylindrical roller bearings (N10xxxHS type).

### 2.2.1 Double-row cylindrical roller bearing

The NN30 type has been the most popular double-row cylindrical roller bearing. NTN has been engaged in the development of the cage material and profile. Some bearings employ resin cages (T2), but the standard bearings use high-strength brass cages. Adoption of resin cages is effective to extend the grease life, and for this reason NTN developed a new resin cage (T6). The new resin cage has been adopted in the new high-speed NN30xxHST6 type and super high-speed NN30xxHSRT6 type, and they are added to "ULTAGE" Series product line.

Table 2 ULTAGE series

<b>The ULTAGE Series</b>	<b>Angular Contact Bearings</b>	<b>For Main Spindles</b>		<b>Standard</b> 70U-type & 79U-type (Contact Angles: 15°, 25° & 30°)	By optimizing the internal design and utilizing a new resin cage, NTN has increased axial capacity and decreased heat generation. Available bore sizes: 10~130 mm. Also available with ceramic balls ("5S" prefix).
				<b>High-Speed</b> 5S-2LA-HSE-type (Contact Angles: 15°, 20° & 25°)	The use of special materials and surface improvements have greatly increased wear resistance and seizure resistance. The optimization of internal specifications has resulted in a high-speed, high-rigidity and highly reliable bearing. Also available with steel balls (no "5S" prefix).
				<b>Ultra High-Speed</b> 5S-2LA-HSF-type (Contact Angle: 25°)	In addition to the features of the HSE-type bearing, this bearing also uses small ceramic balls to achieve greater speed due to less heat generation.
				<b>Eco-Conscious Model High-Speed</b> 5S-2LA-HSL-type (Contact Angles: 15°, 20° & 25°) <b>Ultra High-Speed</b> 5S-2LA-HSFL-type (Contact Angle: 25°)	These bearings use special materials and surface improvements for greatly increased wear resistance and seizure resistance. Based on the high-speed HSE-type and ultra high-speed HSF-type bearings, this design has an eco-conscious nozzle that should be used exclusively with air-oil lubrication. These bearings provide the same high-speed operation as HSE and HSF bearings, but operate more quietly and reduce air and oil consumption. Therefore, they contribute to a cleaner working environment and save energy. HSL-type is also available with steel balls (no "5S" prefix).
				<b>Standard Non-Contact Seal Model</b> 70 LLB-type & 79 LLB-type (Contact Angles: 15° & 25°)	For this design, non-contact seals are utilized on both sides, special grease is used and the internal design has been optimized to create a pre-greased bearing that is resistant to heat generation. Also available with ceramic balls ("5S" prefix).
				<b>High-Speed Non-Contact Seal Model</b> 5S-2LA-BNS LLB-type (Contact Angles: 15°, 20° & 25°)	This bearing utilizes special materials and surface improvements for greatly improved wear resistance and seizure resistance. Various improvements have also been made to the internal design and the non-contact seals at both ends, and the utilization of special grease. The result is a pre-greased bearing that provides longer bearing life. Also available with steel balls (no "5S" prefix).
				<b>For Axial Loads</b> HTA U-type (Contact Angles: 30° & 40°)	Internal specifications have been optimized to create an angular contact bearing for axial loads that offers the same level of rigidity as the conventional HTA-type, but with increased axial capacity and a higher operating speed. Also available with steel balls (no "5S" prefix).
	<b>For Ballscrew Supports</b>		<b>Open Model</b> 2A-BST-type (Contact Angle: 60°)	This open-model bearing provides longer service life and improved fretting wear resistance due to bearing ring surface improvements.	
			<b>Light Contact Model</b> 2A-BST LXL-type (Contact Angle: 60°)	Bearing raceway surface improvements and special grease greatly increase service life and fretting wear resistance. This pre-greased bearing also has a low-torque, light-contact seal that provides greater dust resistance, longer grease life and improves bearing handling and installation characteristics.	
	<b>Cylindrical Roller Bearings</b>	<b>For Main Spindles</b>		<b>Ultra High-Speed</b> N10HSRT6(K)-type	Optimization of the internal design and utilization of a special resin cage that allows for high-speed operation have resulted in a high-speed bearing that is resistant to heat generation. This bearing provides better speed performance than the standard N10HS single-row cylindrical roller bearing.
				<b>Eco-Conscious Model Ultra High-Speed</b> N10HSLT6(K)-type	This bearing is based on the N10HSRT6-type and has an eco-conscious nozzle that should be used only with air-oil lubrication. This bearing provides the same high-speed performance as the N10HSRT6-type, but operates more quietly and reduces air and oil consumption. Therefore, it contributes to a cleaner working environment and saves energy.
			<b>High-Speed</b> NN30 HST6(K)-type <b>Ultra High-Speed</b> NN30 HSRT6(K)-type	Optimization of internal specifications and the use of a new resin cage result in bearings that achieve high-speed operation with low levels of heat generation. Both grease lubrication and air-oil lubrication are acceptable.	

### 2.2.2 Single-row cylindrical roller bearing

The standard single-row cylindrical roller bearing used to be the N10 type bearing. When high speed performance was demanded in the late 1980's to early 1990's, NTN developed a high-speed N10xxHS type which used smaller rolling element diameter than that of the N10 type. The single-row cylindrical roller bearing was once again challenged by the needs for even faster speed, NTN announced in the 2002 JIMTOF two new type bearings for the main spindle rear application. They are the super high-speed N10xxHSRT6 type that adopted resin cages and the eco-conscious N10xxHSLT6 type that reduced noise and air-oil consumption.

### 2.3 Ball screw support bearing

Demands for high-speed with oil lubrication increased for ball screw support bearings in the late 1980's. NTN developed the BSTxx-1B type bearing then, and later in the early 1990's, announced the BSTxx-1E type which used a larger rolling element diameter to extend life. Then, during the 2000 JIMTOF, NTN announced the open type 2A-BSTxx-1B and the light contact seal type 2A-BSTxx-1BLXL for higher speed, longer life, and better resistance against fretting.

## 3. Configuration of ULTAGE Series product line

As shown in the preceding page, the new ULTAGE series bearing product line has added four new types (indicated in bold characters below) and includes name changes of the HSE type products. In the end, the new series now has 14 types of products, which are shown in **Table 2** on the preceding page.

The configuration of the "ULTAGE" series has been reorganized for easy understanding, comprising three types of angular contact ball bearings for radial loads, **standard (7xxxU type)**, high-speed (HSE type), and super high-speed (HSF type), two types of sealed angular contact ball bearings, standard (7xxxLLB type) and high-speed (BNSxxxLLB type), and two types of eco-conscious angular contact ball bearings, high-speed (HSL type) and super high-speed (HSFL type).

Angular contact ball bearings for axial loads are available in only 1 type, **standard (HTAxxxU type)**.

There are four types of cylindrical roller bearings. The double-row resin cage model comes in **high-speed (NN30xxHST6 type)** and **super high-speed (nn30xxHSRT6 type) types**, and the single-row resin cage model comes in super high-speed (N10xxHSRT6 type) and the eco-conscious (N10xxHSLT6 type) types.

The ball screw support bearings are largely divided

into two types, open (BSTxx-1B type) and sealed (BSTxx-1BLXL type).

## 4. About publication and revision of the Precision Rolling Bearings catalog

To become a comprehensive catalog for the precision rolling bearings, this catalog was renewed in the fall of 2003 (catalog No. 2260/J) with addition of the "ULTAGE" series product line and review of some of the technical contents.

The new catalog not only changed the bearing product configuration by adding the "ULTAGE" series, but also it made the following two major changes.

- 1) **The bearing specifications were reviewed, changes made to the allowable rotating speeds, and the speed coefficients were adopted.**
- 2) **The allowable axial loads for the angular contact ball bearings were changed. The catalog has been revised incorporating the new four types of the "ULTAGE" series bearings. Please see the catalog for the details.**

## 5. Conclusion

For the past 4~5 years, NTN has made an overall improvement and introduced new models to the precision bearings line-up for machine tools. The final product is the "ULTAGE" series product line. We believe that the "ULTAGE" series is the most advanced precision bearing series that provides improved reliability and high functionality to the machine tool main spindles.

We know that users will demand more. NTN is committed to perform our duties as a supplier of precision bearings and serve our customers as their good partner. We will continue to seek improvement and undertake development projects to become "NTN, the maker of precision bearings."

### Photos of authors



Hiroshi TAKIUCHI

Industrial Engineering Dept.  
Industrial Sales headquarters



Futoshi KOSUGI

Industrial Engineering Dept.  
Industrial Sales headquarters

## ULTAGE Standard Angular Contact Ball Bearings, 79U/70U type



Keiichi UEDA\*

Machine tool bearings require high speed capability, long life, and consideration of the operating environment. To meet such needs, NTN has developed a new standard angular contact ball bearing, the 79U/70U type, which has superb performance and adds rich variation to our ULTAGE Series product line. This paper describes the features of NTN's standard angular contact ball bearings that have created a new epoch in the areas of high-speed, load resistance, and lubrication performance. These improvements make the 79U/70U ULTAGE Series worthy of the title "The New World Standard."

### 1. Introduction

Machining centers and machine tools are becoming faster, more efficient, and more precise. Today, the machining centers that are used primarily for mold fabrication have reached a  $d_{mn}$  value of 3.5 million ( $d_m$ : ball pitch circle diameter of bearing rolling elements mm,  $n$ : rotating speed  $\text{min}^{-1}$ )<sup>1)</sup>. In addition, increased productivity (higher efficiency achieved through reducing the non-processing time) is actively sought by consolidating multiple machining processes, including the cutting process, into a single machine. Recently, environmentally friendly technologies have become commercially available, which include "dry machining" where no cutting oil is used and "semi-dry machining" where an extremely small amount of cutting oil is used in the processes. The key words in this field are "High-speed", "Compound", and "Eco-conscious technology."

To meet such market trends, NTN created the "ULTAGE" series machine tool bearings and introduced them at JIMTOF (Japan International Machine Tools Fair) in 2002. Since then, NTN has been expanding this series mainly by adding angular

contact ball bearings and cylindrical roller bearings which have superb high-speed performance to be suitable for the machine tool main spindles. More recently, NTN has improved the functionality of the standard angular contact ball bearing and added it to the "ULTAGE" series product line as a new series in the bearing family. (Photo 1)



Photo 1 ULTAGE standard angular contact ball bearing 79U/70U type

\*Industrial Engineering Department Industrial Sales Headquarters

## 2. Optimization of internal design

### 2.1 Adoption of optimal design for high-speed, high-rigidity performance

Standard angular contact ball bearings are superior to high-speed angular contact ball bearings utilizing small diameter balls in terms of rigidity and load capacity (a parameter that indicates resistance to rolling fatigue life). On the other hand, applications of these bearings are limited by speed. The recent design change was aimed at improving high-speed performance, thereby expanding its application. NTN reviewed the internal design and solved the conflicting high-speed performance and high rigidity at the same time (establishing the specifications that achieve high-speed performance while retaining rigidity of the current bearing).

More specifically, impact of the designs of the rolling elements and raceways on rigidity were assessed. Effort was made to change the design of the areas that had less impact on rigidity to improve high-speed performance. However, changes to those areas that have definite impact on rigidity were kept at a minimum. "ULTAGE" 79U/70U type standard angular contact ball bearings utilized the above approach and accomplished both high-speed and high rigidity. Furthermore, this bearing uses a new resin cage, described later, and attained the  $d_{mN}$  value of 0.95 million with grease lubrication, about 1.5 times that of the current bearing, and 1.5 million with air-oil lubrication, about 1.8 times that of the current bearing (both bearings used a contact angle of 15° and steel

balls).

**Figs. 1** and **2** compare rigidity in the current and new designs. The new design has a slight decrease in rigidity, but maintains the rigidity at nearly the same level.

### 2.2 Improvement in load resistance

The bearings for machine tool main spindles can be subject to large axial loads during tool change while machine is stopped. If the load exceeds the allowable limit of the bearing, it can cause dents or other damage to the raceways. Such characteristics that indicate limitations to axial loads are called "allowable axial loads." NTN defines these as follows:

- The end of contact ellipse on the raceway surface reaches the shoulder of either an inner or outer ring (contact ellipse formed between the rolling element and the raceway protrudes out of the raceway: **Fig. 3**).
- The contact surface pressure on the raceway surface reaches 3650MPa in either the inner or outer ring raceway.

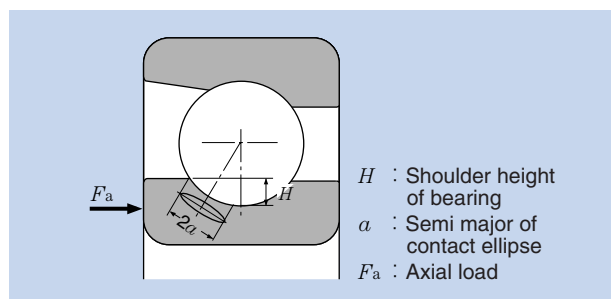


**Fig.3** Rolling elements protrude over the raceway shoulder

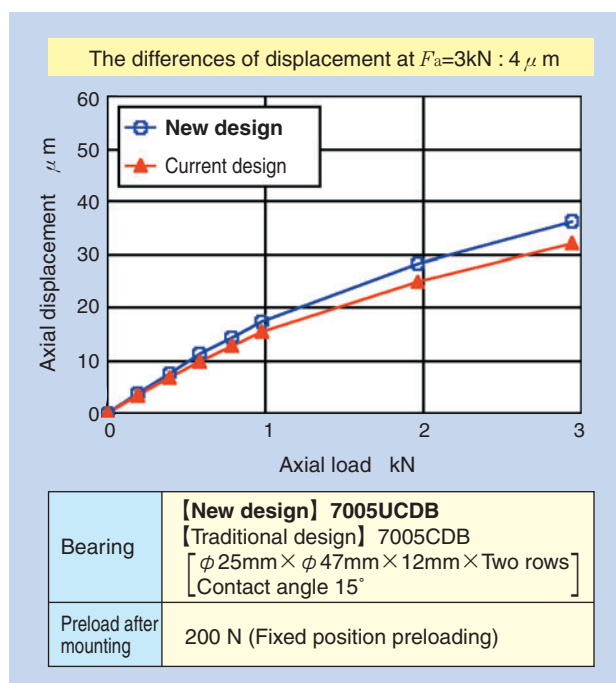


**Fig.1** Axial rigidity (7005CDB)

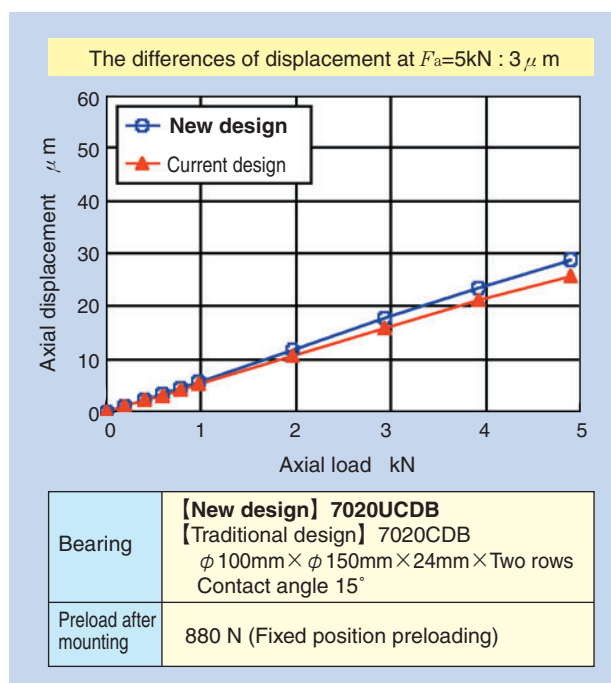


**Fig.2** Axial rigidity (7020CDB)



With ULTAGE 79U/70U type standard angular contact ball bearings, optimization of the internal design (described earlier) took these characteristics, into consideration. The review included the shoulder

height and attained allowable axial load far greater than (about 2.5 times) that of the current design. (Figs. 4 and 5)

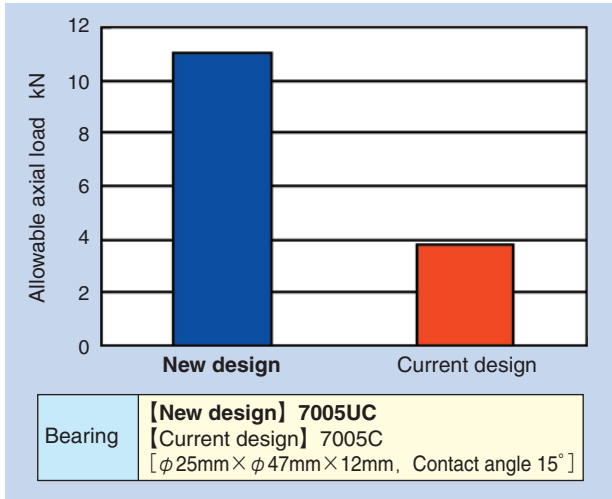


Fig.4 Allowable axial load (7005CDB)

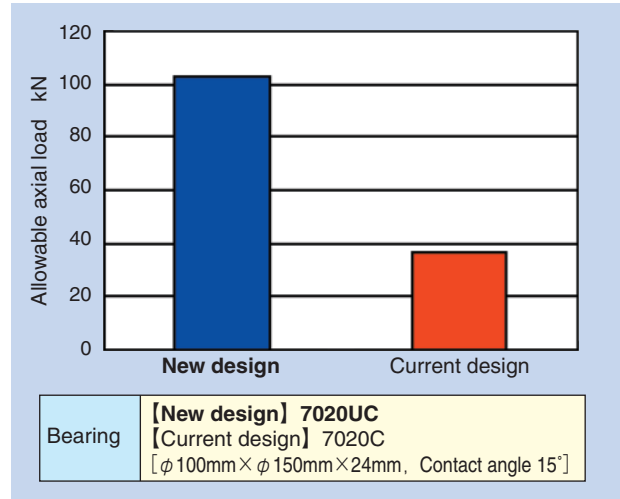


Fig.5 Allowable axial load (7020CDB)

### 2.3 Optimal design for lubrication

In air-oil lubrication, oil delivery into the bearing is important, as is the discharge of used oil (exhaust of air-oil). Unless there is a smooth discharge of used oil, lubricant can collect inside the bearing, which increases stirring resistance and results in temperature rise or seizure<sup>1)</sup>. Consequently, attention must be paid not only to optimization of the rolling elements, raceway profile, or other internal design but also to the above issue in order to establish stable temperatures under high-speed operation.

In grease lubrication, deterioration of grease by heat and lubrication life are critical. For this reason, internal structures having excellent grease retention have an advantage.

ULTAGE 79U/70U type standard angular contact ball bearings, have adopted designs that increase reliability of lubrication both in air-oil and grease lubrication. The following sections describe the key designs.

#### 2.3.1 Molded cage with new profile

(Polyamide resin: Figs. 6 (a) and (b))

##### (a) Characteristics in air-oil lubrication

To ease delivery of lubricant to the rolling element and the raceway contact area (aiming) and to promote the discharge of used oil outside the bearing (purging), the bore of the cage was tapered and the spaces for lubricant delivery and discharge inside the bearing were expanded.

In addition, slits were created at four corners of the ball pockets (where rolling elements are located) to secure oil passage from the inner to the outer ring (flow of lubricant created by centrifugal force).

These measures will prevent stirring resistance caused by stagnant lubricant.

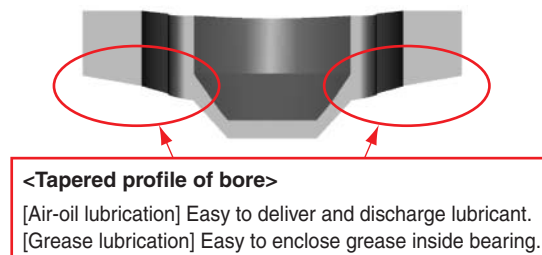


Fig.6(a) New resin cage (section of the ball pocket)

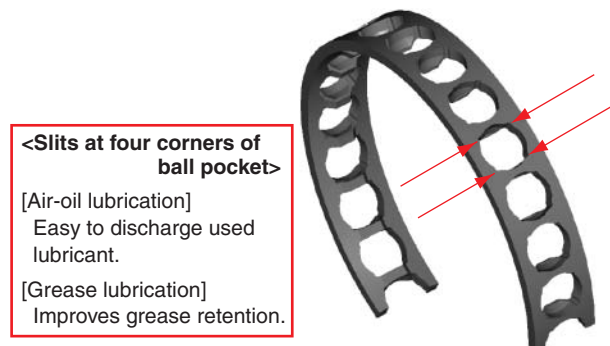


Fig.6(b) New resin cage (appearance)

**Fig. 7** compares the current cage to the new profile cage in a high-speed operation test (air-oil lubrication). The graph shows less bearing temperature rise with the new profile cage than with the current cage.

**(b) Characteristics in grease lubrication**

In grease lubrication, the slits at the pockets function to retain grease. Adoption of the tapered profile increases the bearing space (increases opening at bearing width), which makes it easy to enclose grease inside the bearing. Thus, this profile improved lubrication reliability and simplified grease handling.

**Fig. 8** compares the current cage to the new profile cage in a high-speed operation test (grease lubrication). The graph shows equal or less bearing temperature rise with the new profile cage than with the current cage.

ULTAGE 79U/70U type standard angular contact ball bearings, with applications reaching the  $d_{m\dot{n}}$  value of 1.05 million use this new cage profile as standard, whereas those for high-speed application (air-oil lubrication) beyond this speed use phenol machined cages that have been field proven in many super high-speed applications.

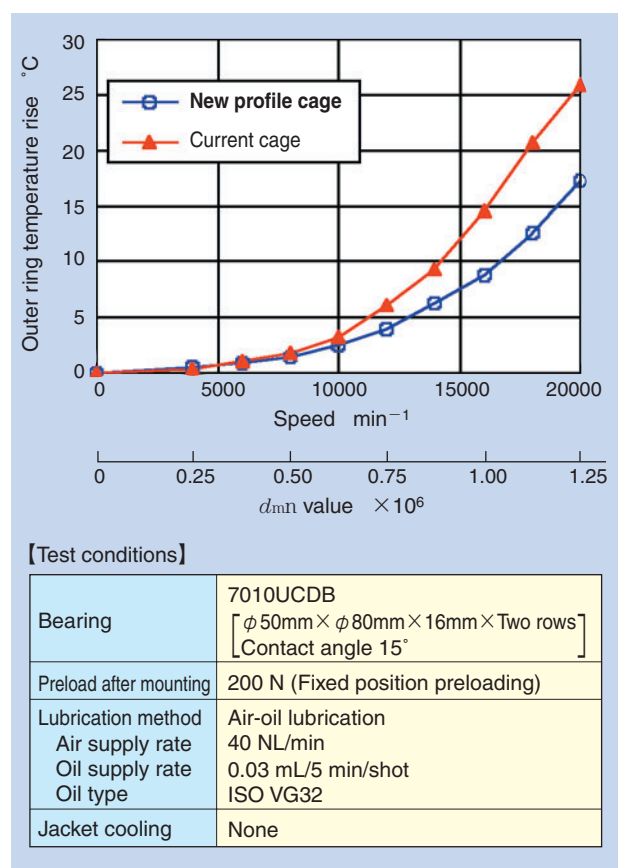


**Fig.7** High-speed test (air-oil lubrication)

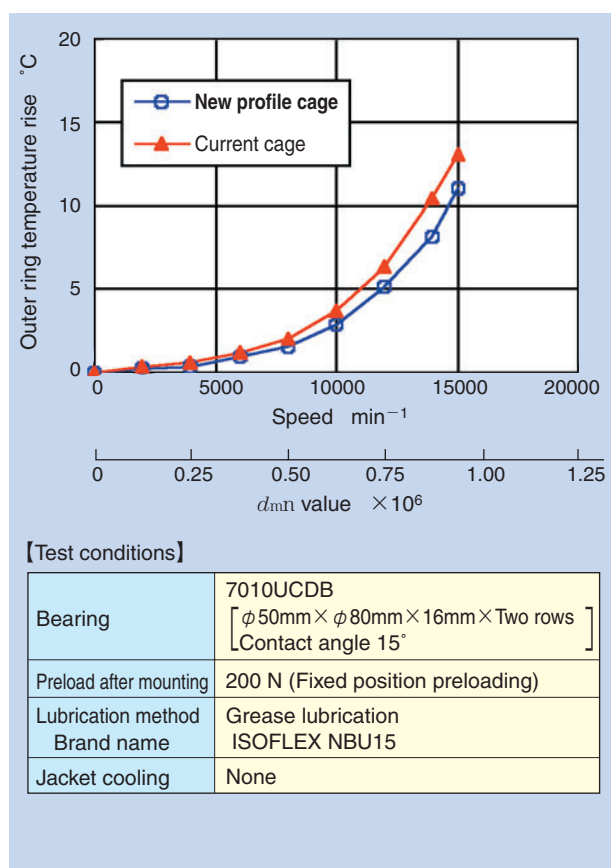


**Fig.8** High-speed test (grease lubrication)

### 2.3.2 Changes in inner ring profile (Fig. 9)

The lubricant delivery space was expanded by designing the outer diameter of the inner ring of the back side, or non-load side, lower than that of the current bearing and combining it with the above mentioned new cage profile. This structure allows for easier oil delivery to the cage-inner ring gap suitable for high-speed operation (with excellent oil delivery in air-oil lubrication) and allows oil delivery (aim of nozzle) at an angle. This reduces the dimensional restriction on the spacer with respect to the nozzle and improves freedom of design for the bearing peripheral structure.

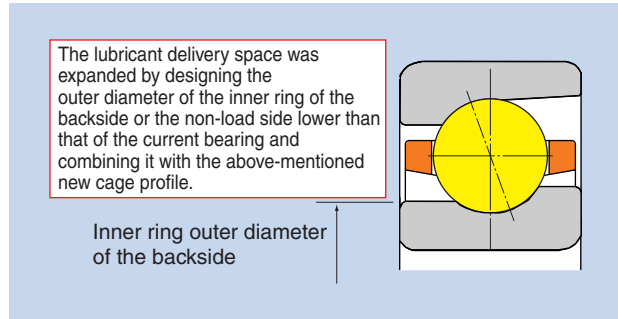
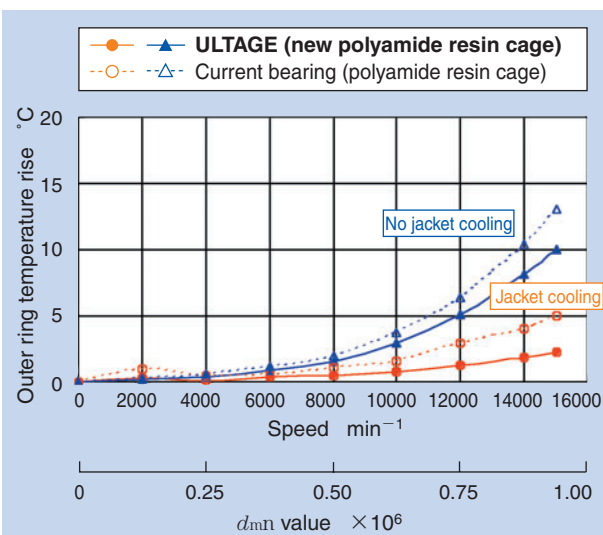


Fig.9 Section of 79U/70U type

## 4. High-speed operation test results

The test results (grease lubrication) of ULTAGE 79U/70U type standard angular contact ball bearings, are shown in Fig. 10. The temperature rise with the new series is lower than that of the current bearings with or without jacket cooling, and the speed reached a  $d_{mN}$  value of 0.95 million.

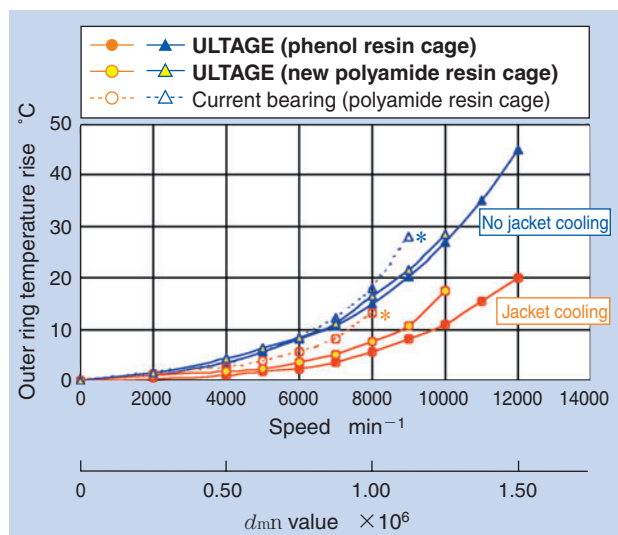
Like grease lubrication, air-oil lubrication evaluation (Fig. 11) also found lower temperature rise in the new series with or without jacket cooling than that of the current bearing. The current bearing showed unstable temperature rise at around a  $d_{mN}$  value of 1.05 million (indicated by  $\circ*$ ,  $\triangle*$ ), while the new series showed stable temperature rise at a  $d_{mN}$  value of 1.5 million.



【Test conditions】

Bearing	<b>[ULTAGE] 7010UCDB</b> [Current bearing] 7010CDB [ $\phi$ 50mm × $\phi$ 80mm × 16mm × Two rows ] [ Contact angle 15° ]
Preload after mounting	200 N (Fixed position preloading)
Lubrication method	Grease lubrication
Brand name	INSOFLEX NBU15
Jacket cooling	Provided, Not provided

Fig.10 High-speed test (grease lubrication)



【Test conditions】

Bearing	<b>[ULTAGE] 7020UCDB</b> [Current bearing] 7020CDB [ $\phi$ 100mm × $\phi$ 150mm × 24mm × Two rows ] [ Contact angle 15° ]
Preload after mounting	150 N (Fixed position preloading)
Lubrication method	Air-oil lubrication
Air supply rate	40 NL/min
Oil supply rate	0.03 mL/5 min/shot
Oil type	ISO VG32
Jacket cooling	Provided, Not provided

Fig.11 High-speed test (air-oil lubrication)

## 5. Series

ULTAGE 79U/70U type standard angular contact ball bearings, series configuration is shown in **Table 1**. The bearing models are either 0 series or 9 series, and each series has three different contact angles (15°, 25°, 30°). The bearing sizes (bore diameter) for these series are  $\phi$  10mm ~  $\phi$  130mm (common to all series). In addition to the current steel balls, the materials for rolling elements include ceramic balls to provide ample variation.

**Table 1** 79U/70U Series

Steel ball series	Contact angle 15°	79xxUC/70xxUC
	Contact angle 25°	79xxUAD/70xxUAD
	Contact angle 30°	79xxU/70xxU
Ceramic ball series	Contact angle 15°	5S-79xxUC/5S-70xxUC
	Contact angle 25°	5S-79xxUAD/5S-70xxUAD
	Contact angle 30°	5S-79xxU/5S-70xxU

Available bearing size (shaft diameter):  
 $\phi$  10mm ~  $\phi$  130mm (common to all series)

## 6. Conclusion

ULTAGE 79U/70U type standard angular contact ball bearings, are products suitable for machine tools that are used under more and more severe environments. NTN will continue to improve and develop machine tool bearings under the fundamental philosophy of "people and environment-friendly bearing technology" and "more advanced functionality and ease of use."

## Reference

- 1) Keiichi Ueda, THE TRIBOLOGY No.188 (2003), 19 (in Japanese)

Photos of author



Keiichi UEDA

Industrial Engineering Dept.  
 Industrial Sales headquarters

## HTA U Type ULTAGE Angular Contact Ball Bearings for Axial Loads



Yasuyuki HIROTA\*

A new angular contact ball bearing has been developed for machine tool applications, particularly lathes, that require a high-speed main spindle with high rigidity and load resistance. This paper introduces the HTA U-type angular contact ball bearing for axial loads, which offers high-speed performance while maintaining the rigidity and load resistance of current bearings.

### 1. Introduction

Angular contact ball bearings for axial loads are used for machine tool main spindles, particularly for lathes, that require high rigidity and load resistance. These bearings are primarily used at low and medium rotating speeds. In recent years, however, there has been a growing need for more efficient and precise machining centers and other machine tools. As machining processes are improved to achieve greater efficiency. High-rigidity main spindles for lathes, etc. Will likely be required to operate at higher speeds. To answer the needs for high-speed operation, NTN improved the high-speed performance of the current HTA type angular contact ball bearing for axial loads and developed the HTA U type bearing. This paper describes the features of this product along with the evaluation results.

### 2. Structure of lathe main spindle and bearing

**Fig. 1** shows an example of a lathe main spindle. An angular contact ball bearing for axial loads is used together with a double-row cylindrical roller bearing. The former is to bear axial loads and the latter radial loads. To accomplish this division of load bearing, the bearing OD of the HTA type angular contact ball bearing for axial loads was made smaller than that of the double-row cylindrical roller bearing. This will cause the HTA type angular contact ball bearing for axial loads to receive axial loads only. **Table 1** shows the tolerances for the bearing OD. The HTA type bearings offer two contact angles, 30° and 40°. Bearings of 40° contact angle are typically used when axial rigidity of main spindles is critical. Bearings of 30° contact angle are used when low temperature rise during operation is important.

\*Industrial Engineering Department Industrial Sales Headquarters

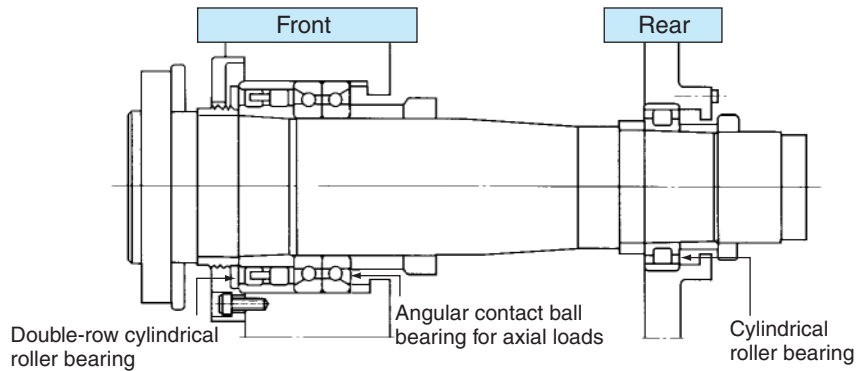


Fig.1 Structure of main spindle for turning machine

Table 1 Outside diameter deviation

Nominal bearing outer diameter mm		Outer diameter tolerances $\mu\text{m}$			
		HTA type P4 L accuracy		Cylindrical roller bearing P4 accuracy	
Over	Incl.	Upper limit	Lower limit	Upper limit	Lower limit
30	50	-25	-36	0	-6
50	80	-30	-43	0	-7
80	120	-36	-51	0	-8
120	150	-43	-61	0	-9
150	180	-43	-61	0	-10
180	250	-50	-70	0	-11
250	315	-56	-79	0	-13
315	400	-62	-87	0	-15
400	500	-68	-95	-	-



Photo 1 HTA U type

### 3. Features

#### 3.1 Allowable rotating speed

The HTA U type (Photo 1) is different from the current bearings in the following areas.

- Internal design (Fig. 2) that limits temperature rise at high-speed range
- Inner/outer ring profiles that improve oil discharge in oil lubrication
- Polyamide resin molded cage with its rolling element contact profile that improves lubrication efficiency in grease and air-oil lubrication

The design specifications described above made the bearing run at high-speed and limit temperature rise, thus reaching the allowable  $d_{mn}$  value shown in Table 2. The operation test results are explained in Section 4.

However, the  $d_{mn}$  value of 1.25 million ( $30^\circ$  contact angle, air-oil lubrication) in the table is of the phenol machined cage specifications. The allowable  $d_{mn}$  value for the HTA U type standard polyamide molded cage specifications is up to 1.05 million.

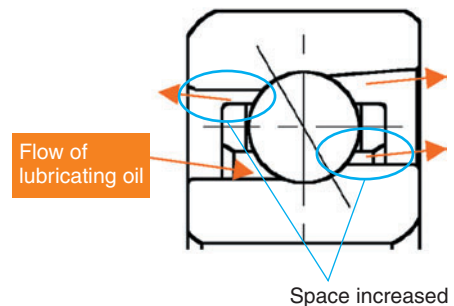


Fig.2 Flow of lubricating oil

Table 2 Allowable  $d_{mn}$  value

	Grease lubrication	Air-oil lubrication
Contact angle $30^\circ$	$100 \times 10^4$ over the current type 60%UP	$125 \times 10^4$ over the current type 25%UP
Contact angle $40^\circ$	$75 \times 10^4$ over the current type 30%UP	$95 \times 10^4$ over the current type 10%UP

### 3.2 Axial rigidity

The internal design of the HTA U type was made to improve high-speed performance at the expense of axial rigidity. However, as shown in Fig. 3, the difference in axial deflection between the HTA U and the current HTA types was 1.5 μm or smaller (at 30° contact angle) when axial load of 5kN was applied, hence the axial rigidity of the HTA U type can be called almost equal to that of the current HTA type.

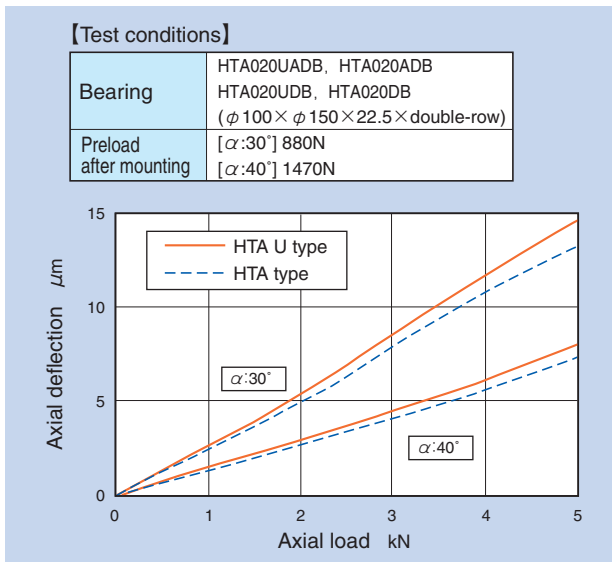


Fig.3 Displacement in axial direction

### 3.3 Load resistance (allowable axial load)

The allowable axial load for bearings is as important a characteristic as axial rigidity. Fig. 4 compares the current HTA type to the HTA U type in axial rigidity. As you can see, by reviewing the internal design, the allowable axial load for the HTA U type was about 1.3 times that of the current HTA type at the contact angle of 30° and about 1.2 times at 40°.

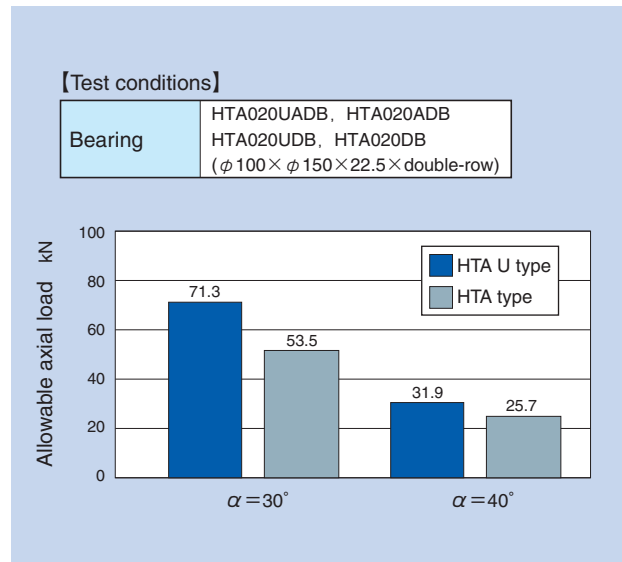


Fig.4 Allowable axial load

## 4. Operation test results

The structure of the test machine used in the operation test and the test results are shown below.

### 4.1 Structure of test machine

Fig. 5 shows the structure of the test machine. To simulate actual service conditions, the test bearing is structured not to receive radial loads.

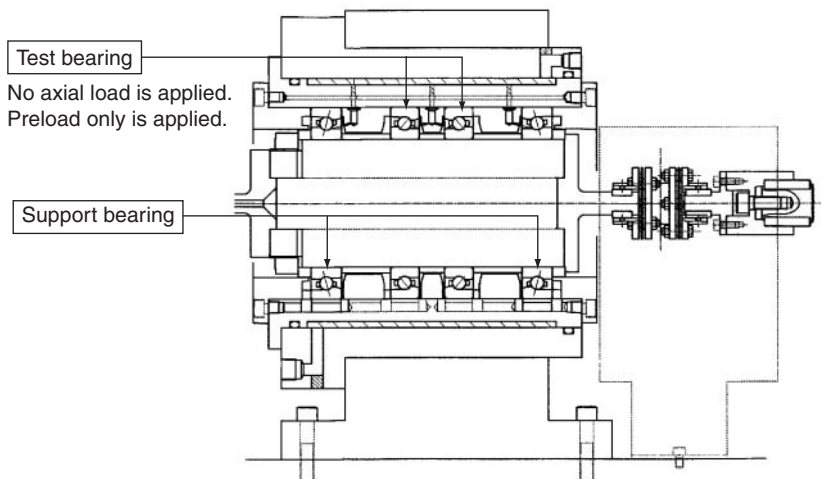


Fig.5 Test rig for measuring temperature rise

### 4.2 Test results

Figs. 6, 7, 8, and 9 show the operation test results of the bearings with grease lubrication and air-oil lubrication.

All the test bearings showed steady temperature rise up to the allowable dmn values as shown in Table 2.

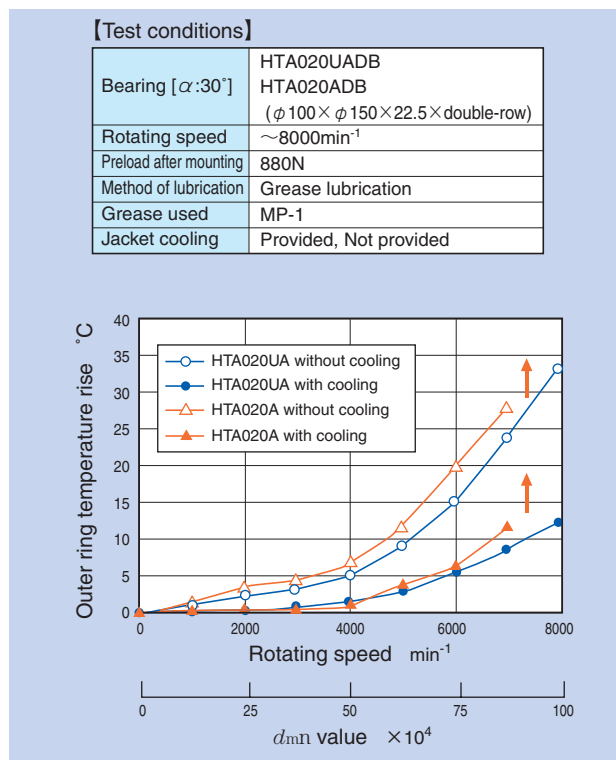


Fig.6 Results of high-speed test (grease lubrication) ( $\alpha:30^\circ$ )

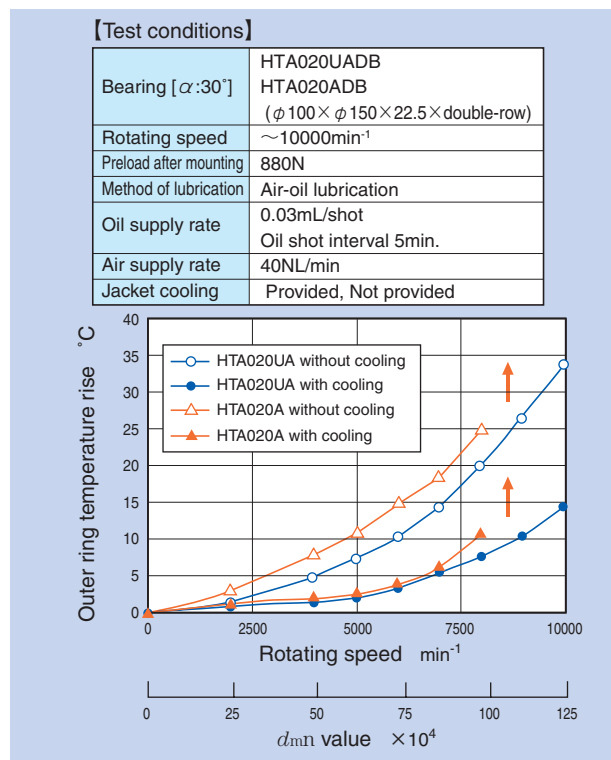


Fig.7 Results of high-speed test (air-oil lubrication) ( $\alpha:30^\circ$ )

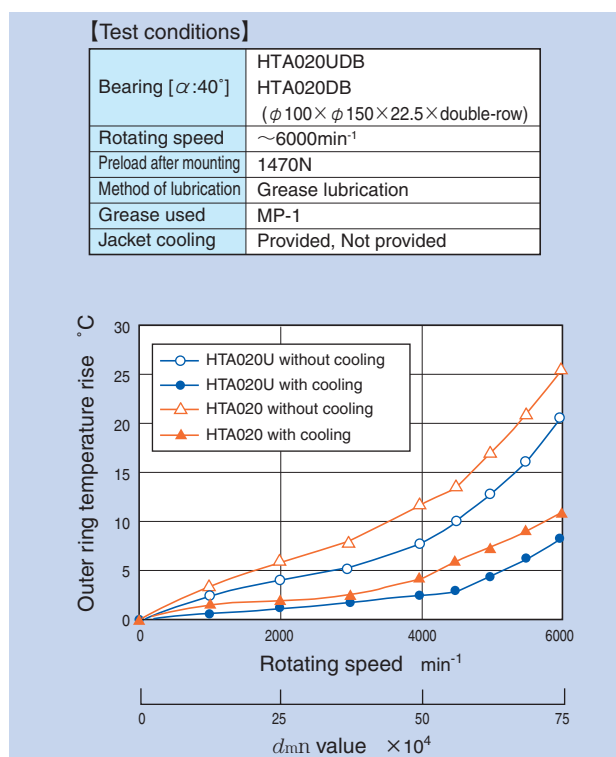


Fig.8 Results of high-speed test (grease lubrication) ( $\alpha:40^\circ$ )

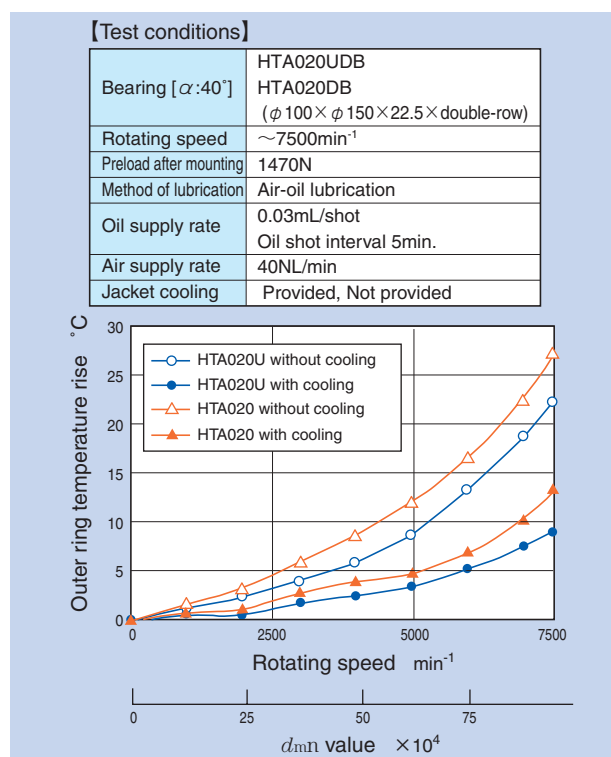


Fig.9 Results of high-speed test (air-oil lubrication) ( $\alpha:40^\circ$ )



## 5. Standard series

The standard specifications of the HTA U type axial load angular contact ball bearing for machine tool main spindles include, like those of the current HTA type, 30° and 40° contact angles and the 0-series and 9-series diameters. The compatible bearing size for the 0-series is  $\phi 50 \sim \phi 320$ , and that for the 9-series is  $\phi 100 \sim \phi 320$ . The rolling elements can be either steel or ceramic balls.

## 6. Conclusion

The HTA U type bearings have achieved high allowable  $d_{min}$  values, 60% over the current type bearings with grease lubrication and 25% over the same with air-oil lubrication, while maintaining rigidity and load resistance equal to those of the current series. This bearing will meet the needs of high-speed and high-rigidity main spindles that are expected to increase in the near future. NTN will continue to develop bearings of longer life and improved handling.

Photos of author

---



Yasuyuki HIROTA

Industrial Engineering Dept.  
Industrial Sales Headquarters

## High Speed and Long Life Double-Row Cylindrical Roller Bearings



Naota YAMAMOTO\*  
Mamoru MIZUTANI\*

NTN has developed a new high-speed and long-life double-row cylindrical roller bearing (NN30xxHSRT6 type) for the **ULTAGE Series** product line. High-speed is accomplished by optimization of the internal design and adoption of a light-weight and high-strength PEEK® resin retainer. Furthermore, the addition of grease reservoirs inside the retainer pockets extends the lubrication life. This paper outlines the development process.

### 1. Introduction

Double-row cylindrical roller bearings are widely used in lathes, machining centers, and other machine tool main spindles that require high rigidity and high accuracy. Nowadays, these machines are increasing their functionality and efficiency. To support the advanced features of modern machinery, the main spindle bearings must run faster and last longer.

Lubrication of the main spindle bearings is primarily air-oil lubrication and grease lubrication. Conventional double-row roller bearings can run up to a  $d_{m11}$  value of 1.2 million under air-oil lubrication and 0.8 million under grease lubrication. Therefore, if higher speed was needed, either angular contact ball bearings or single-row cylindrical roller bearings had to be used.

The ULTAGE Series double-row cylindrical roller bearing offers dramatically faster and longer life performance in both types of lubrication than conventional bearings.

### 2. Features

The development model focused on optimization of the internal design. The retainer especially, went through a comprehensive review. **Fig. 1** shows the configuration of the development model and the conventional model.

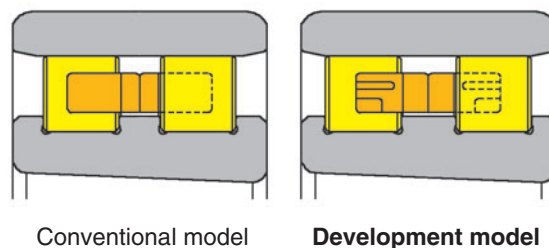


**Fig.1** Conventional design and new design (HSRT6 Type)

\*Industrial Engineering Department Industrial Sales Headquarters

**1) Light weight**

The retainer material was changed from the conventional high-strength cast brass to PEEK resin (polyether ether ketone). This material change reduced the retainer weight to below 1/4 the conventional retainer weight and also successfully limited heat generation and wear that results from contact between the retainer and the rolling elements during high-speed operation. PEEK is a highly rigid resin and is excellent in heat, wear, and hydrolysis resistance.

**2) Super high-speed design for air-oil lubrication**

To optimize the retainer profile, a FEM analysis was conducted to determine retainer deformation by centrifugal force in super high-speed operation. (Fig. 2 shows the analysis example.)

Fig. 3 is the analysis result of the ring thickness. This dimension particularly affects deformation. In the area where the ratio of the ring thickness to the length of the rolling element was below 30%, significant

deformation was noticed. To accommodate super high-speed operation, this ratio should be 30% or greater. Furthermore, off-sets were installed at the column ends that could make abnormal contact with the rolling elements, especially during deformation. These off-sets also serve as grease pockets.

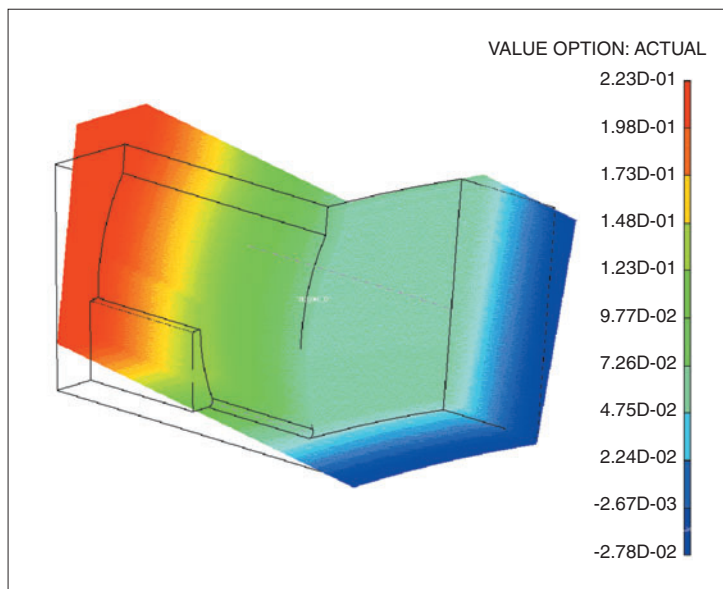


Fig.2 FEM analysis of deformation

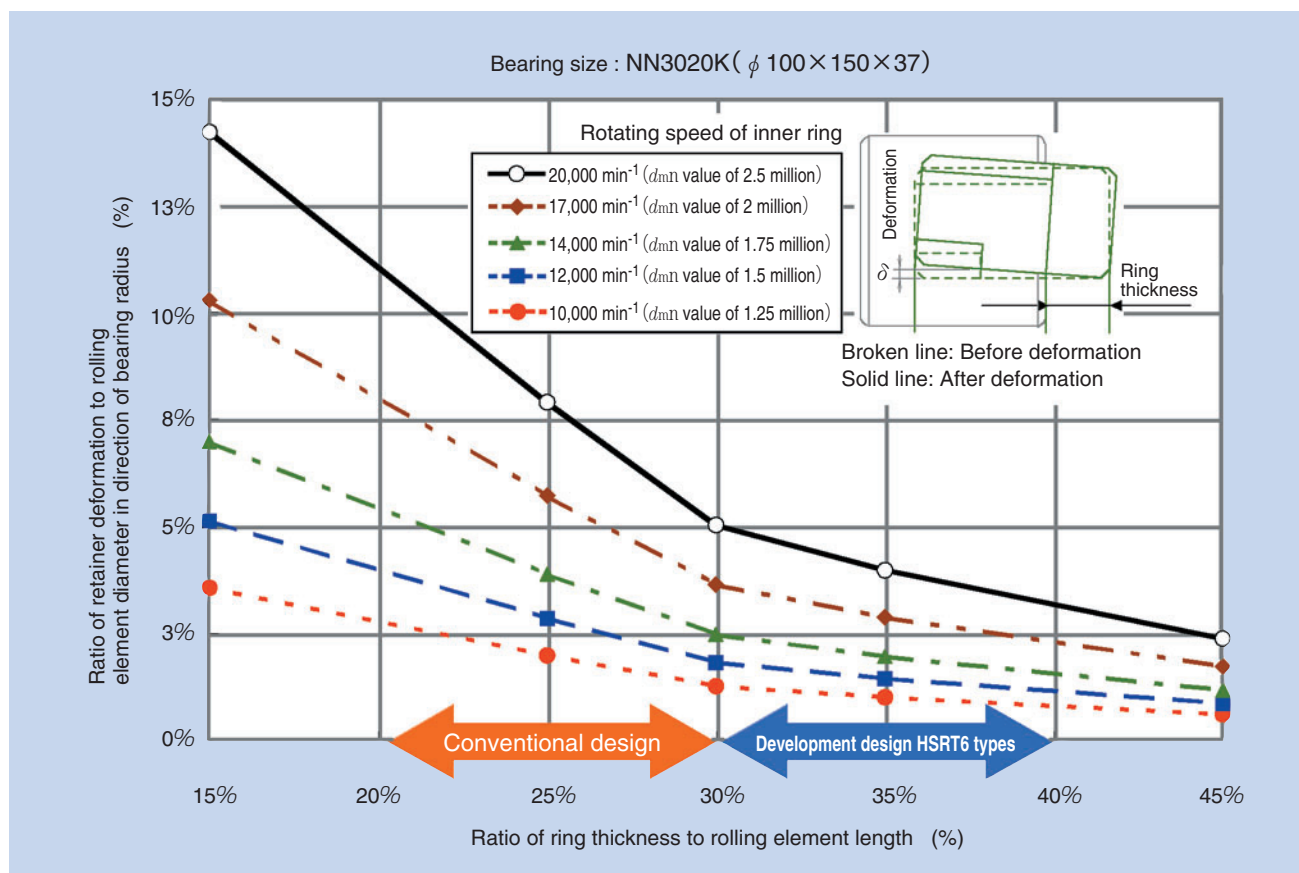


Fig.3 Relation between ring thickness and deformation at super high-speed (FEM analysis of deformation)

### 3) Long-life design for grease lubrication

Fig. 4 shows the outline of the new retainer structure. As shown, grease pockets are created on the retainer columns to improve grease retention for longer grease life.

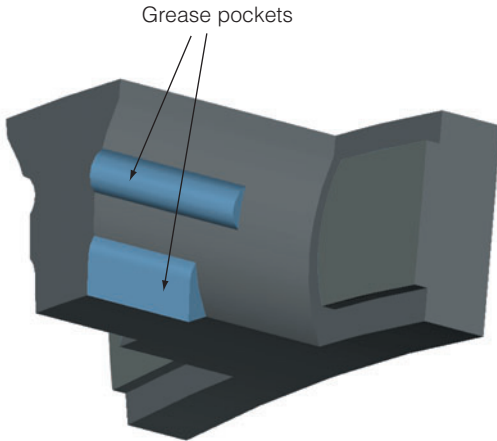


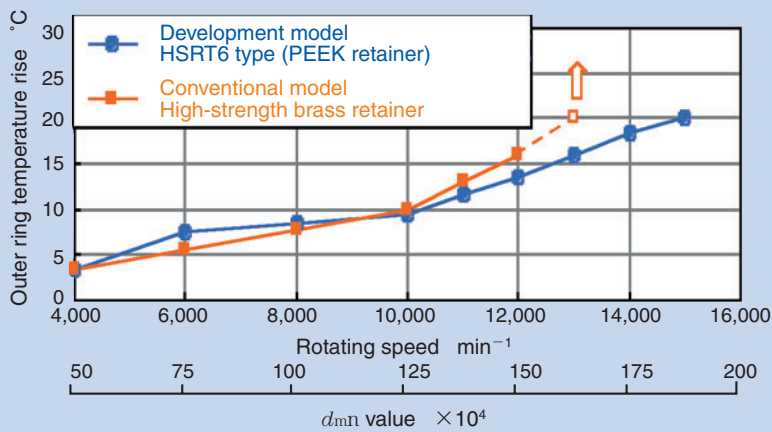
Fig.4 Drawing of the retainer

### 3. Test results in air-oil lubrication

Fig. 5 shows the test results of this retainer in air-oil lubrication. The conventional retainer (high-strength cast brass retainer) showed a sudden temperature rise at 13000min<sup>-1</sup>, but the development model (PEEK retainer) was able to withstand high-speed operation up to 15000min<sup>-1</sup> ( $d_{mN}$  value of 1.9 million).

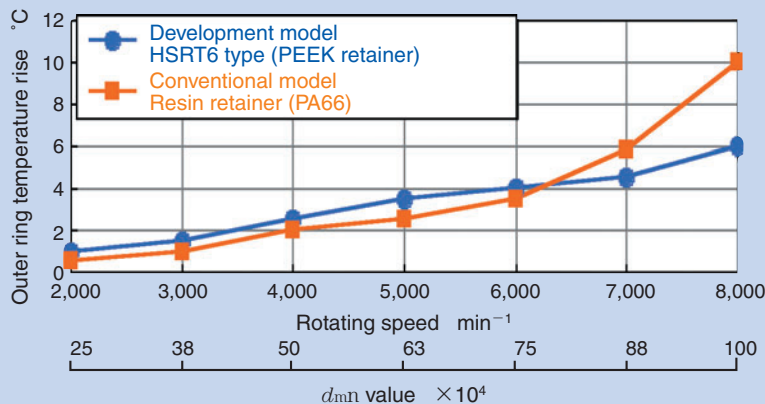
### 4. Test results in grease lubrication

Fig. 6 shows the test results of this retainer in grease lubrication. A comparison of the conventional retainer (PA66 retainer) to the development model (PEEK retainer) showed temperature rise of the outer ring at 7000min<sup>-1</sup> and a distinctive difference between the two was observed at 8000min<sup>-1</sup> ( $d_{mN}$  value of 1 million). In the endurance test, the conventional retainer developed high vibration after 1500 hours and the test had to be terminated. Though the bearing didn't sustain any major damage, the rolling elements and the retainer columns had little lubrication.



- <Test conditions>  
**[Development model HSRT6 type (PEEK retainer)]**  
 [Conventional model High-strength brass retainer]
- Bearing size : NN3020K  
( $\phi 100 \times \phi 150 \times 37$ )
  - Rotating speed :  $\sim 15,000 \text{ min}^{-1}$   
( $d_{mN} = 1.9 \text{ million}$ )
  - Clearance after mounting :  $0 \mu\text{m}$
  - Oil supply rate :  $0.02 \text{ mL}/20 \text{ min}$  (VG32)
  - Air supply rate :  $30 \text{ NL}/\text{min}$
  - Jacket cooling : Provided

Fig.5 Temperature rise test results (air-oil lubrication)



- <Test conditions>  
**[Development model HSRT6 type (PEEK retainer)]**  
 [Conventional model Resin retainer (PA66)]
- Bearing size : NN3020K  
( $\phi 100 \times \phi 150 \times 37$ )
  - Rotating speed :  $\sim 8,000 \text{ min}^{-1}$   
( $d_{mN} = 1 \text{ million}$ )
  - Clearance after mounting :  $-5 \mu\text{m}$
  - Grease : MP-1
  - Jacket cooling : Provided

Fig.6 Temperature rise test results (grease lubrication)

Consequently, it was determined that the bearing had reached its limit of operation.

On the other hand, the development model retained grease in the retainer's grease pockets after 2000 hours of operation, and was able to continue operation (Photo 1).

To confirm the endurance performance of the development bearing, an endurance test is currently on-going at  $8000\text{min}^{-1}$  ( $d_{m\text{N}}$  value of 1 million) (Fig. 7).

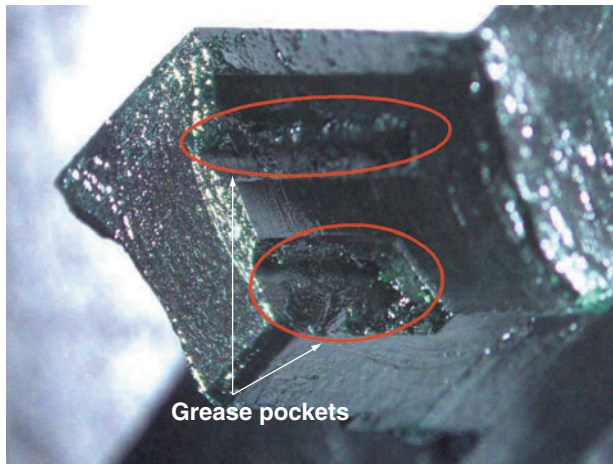


Photo 1 Grease remaining in the reservoirs after 2000(h) running test

### 5. Bearing composition

The bearing specifications developed in this project should apply to NN3013 ~ NN3026 (Inner Diameter  $\phi$  65 ~  $\phi$  130).

### 6. Conclusion

The ULTAGE series double-row cylindrical roller bearing, bearing type NN30xx HSRT6, runs at high speeds and lasts longer under air-oil and grease lubrication than conventional double-row cylindrical bearings. This bearing should contribute to increasing functionality and efficiency needs of the lathe main spindles. It will support the development of high-speed and high-rigidity main spindles that will see a growing need in today's market.

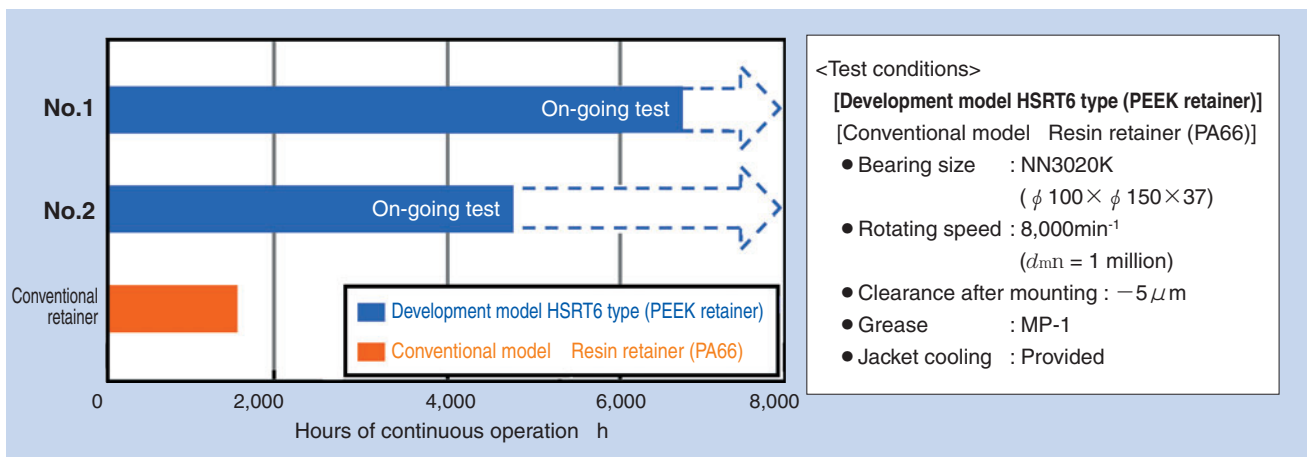


Fig.7 Endurance test results

#### Photos of authors



Naota YAMAMOTO

Industrial Engineering Dept.  
Industrial Sales Headquarters



Mamoru MIZUTANI

Industrial Engineering Dept.  
Industrial Sales Headquarters

## Next Generation Deep Groove Ball Bearing for High-Speed Servomotor



Chikara KATAGIRI\*  
Kenichiro NAITO\*

In the past, servomotors have been developed by focusing mainly on machine tool and robot use. Recently, servomotors are being more widely used in general industrial apparatus and in manufacturing equipment for products such as semiconductors or electronic parts.

Due to the growth of these applications in recent years, demand has increased for high-speed servomotors with high accuracy. High-speed angular contact ball bearings are typically used in these servomotors. Since they are easier to handle than angular contact ball bearings, the demand for deep groove ball bearings has also increased for high-speed applications.

Because of this increased demand, NTN has developed the "Next Generation Deep Groove Ball Bearing for High-speed Servomotor" that can be used in applications with  $d_{m1}n \leq 950,000$  ( $d_m$  = ball pitch circle diameter,  $n$  = speed). In the past, only angular contact ball bearings could be used at this high  $d_{m1}n$  value. This new bearing also has a longer life than the previous deep groove ball bearing used in a servomotor application.

This report introduces the characteristics, including several test results, of NTN's new design named the "Next Generation Deep Groove Ball Bearing for High-speed Servomotor."

### 1. Introduction

In recent years, machine tools are becoming faster, more efficient, more accurate, and more compact. Accordingly, there is a great demand for faster, more rigid, longer-lasting, higher output, and smaller main-spindle servomotors. To meet the engineering needs of such servomotors, bearings must run faster or achieve high  $d_{m1}n$  values. Today, a low-cost and easy-handling deep groove ball bearing is desired to satisfy those needs in the operation range traditionally and primarily served by angular contact ball bearings.

Having realized the situations, NTN developed a "next generation deep groove ball bearing for high-speed servomotors" that provides "high-speed" and "long life."

This paper outlines this new bearing.

### 2. Bearing structure

Sealed and greased deep groove ball bearings are typically used for motors. Among those bearings, some are used for high-speed motors. Because the cage of such a bearing is subject to large centrifugal force, the bearings for high-speed motors typically use pressed steel cage that is made of highly rigid metallic sheet.

The pressed steel cage can produce relatively large collision noise (cage noise) upon impact with the balls.

For this reason, more synthetic-resin cages are used now. They are easy to manufacture, light-weight, and self-lubricating. The synthetic-resin crown-type cage, however, is subject to deformation due to centrifugal force at high-speed ranges. The deformation causes interference between the cage

\*Industrial Engineering Department Industrial Sales Headquarters

and other parts, resulting in temperature rise of the bearing and increase in the rotational torque.

The deep groove ball bearing developed this time has resolved the above problems with the synthetic-resin crown-type cages and improved its "high-speed" performance. This new bearing also improved endurance of the grease, thereby "extending bearing life."

**(1) New cage**

**[Features of new cage]**

- ① High-speed
- ② Improved lubrication
- ③ Improved productivity designing

**① High-speed**

The traditional synthetic-resin crown-type cage (see **Photo 1**) is open to one side. This profile causes the prongs on the open side to widen due to centrifugal force in high-speed operation (see **Fig. 1**). This deformation leads to interference with the balls and other components, which in turn contributes to the rise in the bearing temperatures and the rotational torque.



**Photo.1** Synthetic-resin crown-type cage

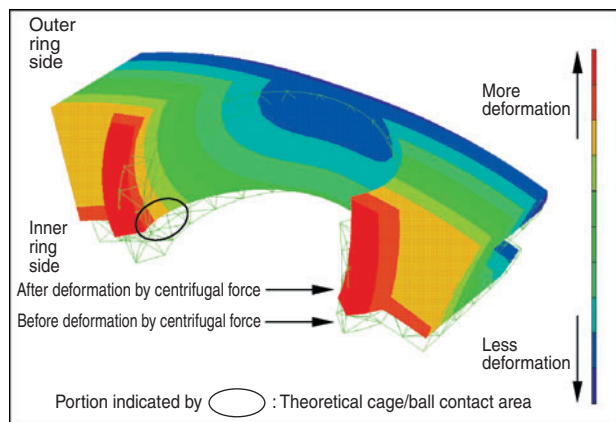


**Fig.1** Example of FEM analysis of synthetic-resin crown-type cage under centrifugal force

The configuration of the new cage assumed the structure of a traditional pressed steel cage and combined two resin-molded wave-type rings of identical shapes (see **Photo 2**).

Compared to the traditional crown-type cage, the new cage does not have openings, which improves rigidity of the pockets and dramatically reduces deformation by centrifugal force in high-speed operation.



**Photo.2** New synthetic-resin cage design

**[FEM analysis of new cage deformation by centrifugal force]**

**Table 1** shows the analysis conditions.

**Table 1** Condition of FEM analysis

Bearing	6308
Inner ring rotating speed, min <sup>-1</sup>	15,000 ( <i>d<sub>n</sub></i> value=0.6 million, <i>d<sub>m</sub></i> value=0.95 million)
Ambient temperature, °C	60
Material	PA66+GF25%
Density	1.32
Modulus of vertical elasticity of material, MPa	2200
Modulus of linear expansion of material, /k	7×10 <sup>-5</sup>

\**d*: Bearing ID mm, *d<sub>m</sub>*: Rolling element pitch circle diameter mm, *n*: Rotating speed min<sup>-1</sup>

**[FEM analysis results]**

The analysis was made to the pocket and a single joint. The calculations assumed that the cage was subject to centrifugal force only in high-speed operations.

**Fig. 2** shows the analysis results of the cage deformation. Expansion was observed generally in the radial direction. The largest deformation was found at the joints due to the joint clearance (set in the radial direction for easy assembly). Nevertheless, deformation of the pockets is restricted and the calculations confirmed that there would be no interference between the cage and other components.

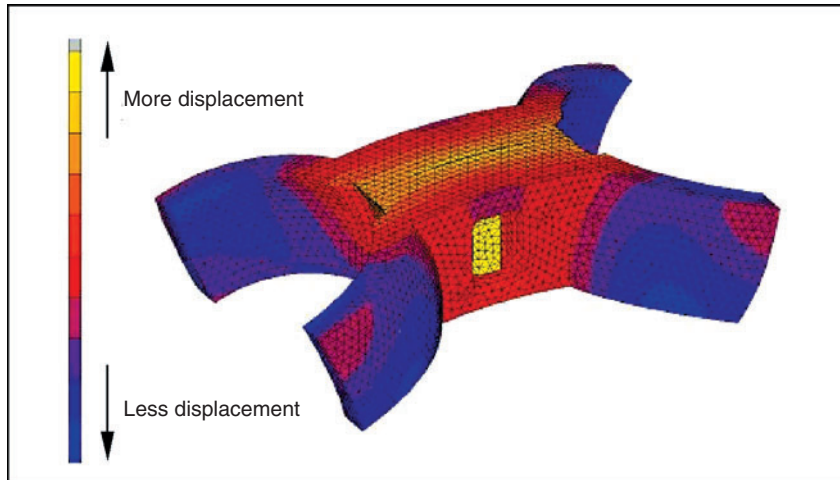


**Fig.2** Example of FEM analysis of new synthetic-resin cage design under centrifugal force (displacement in radial direction)

**② Improved lubrication**

The new cage has grease grooves inside the pockets (see **Photo 3**), thus improving lubrication inside the pockets. They also improve the bearing life and reduce the bearing noise.

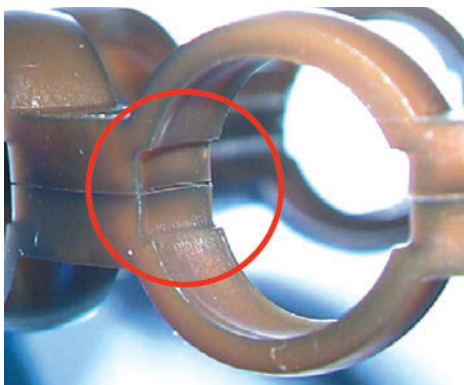


**Photo.3** Grease groove

**③ Improved productivity designing**

With the metallic-sheet wave-type cages, coupling is typically accomplished by crimping the rivets (see **Fig. 3**). However, the new synthetic-resin cage simply requires pressing together the coupling prongs of the two wave-type rings, reducing the assembly time.

The coupling portions are designed such that the two wave-type rings are of an identical profile, which requires only one mold for manufacturing (see **Fig. 4**).

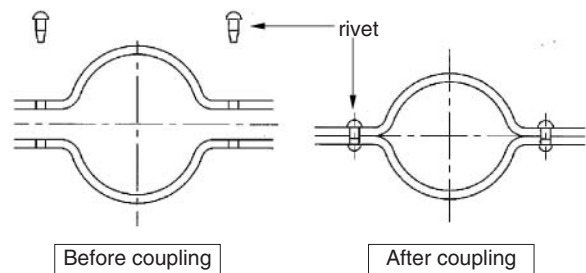


**Fig.3** Cross section of pressed-steel cage

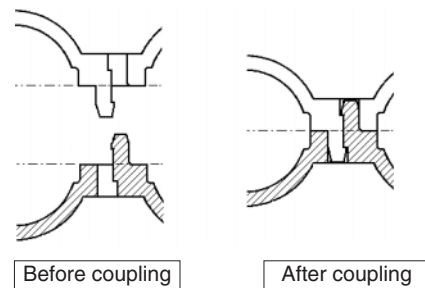


**Fig.4** Cross section of new synthetic-resin cage design



**(2) Long-life grease "ME-1"**

(For details, see Page 20, "Development of high-speed, long-life grease.")

The new long life grease "ME-1" was developed with attention paid to oxidation stability of the base oil and selection of the most effective oxidation inhibitor. This grease almost doubled the life of NTN's standard motor grease (MP-1). This grease is now adopted as standard for the "next generation deep groove ball bearing for high-speed servomotors."

**① Composition and properties of ME-1 grease**

ME-1 grease uses urea compound as thickener and, for the base oil, it uses a mixture of special ester oil and PAO. To prevent oxidation of the base oil, an appropriate anti-oxidant is added, increasing the grease life.

Table 2 shows the composition and properties of ME-1 grease.

**Table 2** Typical properties of ME-1 grease

	ME-1	Test method
Thickener	Urea	—
Base oil	Ester/PAO	—
Viscosity of base oil, mm <sup>2</sup> /s	60	JIS K2220.23
Mixture thickness, 60W 25°C	250	JIS K2220.7
Dropping point, °C	250 or higher	JIS K2220.8

**② High temperature endurance**

A high-temperature endurance test (ASTM D3336) was carried out on the new grease (ME-1). Fig. 5 shows the test results of a commercially available grease and ME-1 grease.

As compared to commercially available grease A, endurance of ME-1 grease is more than five times, and to commercially available urea grease B and MP-1 it is 1.5 to 2 times.

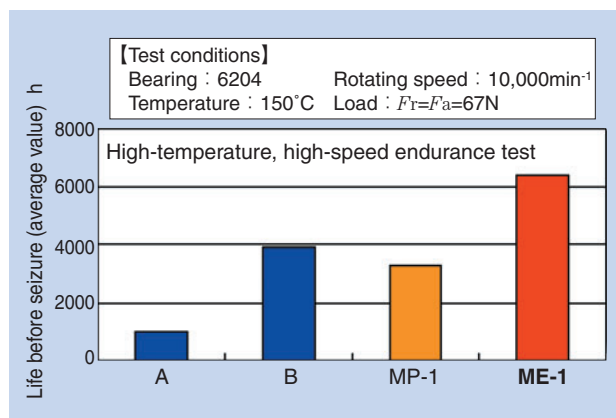


**Fig.5** Endurance test result

**3. Results of functionality confirmation test**

**(1) High-speed operation**

To evaluate the high-speed performance, a temperature rise test was conducted.

**① Bearing specifications: See Table 3.**

**Table 3** Test bearing

Bearing	Cage	Grease	Amount of grease sealed	Seal
6308	Synthetic resin crown type cage	New grease (ME-1)	80% of static space	Non-contact type rubber seal
Same as above	New synthetic resin cage	Same as above	Same as above	Same as above

※ Synthetic resin: PA66 + GF25%

**② Test conditions**

**[Maximum rotating speed]**

n=15,000min<sup>-1</sup>

(d<sub>n</sub> value=0.6 million, d<sub>m</sub>n value=0.95 million)

**[Temperature]**

Room temperature

**[Test machine]**

Rapid acceleration/deceleration test machine (see Fig. 6)

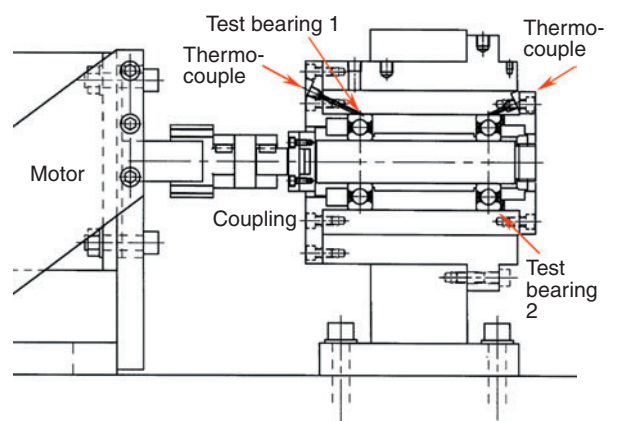


**Fig.6** Rapid acceleration/deceleration test machine

③ Test results

Fig. 7 shows the relationship between the rotating speed and the outer-ring temperature rise.

Temperatures were read when it stabilized. The test was terminated as soon as the temperature exceeded 100°C.

No significant difference was observed between the synthetic-resin crown-type cage and the new synthetic-resin cage up to  $n=12,000\text{min}^{-1}$  ( $d_n$  value=0.45 million,  $d_{m\Omega}$  value=0.75 million). At  $n=15,000\text{min}^{-1}$  ( $d_n$  value=0.6million,  $d_{m\Omega}$  value=0.95 million), the crown-type cage showed abnormal temperature rise and the test was interrupted. No abnormal temperature rise was noticed with the new cage except for that possibly caused by grease resistance.

The bearing inspection after the test and the FEM analysis results confirmed that the abnormal temperature rise found with the crown-type cage was caused by its contact with the other bearing components due to cage deformation by centrifugal force.

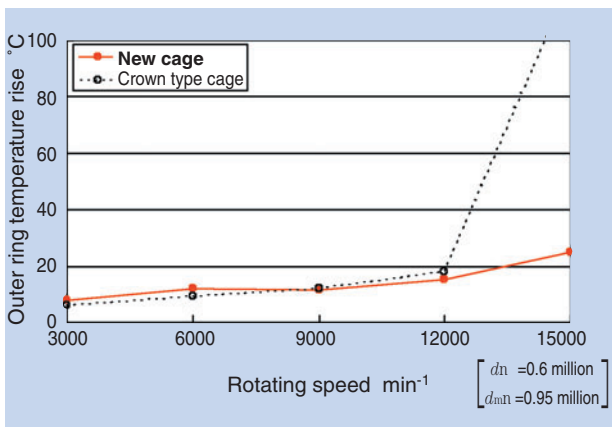


Fig.7 Temperature rise test result

(2) Endurance

To evaluate high-temperature endurance of the cages, a high-temperature, high-speed endurance test was conducted.

① Bearing specifications: See Table 4.

Table 4 Test bearing

	Bearing	Cage	Grease	Amount of grease sealed	Seal
A	6209	Pressed steel cage	Traditional grease (MP-1)	90% of static space	Non-contact type rubber seal
B	Same as above	New synthetic resin cage	New grease (ME-1)	Same as above	Same as above

※ Synthetic resin: PA46 + GF25%

② Test conditions

[Rotating speed]

A:  $n=11,111\text{min}^{-1}$

( $d_n$  value=0.5 million,  $d_{m\Omega}$  value=0.7 million)

B:  $n=13,333\text{min}^{-1}$

( $d_n$  value=0.6 million,  $d_{m\Omega}$  value=0.85 million)

[Bearing temperatures]

130°C (at bearing's outer diameter)

[Test machine]

High-temperature, high-speed endurance test machine (see Fig. 8)

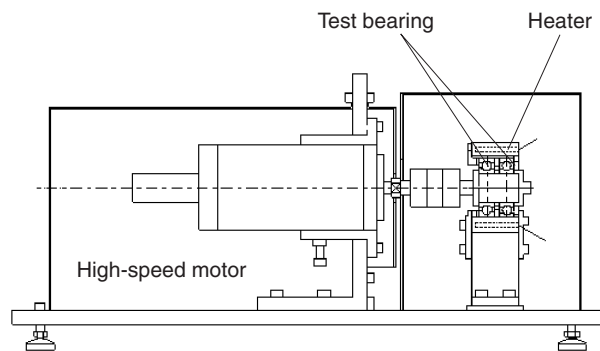


Fig.8 High temperature and high speed endurance test machine

### ③ Test results

**Fig. 9** shows the relationship between the cage type and the test duration.

The new synthetic resin cage + new grease (ME-1) demonstrated three time and greater endurance than the pressed steel cage + traditional grease (MP-1), despite the fact that it was run at even higher rotating speeds.

This superb endurance is attributable to excellent high-temperature endurance of the new grease (ME-1) and to improved lubrication characteristics of the new cage.

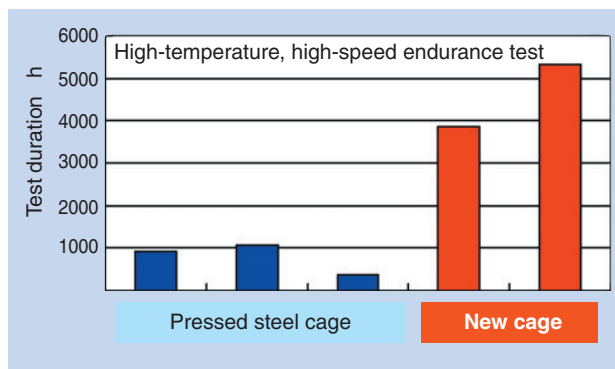


**Fig.9** High-temperature and high-speed endurance test result

## 4. Conclusion

By adopting the new synthetic-resin cage, the "Next generation deep groove ball bearing for high-speed servomotor" can successfully prevent abnormal temperature rise at the  $d_{11}$  value of 0.6 million (the  $d_{m11}$  value of 0.85~0.95 million) which the traditional design was unable to resolve. Additionally, adoption of the new grease "ME-1" realized a longer life of this bearing. Furthermore, the unique cage profile has reduced the assembly time and minimized the cost-increase associated with the traditional types (pressed steel cage, synthetic-resin crown-type cages) by controlling the mold costs.

We believe that this bearing can contribute to the development of the servomotors for machine-tool main spindles in the areas of high-speed operation and longer service life. We will continue to develop new products that support advancing performance of the latest machine-tool motors.

### Photos of authors



Chikara KATAGIRI

Industrial Engineering Dept.  
Industrial Sales Headquarters



Kenichiro NAITO

Industrial Engineering Dept.  
Industrial Sales Headquarters

# Multi-Repair System for Color Filters



Masahiro SARUTA\*

NTN has developed a color filter repair system (product name: Multi-Repair System) that is capable of repairing all of the various production defects in liquid crystal color filters. This system was developed jointly with Takano Co., Ltd. and offers new functions such as review and tape grinding in addition to traditional laser cut and ink pasting functions.

Integrating all of these functions into a single unit provides a great benefit in terms of improved repair quality, reduced repair time and equipment cost, and smaller machine footprint. It has already received acceptance by many users. This paper outlines the system and explains the available functions.

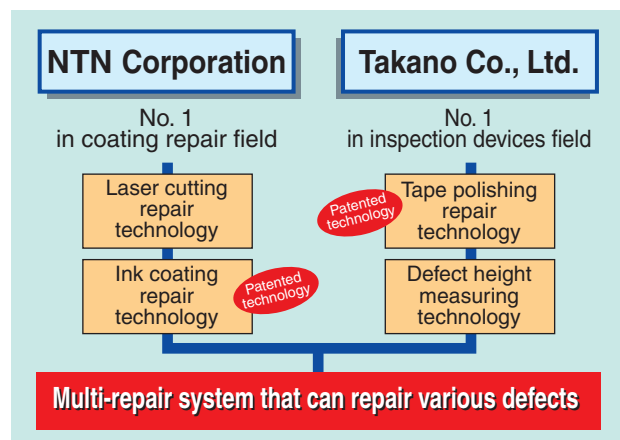
## 1. Introduction

NTN has developed equipment that pastes color ink on defective portions of LCD color filters (see "Repair system for the 6th and 7th generation LCD color filters") and has delivered it to many customers. NTN recently conducted a joint development with Takano Co., Ltd. and added a polish repair function to this equipment. The resulting product is a multi-repair system. NTN has begun sales of this product.

The defects in the LCD color filter manufacturing processes are largely divided into foreign particles, black defects, and white defects. Until today, separate repair machines were used to repair each type of defect. For the first time in the industry, this multi-repair system has consolidated all these repair functions into a single piece of equipment. This system will improve the productivity and quality of production of ever-larger LCD color filters and will free up floor space.

The design concept of this system as well as its field-proven performance was recognized in the 2004 Flat Panel Display Fair, and it won the ADY2004 (Advanced Display of the Year) Grand Prix award in the inspection device division.

Various functionalities of the system and the benefit of function consolidation are discussed below.



\*Precision Equipment Division Product Engineering Department

## 2. Outline of multi-repair system

**Photo 1** is the appearance of the system. The system can handle large glass color filter substrates up to the seventh generation (1870×2200mm) display panels and have the following repair functions.

- (1) Review function to assess defects
- (2) Tape polishing function to repair foreign particle defects
- (3) Laser cutting function to repair black defects and foreign matters
- (4) Ink pasting function to repair white defects and to fill laser cut portions



**Photo 1** Multi-repair system for color filters

The defect repairing process is as follows. First, defect data is sent from a server or an inspection device to the host computer of the multi-repair system. The defect data contains the types and the locations of the defects, which will be the basis for the subsequent repair works. The system automatically recognizes the alignment mark on the substrate, calculates its inclination on the XY plane, converts the above defect location into coordinates, and then displays it accurately on the monitor screen. At this point, the operator manually determines the method and the range of repair. This system is also characterized by abundance of software that will allow users to deal with various situations.

### (1) Review function

The defect data received by the host computer is displayed on the monitor. Operators can select any of these defects, and the computer will automatically display the selected defects on the monitor for review.

In the review process, users may engage themselves primarily in observing or measuring the profiles of the defects.

To make defect observation easy, the system

employs a large glass surface plate at the glass substrate chucking surface. It allows both backlight and incident lighting. In an observation using the backlight lighting, the machined surface of the glass surface plate may cause uneven light intensity, which can create dead angles. To avoid such dead angles, the system has a function to offset the substrates to display the whole images without such dead angles.

For profile measurement, the system utilizes contact type height sensors to measure projection heights. There are other functions in this system that allow dimensional measurement of the defects and many other inspection functions.

### (2) Tape polishing function

**Photo 2** shows the appearance of the tape polishing unit.

The polishing unit consists of a polishing head, tape drive mechanism, two height sensors, etc. and performs polishing of foreign particles by moving the tapes with appropriate grain size.

The pressure on the polishing head can be set at any pressure, which allows the system to run at the most suitable conditions for different materials. The polishing head is also equipped with displacement sensors that detect height. Consequently, the amount of material removal can be controlled not only by time but also by height.

One of the two height sensors can scan the contact point, and by selecting two nearby points of a projection defect, the system can measure the height of the defect.

The other height sensor is combined with the above-mentioned height sensor in determining the inclination of the glass substrate. With these measurements as basis, the system applies numerical control of the height of the polishing head located in between the two height sensors, thus performing highly accurate repair works.

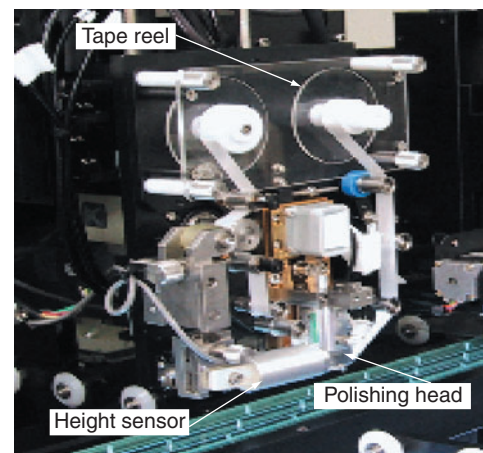


**Photo 2** Tape grinding unit

**(3) Laser cutting function**

The YAG (Yttrium Aluminum Garnet) laser with an EOQ (Electro Optic Q) switch is the most common laser used in the LCD color filter repair. The basic frequency is the second high-order harmonic at 532nm, but a laser of even higher-order harmonic may be installed if necessary.

The laser optical unit shown in Fig. 1 is an image-formation optical unit that focuses the slit profile of cutting on the color filter, and consists of a slit mechanism which determines cutting profiles, a power control mechanism to adjust laser output, and a revolver mechanism which selects an appropriate objective lens.

Since the pixel of a color filter may not always be rectangle in shape and some pixels may be deformed or all may be angled, the  $\theta$  slit mechanism which rotates the whole slit mechanism is often installed.

Selection of the slit profile, angle, laser power, and the objective lens can be done on the GUI (Graphical User Interface) screen or on the control panel.

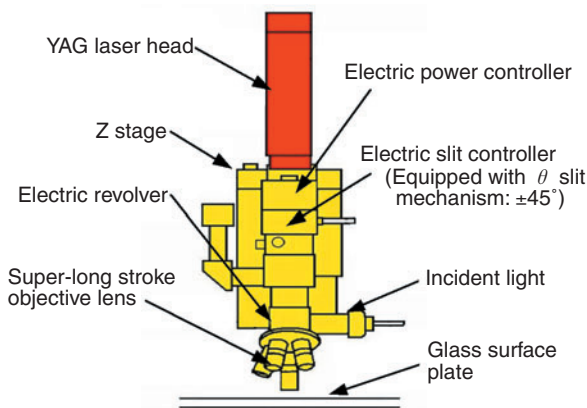


**Fig.1** Optical unit with YAG laser

**(4) Ink coating function**

Another feature of this system is the ink coating mechanism using a coating needle. The methods of ink coating include coating needle method, dispenser method, injection method, etc. The reason why this system has adopted the coating needle method is because it offers coating at fine diameters, the paste does not clog, and because it accommodates various types of paste used by customers.

Fig. 2 shows the structure of the coating needle method. The coating needle is mounted on the

positioning actuator via the slide. The coating needle picks up the paste in the ink container located on the index disc and transfers it to a defective portion on the substrate by touching it. The needle tip diameter can be selected at will depending on the pattern width of the defect, but the needle tip diameter of  $\phi 30 \sim \phi 70\text{mm}$  is typically used. If the defect portion is long, a continuous pattern should be used by repeating coating of a pitch smaller than the coating diameter.

For repairing color filters, up to four different resists (ink) may be used. In preparation for needs of washing the needle tips along with the paste change, the system is equipped with mechanisms that agitate detergent, wash the needles, and air purge them after washing.

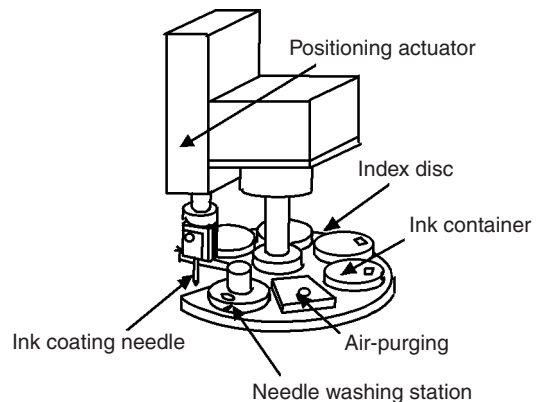


**Fig.2** Pasting needle unit

Photo 3 shows an example repair operation where a foreign matter on the color filter was removed by laser cutting followed by color coating using the ink coating mechanism.

In this example, the defect is small and resides in the R (red) region only. Therefore, it needed laser cutting and coating repair of one color only. However, as the area of a defect becomes larger, repair would require multiple processes including tape polishing, coating of RGB colors, etc.

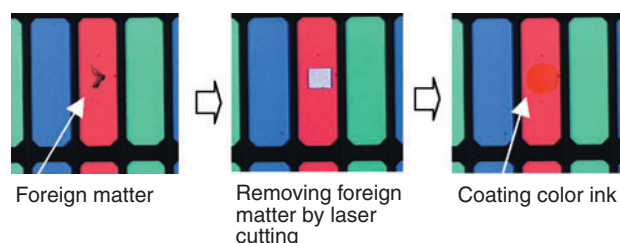


**Photo.3** Example of defect repair process

## 2. Advantages of consolidating multiple functions into single equipment

Needless to say one of the advantages of consolidating the three processes, polishing, laser cutting, and ink coating, is to be able to repair all defects with one machine. Another big advantage is improvement in the quality of repair. If, for example, multiple exposures to laser are a concern of damaging the substrate, you can first apply tape polishing and then cut out the defective portion with a low power laser. The subsequent coloring process should achieve good chromaticity because the laser has left little irradiation damage.

Reduction in the repair time is another big benefit. If multiple devices are used to repair defects, they incur transfer time between the devices, time to align the glass substrates within the devices, and time to position in each device. Time is saved, resulting in significant repair time reduction. Other advantages include reduction in the total equipment costs through sharing the glass surface plate and other components or saving in the required floor space.

## 3. Conclusion

Demands for LCD's for large-size TV's are growing rapidly and so are the demands for high-quality repair equipment for various defects of color filters. NTN's new multi-repair system should satisfy those demands.

This paper describes this system with a focus on the mechanical aspects. However, the system is loaded with CIM (Computer Integrated Manufacturing), GUI (Graphic User Interface), and other software that makes this system qualify as in-line equipment. There has been an increase in the in-line use of this system. We believe that the market will be demanding even larger systems, reduction in repair time, reduction in labor, and more efficient repair performance. We are committed to improve this system so that it can offer greater productivity to our customers.

### Reference

- 1) SARUTA, Semiconductor FPD World 2004. 7
- 2) SATOU, Semiconductor FPD World 2004. 5

Photos of author

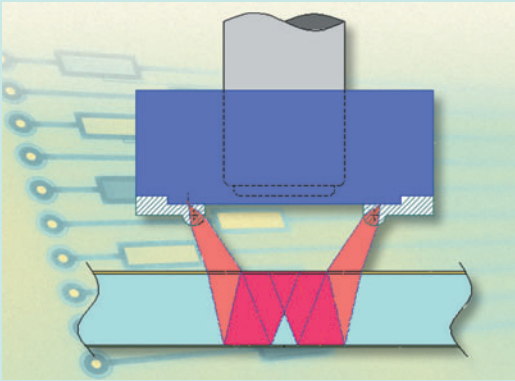
---



Masahiro SARUTA

Precision Equipment Division  
Product Engineering Dept.

## Repair System for Sixth and Seventh Generation LCD Color Filters



**Akihiro YAMANAKA\***  
**Akira MATSUSHIMA\***

NTN's color filter repair system fixes defects in color filters, which are the primary components of liquid crystal displays. The most important feature of this system is its ability to apply ink to a white spot, commonly referred to as a "white defect" on the color filter. The repair process of the liquid crystal color filter involves a backlight observation mechanism that verifies the conditions before and after the repair. LCD screens have gotten larger in recent years and, consequently, the size of the glass used for production is also increasing. Naturally, the repair system for these new screens must also be larger. The growth in screen size could pose a problem for traditional backlight observation mechanisms in the near future. This paper details a reflective-type backlight mechanism that NTN recently developed for large-size substrates (Sixth and Seventh generation).

### 1. Introduction

In the past, televisions have primarily used CRT's (Cathode Ray Tubes) for their display screens. CRT's are now being replaced by LCD's (Liquid Crystal Displays) and PDP's (Plasma Display Panels), also known as Flat Panel Displays or FPD's. By 2006, domestic sales of FPD's are expected to exceed that of the CRT's.

NTN has had a pattern repair system on the market for well over 10 years. It repairs color filter defects that occur during FPD production. Recently, as the market has trended towards larger and higher resolution FPD's, the repair process has been widely recognized as an integral part of production. For this reason, NTN's LCD color filter repair system has been installed in many production facilities.

The size of mother glass substrates used in the production of FPD's is rapidly becoming larger. For example, the Sixth generation has a size of 1500×1850mm and the Seventh generation measures 1850×2200mm. Consequently, the size of the pattern repair systems has increased dramatically.

This paper details NTN's newly developed backlight mechanism that is compatible for large-size substrates.

\*Precision Equipment Division Product Engineering Department



## 2. Backlight mechanism for LCD CF repair system

As shown in **Fig. 1**, an LCD panel is made up of TFT and CF substrates bonded together with spacer balls and filled with liquid crystal and a backlight at the bottom of this structure. A CF glass substrate has red (R), green (G), and blue (B) pixels arranged in a matrix format (see **Fig. 2**).

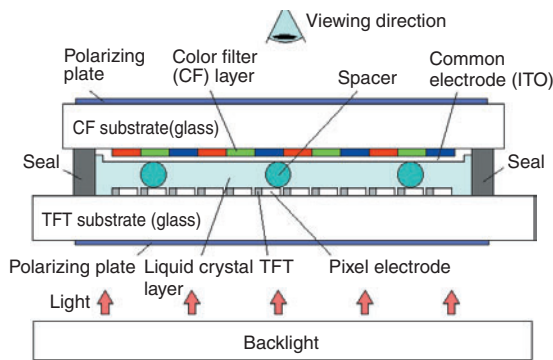


**Fig.1** LCD structure

A CF substrate adds color information to light and is turned "on" or "off" by the liquid crystal. Light going through the CF substrate will display the color information for that pixel: enabling an LCD to display color images.

As described above, a CF substrate functions by allowing light to pass through it. Consequently, a CF substrate repair system must have a backlight mechanism to verify the quality of the repair.

A CF repair system is equipment that is designed to repair defects on CF panels as shown in **Fig. 2**.

White defects are spots on pixels where color is missing. These defects are repaired by coating the white spot with ink of the same color as the rest of the

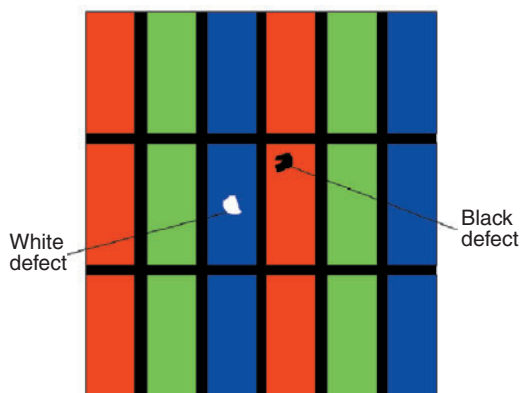


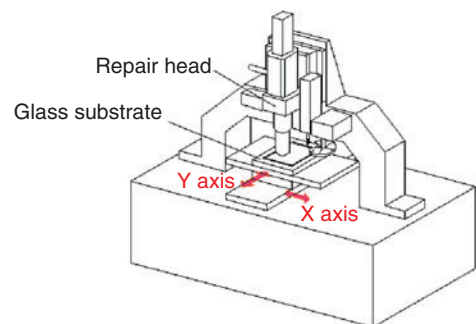
**Fig.2** Defects in a CF panel

pixel. Black defects are caused when colors are mixed on a pixel or dust adheres to a pixel. They may be repaired by first removing them by laser cutting followed by coating them with ink of the same color.

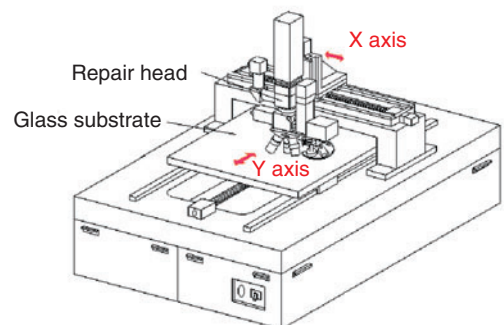
### 2.1 Evolution of CF repair system configuration

As mentioned before, the size of FPD's is increasing at an amazing rate. In response, the size and the configuration of the repair systems are also changing rapidly. The primary purpose for the changes is to limit the necessary floor space for the system inside clean rooms.

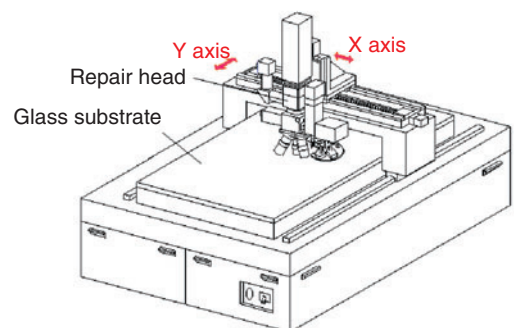
**Fig. 3** shows the evolution of the CF system configurations.



**a. Third and earlier generations**



**b. Fourth and Fifth generations**



**c. Sixth and future generations**

**Fig.3** Transition in the construction of repair systems related to generation change of LCD substrate

In the repair system configurations for Third and earlier generations, substrates were placed on the XY tables. The tables moved horizontally while the repair heads were fixed. The systems for the Fourth and Fifth generations generally had separate tables for the X-axis and the Y-axis and the substrates were moved in one axis while the repair head was moved in the other.

Most of the Sixth and Seventh generation repair systems secure substrates in a fixed position and employ the gantry method which moves the repair head in both the X and Y directions.

### 2.2 Traditional backlight mechanism and its Issues

The backlight mechanism, as shown in Fig. 4, illuminates the back of the surface plate so the light transmitted through the CF substrate can be observed. For this reason, the support for the CF substrate needs to be transparent. Therefore, most surface plates are made out of glass.

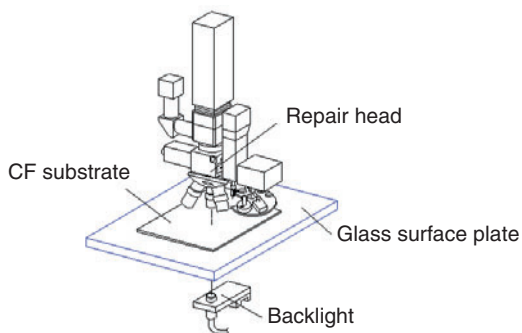
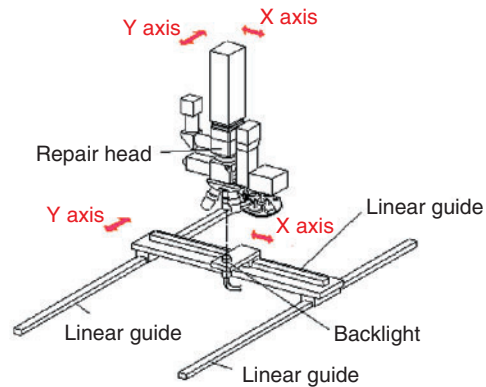


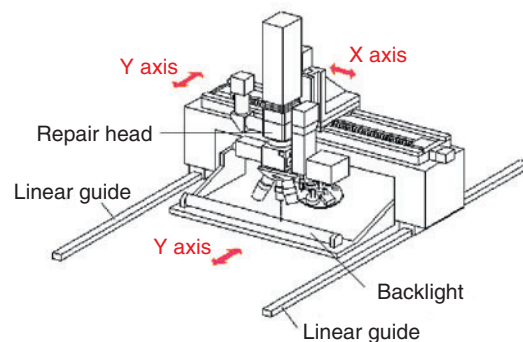
Fig.4 Glass surface plate

The gantry method used in the Sixth and the Seventh-generation systems moves the repair head in both X and Y directions. It requires a synchronized movement of the backlight mechanism. This results in a very complex system construction. Fig. 5 shows the backlight mechanism that has been adopted for the traditional gantry method. Fig. 5-a shows the complex structure of the backlight mechanism that moves synchronously with the repair head in X and Y directions.

Fig. 5-b is a simpler design in terms of both its structure and control where the linear backlight moves synchronously with the repair head in a single axis. This design does not require any additional control mechanism and is used in many systems. However, this method presents many system configuration issues when it comes to meeting the needs of Sixth and Seventh generation FPD's. Also, it is difficult to build backlight mechanisms for increasingly larger



a. XY moving backlight system



b. Y moving backlight system

Fig.5 Conventional backlight mechanism

systems with this design.

In the configurations illustrated in Figs. 5-a and 5-b, the light source of the backlight moves underneath the glass surface plate on which CF substrates are placed. This means that support members must be located at the perimeter of the glass surface plate.

To accommodate larger Sixth and Seventh generation FPD substrates, the size of glass surface plate must increase. However, as mentioned above, the glass surface plate must be supported at its perimeter. Therefore, the weight of the glass surface plate can cause deflection in the glass. Also, impact during transportation of the system can damage the glass surface plate.

The glass surface plate needs to have a mechanism for securing the CF substrate in position. Today, many systems use vacuum suction mechanisms for this purpose. The vacuum suction mechanism requires suction grooves to be cut and holes to be drilled on the glass surface plate. It also requires piping to be placed on the back of the glass surface plate. The suction holes and piping can obstruct the backlight.

When placing a CF substrate onto a repair system, a transfer device normally is used. Today, robots are used as transfer devices most of the time.

Lift mechanisms need to be installed on the repair systems so that they can receive the CF substrates transferred by the robots. A typical lift mechanism used for such an application is shown in Fig. 6. The lift mechanism raises the lifter pins to receive the substrate from the robot, and then lowers the lifter pins to place the substrate on the glass surface plate.

Holes must be drilled into the glass surface plate, as shown in Fig. 6, so the lifter pins can pass through. These holes affect the function of the backlight.

These are the major issues currently affecting the present backlight mechanism. At this time, the strength of the glass surface plate is the biggest issue.

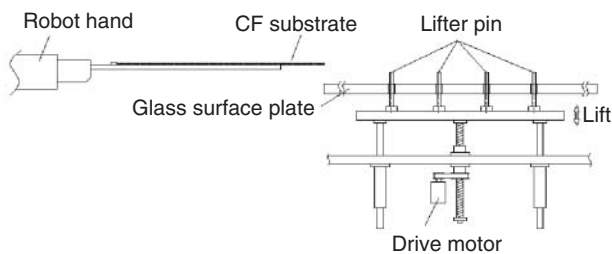


Fig.6 Lift mechanism

### 3. New backlight mechanism

In order to improve the function of the repair system, NTN has developed a new backlight mechanism. Instead of lighting from underneath the repair head, the new mechanism lights from the top of the repair head side to for improved inspection. With this configuration, since the source of the backlight is no longer located underneath the surface plate, the plate can be supported along its entire surface.

#### 3.1 Outline of reflective type backlight mechanism

Fig. 7 shows a diagram of the new backlight mechanism (reflective type).

The reflective-type backlight mechanism has a ring lamp around the objective lens of the repair head. Light is irradiated from around the observation point, utilizing the translucency of a CF substrate. The light is then reflected off the mirror surface on the backside of the glass surface plate, re-entering the CF substrate from the backside, thereby providing backlight for the lens.

Let us now explain the potential issues and corresponding solutions for backlight observation using this method.

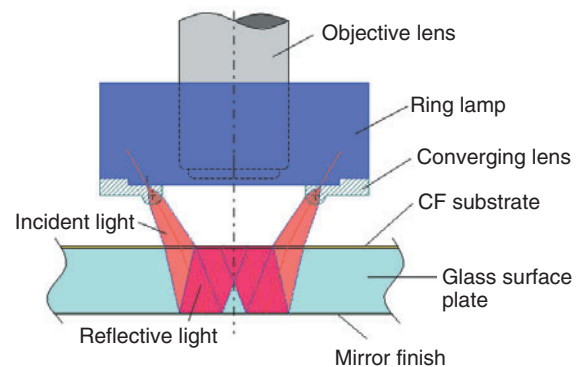


Fig.7 Reflective-type backlight mechanism

#### ① Securing reflective light intensity

##### ● Irradiation angle of light

Since there is a constraint on the arrangement of the ring lamp with respect to interference with the objective lens, the angle of the incident light to the CF substrate was set at  $30^\circ$ . Light emitted by the ring lamp spreads out to about  $30^\circ$ . A ring lens was installed at the light emitter to improve the light convergence, thus increasing the utilization of the light from the ring lamp and increasing the reflective light intensity. Without these measures, the spreading light from the ring lamp reaches the

observation point and prevents clear observation images from forming.

● **Thickness of glass surface plate**

In order to reflect the incident light from the ring lamp onto the mirror surface and then back onto observation point, the glass surface has to be a specified thickness. As shown in **Fig. 8-a**, if the glass surface plate is too thin, the reflected light does not reach the back surface of the observation point and cannot backlight observation images cannot be formed.

The test results indicate that if the glass surface plate has a thickness of 15mm or greater (**Fig. 8-b**), it can direct the reflected light from the mirror surface onto the backside of the observation point. The tests also found that this backlight observation was as good as that with a traditional backlight mechanism.

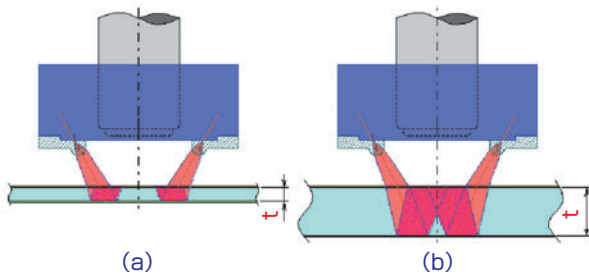


**Fig.8** Influence of glass plate thickness - 1 (Backlight intensity)

② **Solution to impacts of laser cutting**

As mentioned above, black defects on CF's can be repaired by cutting them with a laser and then coating them with ink. The laser cutting could cut the mirror on the back of the glass surface plate. As shown in **Fig. 9-a**, if the thickness ( $t$ ) of the glass surface plate is small, then the diameter of laser convergence ( $\phi D$ ) on the mirror surface is small and the power density of laser is high. In this situation, the mirror surface is vulnerable to damage by the laser.

The test results indicate that, if the thickness of the glass surface plate is 12 mm or greater, as shown in **Fig. 9-b**, then the diameter of laser convergence ( $\phi D$ ) on the mirror surface is large and the laser power density is low. Consequently, the mirror surface should not sustain any damage during laser cutting.

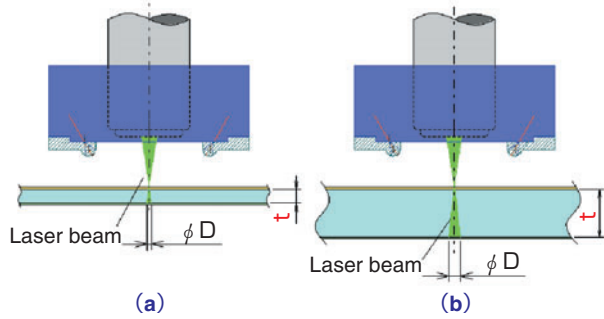


**Fig.9** Influence of glass plate thickness - 2 (Damage on mirror by cutting laser)

③ **Separation from incident light observation**

As the ring lens prevents light from entering the observation point, the incident light does not affect the observed images. However, it is possible for the incident light emitted by the objective lens to be reflected by the mirror on the bottom of the surface plate and impact the observation images.

As shown in **Fig. 10 (a)**, if the thickness ( $t$ ) of the glass surface plate is small, then the diameter ( $\phi D$ ) of light reflecting off the mirror surface and entering the back of the observation point is small and the light density is high. If this occurs, the light that is reflected on the image affects the transmitted light.

The test results indicate that, if the thickness ( $t$ ) of the glass surface plate is 5 mm or greater, as shown in **Fig. 10-b**, then the diameter ( $\phi D$ ) of light reflecting off the mirror surface and entering the back of the observation point is large and the light density is low. When this occurs, reflection on the mirror surface does not affect the observed image.

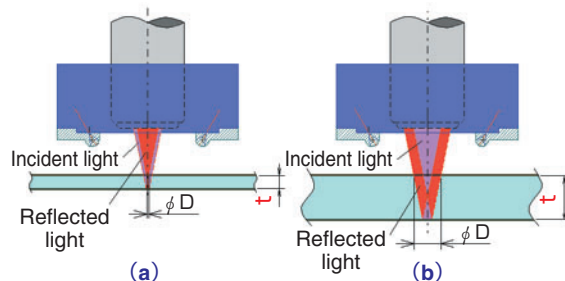


**Fig.10** Influence of glass plate thickness - 3 (Reflection of incident light)

④ **Solution to lifter pinhole issue**

The glass surface plate must have holes for the lifter pins to pass through for loading and unloading CF substrates. Since these holes must pass through the entire plate, a mirror cannot be installed on the back of the glass surface plate at these locations. As a result, light cannot be reflected at these holes and an image cannot be observed.

To resolve this issue, optical fibers were installed inside the lifter pins as shown in Fig. 11. This measure successfully resolved the issue and made backlight observation at the lifter pinholes possible.

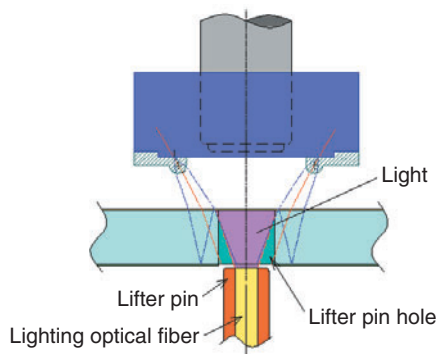


Fig.11 Lighting of lifter pin holes

⑤ **Solution to vacuum hole issue**

Vacuum holes must be made on the glass surface plate to secure CF substrates. Like the lifter pinholes, these holes must pass through the entire plate so no mirror process can be applied at the bottom. However, if the hole diameter is small enough, shown in Fig. 12, backlight observation is possible by the light reflected by the mirror surface around these holes.

The reflected light at the center of the vacuum hole is refracted by the wall of the hole, distorting the backlight observation image compared to the ordinary surface. This distortion in the images was reduced by optimizing the distance between the ring lamp and the CF substrate.

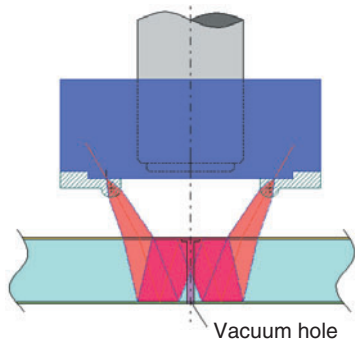


Fig.12 Lighting of vacuum holes

⑥ **Solution to electrostatic charge**

Electrostatic charge is produced by the contact and separation of the glass surface plate and the CF substrate and is a common issue for all backlight mechanisms. Solutions to this issue were studied as a part of this development.

As mentioned above, electrostatic charge occurs due to the contact and separation of the glass surface plate and the CF substrate. Minimizing the contact area between the plate and the substrate should reduce the amount of electrostatic charge. As a result, a special surface texture was used for the top of the glass surface plate (see Fig. 13).

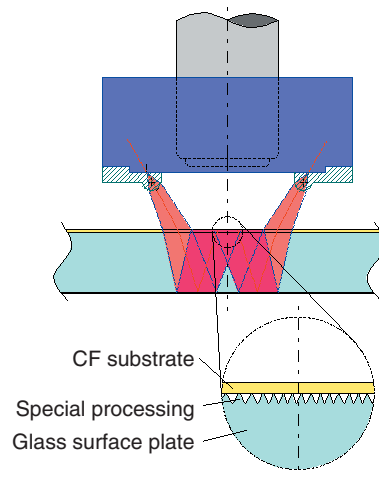


Fig.13 Glass plate surface special processing

Special processing makes micro dents and bumps on the top of the glass surface plate. This special process reduces the contact area between the glass surface plate and the CF substrate, thereby reducing the occurrence of electrostatic charge compared with a regular glass surface. Furthermore, light entering from the back surface of the CF substrate is dispersed by the micro dents and bumps created by the special process. As a side benefit, this dispersion increases the brightness of the backlight observation image.

⑦ **Solution to judgment time**

The repair judgment is an important issue with repair systems. In the preceding discussion about reflective-type backlight mechanisms, the ring lighting was examined. The ring lighting has the following problems.

Most of the current systems offer multiple objective lenses that are exchanged by the rotational movement controlled by the revolver mechanism. Since the revolver mechanism rotates the objective lenses, the ring lamp must retreat during the rotation. This retreat time must be included in the total judgment time. It may only take a few seconds, but any additional judgment time should not be accepted.

The objective of this study was to determine a lighting layout that does not require the ring lamp to retreat during objective lens exchanges and that provides sufficient light intensity for backlight observation.

The study concluded that multiple arc-type lamps could achieve this objective. These lamps were made by dividing a ring lamp in sections to avoid interference with the objective lenses during their rotation.

⑧ **Meeting the needs of the Sixth and Seventh generation FPD's**

Unlike the traditional backlight method, the reflective type backlight method accommodates support mechanisms under the glass surface plate. Therefore, there would be no structural problem as the system becomes larger.

Considering all the above issues, the specifications of a reflective type backlight mechanism were determined as shown in **Table 1**.

**Table 1** Reflective-type backlight mechanism specifications

Size of glass surface plate	Sixth generation Seventh generation	1540 × 1890 mm 1910 × 2240 mm
Thickness of glass surface plate		t=19 mm
Distance between reflective light and CF substrate		W.D.=18 mm
Surface processing of glass surface plate		Special processing
Back surface processing of glass surface plate		Mirror processing
Reflective light		Divided arc lighting

**Photo 1** shows the backlight observation images obtained using the reflective-type backlight mechanism. The images are as good as those of the traditional backlight mechanism.

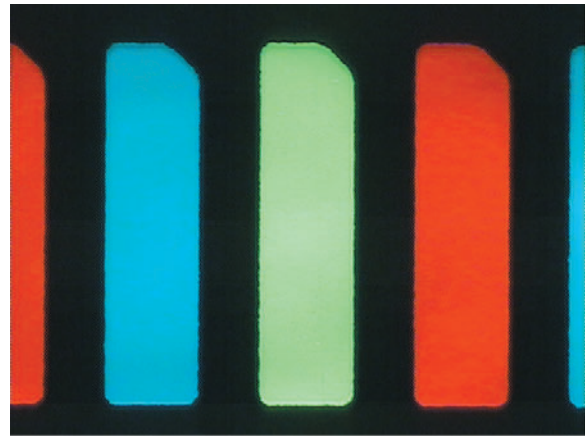


**Photo 1** Image of CF pattern with reflective type backlight

## 4. Conclusion

This paper introduced a new backlight mechanism for the CF repair system. The objective of the new backlight mechanism was to meet the requirements of Sixth and Seventh generation FPD's. However, FPD manufacturers have concepts of even larger mother glass substrates. As described earlier, a backlight mechanism is a necessity for repairing color filters and the traditional backlight mechanism would face structural problems when dealing with increasingly large glass substrates. The reflective-type backlight mechanism has resolved any structural issues associated with the repair of large CF's substrate. This mechanism is a new feature of NTN's CF repair systems. This paper primary focused on backlight mechanism, but as glass substrates become larger, numerous new issues will continue to challenge equipment manufacturers. NTN will continue developing our repair system components to solve these new issues to improve the innovation and quality of our products.

### Photos of authors

---

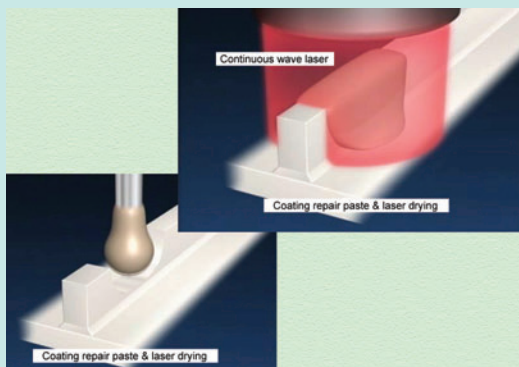


Akihiro YAMANAKA  
Precision Equipment Division  
Product Engineering Dept.



Akira MATSUSHIMA  
Precision Equipment Division  
Product Engineering Dept.

## PDP Rib Repair System



Shizuka YAMAZAKI\*  
Yuji YADA\*

In recent years, PDP is expected to rapidly penetrate into the market. However, rib defects occasionally occur during the manufacture of PDP substrates. If the substrate has a rib defect, the image quality of the PDP is poor. Therefore, equipment that can repair this rib defect is in demand. To meet this demand, NTN has added various functions to NTN's conventional repair equipment and developed a rib repair device.

This device makes repairs by repeatedly applying paste on the defective portion, baking it, and measuring the shape of the repaired portion with a non-contact displacement meter. After filling the defective portion with paste, the upper surface of the rib is finished by machining. Surplus paste is removed from the side surfaces with a cutting laser and scratch needle.

This paper provides an outline of this equipment.

### 1. Introduction

PDP's (Plasma Display Panel) have recently become larger, improved the quality of images, and reduced the manufacturing costs. The civil market for PDP's was first launched in Japan in 2002 and the European as well as the American markets is expected to follow. Plasma TV's are considered the winner of flat and big screen TV's, and demands for PDP's in the market of 30 inch or larger FPD are expected to grow.

The PDP back plate glass substrate has ribs which are subject to notch and projection defects due to adhesion of dust and foreign matters or inclusion of air bubbles during the production processes of the substrates. These defects on the PDP ribs cause color mixing and loss of image quality. Substrates with these defects have been scrapped or repaired.

Recent increase in the PDP production has drawn people's attention to the loss associated with scrapping substrates with these rib defects, the needs for improved productivity and quality, and to the environmental issues relative to the scrapped substrates. Thus, demands are growing for a rib repair system.

To meet these demands, NTN expanded the existing paste application and laser cutting technologies and combined them with additional laser curing, machining, contour measuring functions, etc. to create a rib repair system. The following is an outline of this system.

\*Precision Equipment Division Product Engineering Department



## 2. Structure of PDP

Fig. 1 shows the structure of a typical PDP including ribs. A notch defect on a rib is shown in Fig. 2. A PDP consists of a rear glass substrate with ribs (barrier walls) and a front glass substrate that is placed against the top surfaces of these ribs. The types of the rib profile include the stripe, waffle, meander types, etc. The figure below shows typical stripe type ribs.

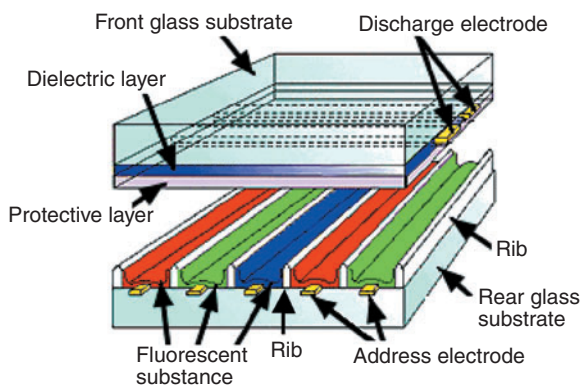


Fig.1 Structure of PDP

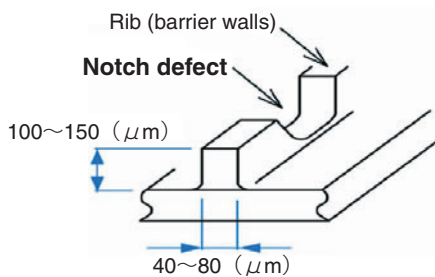


Fig.2 Rib defect

## 3. Outline of system

### 3.1 System configuration

Photo 1 is the appearance of the system and Fig. 3 the system configuration.

This system applies repair paste to notch defects on the ribs, bakes them, machine finishes the rib top, and removes excess paste off the sides of the ribs by laser cutting or use of a scrape needle.

The defect data is sent from the server or the inspection unit to the host computer of the system. Repair operations are conducted based on these data.

As shown in Fig. 3, the head is equipped with an air spindle for machining, laser displacement meter, baking laser, observation optical unit, cutting laser, scrape unit, and a pasting unit. Not shown in Fig. 3 and behind the scrape unit is a squeegee unit.



Photo 1 Rib repair system

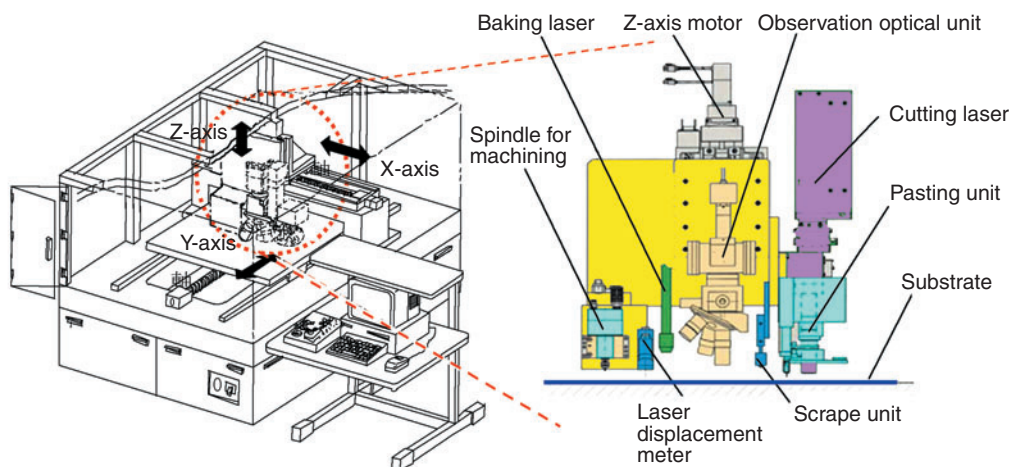


Fig.3 Schematic of rib repair system

A defective substrate placed on the stage moves in the Y-axis direction while the head moves in the X- and Z-axis directions. In other words, the head has relative displacement in the XYZ directions with respect to the defective substrate. **Table 1** lists the stage specifications.

**Table 1** Specifications of stages

Item	Specifications
<b>1. X stage</b>	
Drive	Ball screw or linear motor
Control method	Full closed loop control
Resolution	1 $\mu$ m/pulse
Positioning repeatability	$\pm 3 \mu$ m
<b>2. Y stage</b>	
Drive	Ball screw or linear motor
Control method	Full closed loop control
Resolution	1 $\mu$ m/pulse
Positioning repeatability	$\pm 3 \mu$ m
<b>3. Z stage</b>	
Drive	Ball screw
Control method	Semi closed loop control
Resolution	0.05 $\mu$ m/pulse
Positioning repeatability	$\pm 1 \mu$ m

### 3.2 Feature of system

#### (1) Numerous repair functions

As mentioned above, this system offers various functions necessary for repair works. Users may select functions that are most suitable for specific defects.

Different functions may be manually operated by way of the buttons on the monitor screen or the switches on the operation panel.

The observation optical unit has a CCD camera that sends expanded images of the target areas to the monitor.

The spindle is an air bearing spindle driven by an air turbine. This spindle generates no heat and high rotational accuracy. A small grinding wheel of  $\phi 0.4 \sim 0.3$  mm in diameter is placed at the tip of the rotating shaft for grinding.

When the coating unit has applied the paste at the defective portion, the squeegee unit runs its end tip of a cylindrical resin squeegee head of about  $\phi 3$ mm in diameter over the paste with reference to the adjoining normal rib top, thus smoothing the repaired surface. The scrape unit, then uses the scrape needle and mechanically removes the excess paste on the sides of the rib.

For baking, continuous wave CO<sub>2</sub> laser with long wave length (wave length: 10.4  $\mu$  m) is used for

localized heating, and for cutting. Short wave continuous pulse YVO<sub>4</sub> laser (wave length: 532nm) which has less thermal effects is used.

**Table 2** shows the major specifications of the above functions.

**Table 2** Specifications of functional elements

Items	Specifications
<b>1. Laser displacement meter</b>	
Resolution	0.1~0.01 $\mu$ m
Measuring point	About $\phi 2 \mu$ m
Measuring range	$\pm 0.3$ mm
<b>2. Cutting laser</b>	
Type	LD excited YVO <sub>4</sub> laser
Wave length	532nm
Output	250mW or higher (at 5KHz)
<b>3. Baking laser</b>	
Type	CO <sub>2</sub> laser
Wave length	10.6 $\mu$ m
Maximum output	10W
<b>4. Spindle</b>	
• Type	Externally pressurized air bearing
• Drive (rotation)	Air turbine
• Maximum rotating speed	40,000 rpm
• Tool diameter	$\phi 0.4$ mm ~ $\phi 0.3$ mm
<b>5. Observation optical unit</b>	
• Revolver	Electric revolver
• Objective lens	Magnification 2x ~ 20x

#### (2) Height measurement using noncontact displacement meter

This unit is equipped with a laser displacement meter and off-sets between the Z-axis reference point of the displacement meter and the focal point of the observation optical unit, and between the measuring point on the XY plane and the center of the optical unit are preregistered. Therefore, operators need to view the rib image on the monitor screen and specify the start and end points of measurement. Then the unit automatically corrects each offset amount, moves the displacement meter to the specified location, and simply measures the height.

Since the displacement meter uses a small spot diameter (about  $\phi 2 \mu$  m) and takes measurement without contact, it can accurately measure the profile of the top of the filled portion even though the paste is still soft.

These measurements are converted into graphs and displayed on the observation monitor screen by the measurement locations.

### (3) Specifying positions in different functions

As described above, this unit automatically corrects the reference points in all functions (tip position of the rotating tool, focal point of the cutting laser, focal point of the baking laser, etc.) and the offset amount between the displacement meter (Z-axis) and the observation optical unit (X and Y axis's). Consequently, this unit offers easy machining and baking at the height and the positions specified on the observation monitor screen.

The rib material, profile, and the material for the dielectric layer vary by users and so does the most suitable paste. Before installation of this system, NTN offers assistance with paste selection tests and optimal conditions selection tests using the actual substrates and repair paste.

## 4. Repair procedure

The actual repair works do not always use the same processes. Some rib defects may require repair of projections only, and others may require only height measurement. The system allows independent operation of the functions so that users may combine any of these functions to perform necessary defect repairs.

Fig. 4 shows one example of the rib defect repair processes. Each repair process will be explained following the sequence shown in Fig. 4.

This figure does not show the profile measuring process, but it is necessary to execute this process whenever multiple repair process are necessary. This is to remeasure the profile of the defect after the repair processes.

- ① Dip the needle in paste in container and apply paste to defect by making contact. For long defects, specify start and end points for coating. Then have the unit move needle up and down at constant pitch to accomplish continuous coating.
- ② Bake paste by CO<sub>2</sub> laser. Repeat above coating and baking several times to fill defects with paste.
- ③ Measure height of repaired portion by comparing paste buildup to height of adjoining normal rib. Determine depth of paste removal by amount of buildup, and then machine the rib surface by the tip of rotating tool. Typically, this operation requires several round trip runs of tool to achieve same height as that of adjoining rib top.
- ④ If paste builds up beyond rib width in coating and baking operations, remove excess paste with reference to width of the adjoining normal rib using laser cutting and scrape needle. This completes repair processes.

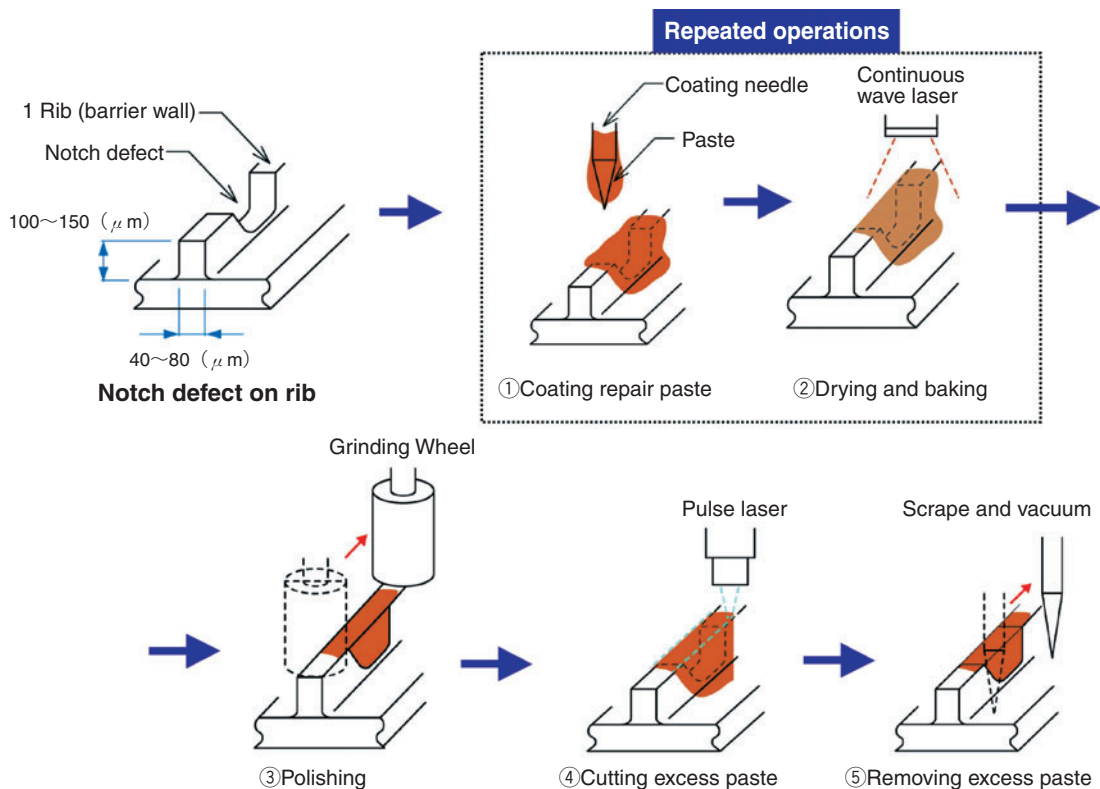


Fig.4 Schematic of rib defect and repair process

## 5. Repair results

**Photo 2** is the measurement of the defect and its repair in the rib direction measured by the displacement meter. The defect on this sample measured about 450  $\mu\text{m}$  in length and 105  $\mu\text{m}$  in depth.

For this sample, the coating and the baking processes were repeated about five times to build up the paste above the normal rib height (about 27  $\mu\text{m}$ ), and then the top surface was polished. **Table 3** lists the baking and the polishing conditions.

As shown by the measurement results in **Photo 2**, the repaired surface after the polishing process is almost undistinguishable from the surrounding ribs.

**Table 3** Heat treatment and grinding conditions

Item	Conditions
1. Baking (CO <sub>2</sub> laser)	
Laser output	0.2W
Spot diameter	$\phi$ 200 $\mu\text{m}$
2. Polishing	
Grinding wheel	$\phi$ 0.3, Electro deposition grinding wheel
Average particle diameter	22~36 $\mu\text{m}$
Feed speed	10 $\mu\text{m/s}$ (cutting: 2 paths)
Rotating speed	40,000 rpm

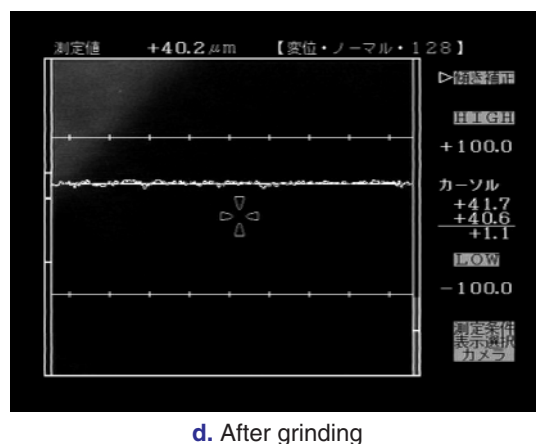
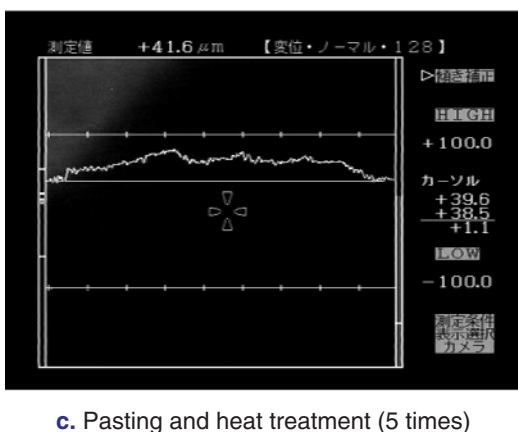
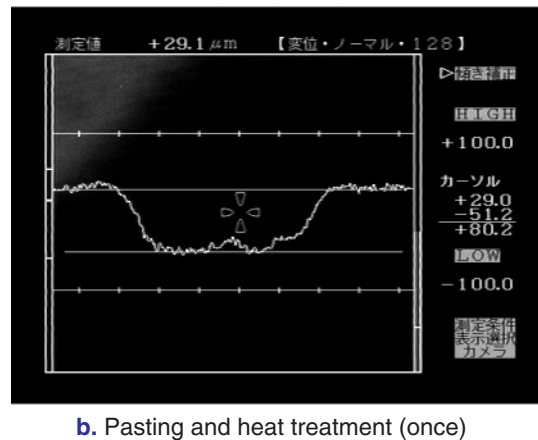
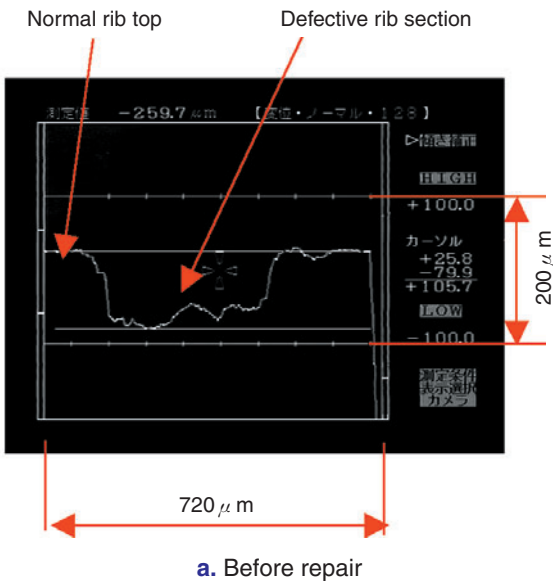


**Photo 2** Shape of rib defect through repair process

## 6. Conclusion

This article introduced the "PDP rib repair system" that was designed to repair the rib defects on the PDP back glass substrate.

As the market for PDP's is expected to grow rapidly, demands for this system should also increase.

With the growing markets for Hi-definition TV broadcasting and DVD or such high-quality graphic media, PDP's must improve resolution, reduce power consumption, and lower the production costs. The repair systems will also have to improve the surface and dimensional accuracy of the rib top, accommodate complex rib profiles and thinner ribs, handle even longer defects, and reduce tact time.

NTN will continue to proactively deal with these demands so that we may improve this system to a higher level of maturity.

### Photos of authors

---



Shizuka YAMAZAKI

Precision Equipment Division  
Product Engineering Dept.



Yuji YADA

Precision Equipment Division  
Product Engineering Dept.

# Improvement of the Accuracy of an Air Spindle of the Nano-meter Order

- Improvement of Rotational Accuracy by Optimization of Feed Hole Positioning -



Yoshio FUJIKAWA\*  
Takashi HARAGUCHI\*  
Kazuyuki AONO\*  
Teruyoshi HORIUCHI\*

NTN's air spindles are used in production and inspection equipment for magnetic discs. The major issue of such air spindles is how to improve the rotational accuracy. NTN studied the correlation of the rotational accuracy and the feed hole arrangement on an aerostatic journal bearing, and as a result NTN has developed a staggered triple-row feed journal bearing. This paper presents the numerical analysis results of the performance of the staggered triple-row feed journal bearing and describes the rotational accuracy of the prototype air spindle that is equipped with this bearing.

## 1. Introduction

Aerostatic bearings offer dynamic accuracy of the nanometer order at realistic costs. They are widely used in advanced production equipment for semiconductors, optical disks, and for magnetic disks as bearing/guide elements. NTN integrated this aerostatic bearing and a motor to develop a high-accuracy air spindle. Today, these air spindles are in production and fulfilling the needs for these products. In this field of technology, however, progress has been dramatic in terms of higher precision and recording density. Air spindles are always expected to reduce the rotational errors.

To facilitate these demands, NTN has developed a new staggered triple-row feed aerostatic journal bearing. This paper describes a case study where this bearing was used on the air spindle for magnetic disk inspection devices or servo track writers and successfully reduced the major contributors to repetitive run-out and non-repetitive run-out.

## 2. Air spindles for magnetic disks

Magnetic head inspection devices for hard disk drives or servo track writers may stack up magnetic disks, as shown in **Fig. 1**<sup>1)</sup>, for rotation. Because the disk stack overhangs significantly with respect to the spindle bearing part, the run-out at the top of the disk stack is large. It is almost like the conical mode. Run-out of disks causes errors in the positioning of the head on the disk. Especially, non-repetitive run-out that does not synchronize with the disk rotation has been viewed as critical. Presently, needs for higher storage density have caused the track pitch to become smaller. Accordingly, allowable errors for head positioning have become tighter. On some occasions, it is necessary to assess repetitive run-out, particularly on higher components.

**Fig. 2** shows the structure of an air spindle for magnetic disks. A shaft is supported by two journal bearings that support primarily radial load, and by a

\*Precision Equipment Division    Product Engineering Department

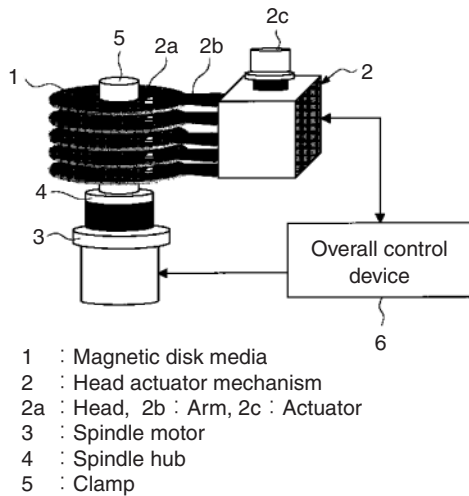


Fig.1 Air spindle for magnetic disk <sup>1)</sup>

pair of thrust bearings located on both sides of the shaft-integrated thrust plate supporting primarily the axial load. Restrictor has significant effects on the characteristics of aerostatic bearings and many types of restrictor are suggested. For applications that require high accuracy, NTN primarily adopts complex restriction that combines an inherent restrictors and shallow circumferential grooves. NTN also uses porous restriction in some applications. The slit plate of the optical rotary encoder and the AC servo motor rotor are directly mounted on the shaft. Such structure makes the rotating portion completely free from contact with the fixed portions, thus minimizing fluctuation in friction resistance with respect to the shaft rotation and making it possible to accurately control the shaft rotation.

To accommodate a vacuum chuck mechanism for mounting/dismounting of disks, etc., a non-contact seal section is placed between the two journal bearings configuring a vacuum exhaust passage between the rotating and the fixed portions. The non-contact seal section has a clearance about equal to that of the journal bearing. Resistance at this small clearance limits entry of outside air into this vacuum exhaust passage. The seal surfaces of the rotating and the fixed portions can be machined simultaneously with the surface of the journal bearing, and therefore very high concentricity to the bearing surface can be obtained, affecting little on the rotating accuracy.

To ensure high rotating accuracy of an air spindle, the motor control technology is important. If rotating speed control of very high accuracy is required for magnetic disk or optical disk related applications, NTN uses a driver that was developed internally by combining PLL control (Phase Locked Loop) and sinusoidal linear drive.

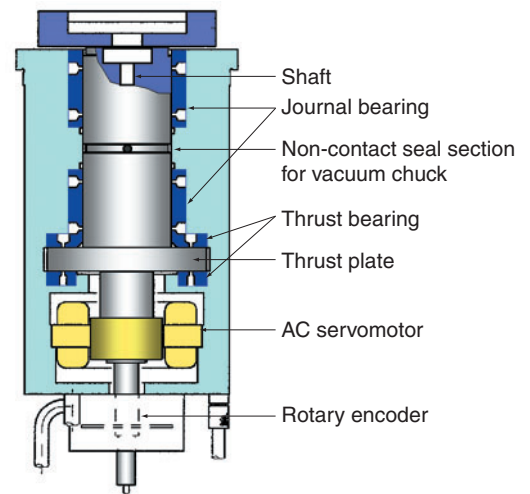


Fig.2 Configuration of air spindle

### 3. Measurement of repetitive run-out using 3-point method<sup>2)</sup>

#### 3.1 Run-out measuring system

The run-out accuracy evaluation used the 3-point method in order to eliminate influence of the profile errors of the target object and to measure minute run-out of the air spindle with good repeatability. Fig. 3 shows the measuring system. To evaluate the run-out under the operating conditions closest to those on an actual unit, dummy clamp and dummy disks were fixed on the spindle by the vacuum chuck mechanism to simulate a disk stack of multiple magnetic disks. In addition, a steel ball of 25.4mm in diameter was installed at the top to be the target for the displacement sensor.

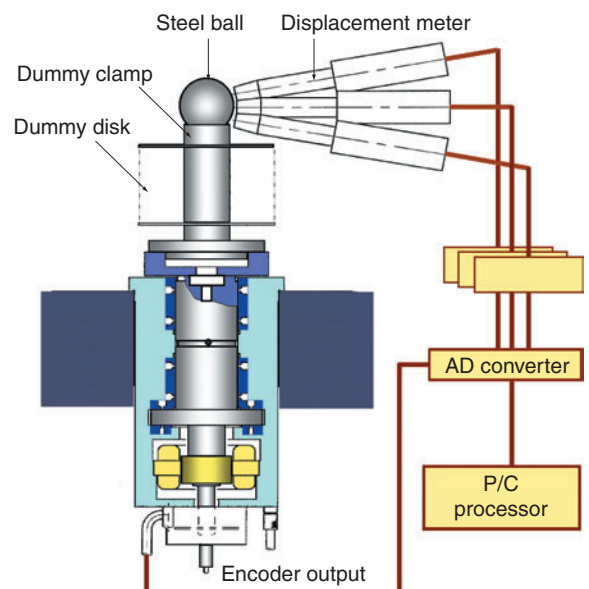


Fig.3 Measurement system for radial runout by 3 point method

The steel ball at the top of the dummy clamp allows run-out measurement to be taken at a point where the amplitude is the largest. However, it adds mass to a point away from the bearing, creating more severe operating conditions in terms of run-out.

A capacitance displacement sensor was used to measure run-out. The output signal of the displacement sensor was stored into the memory via an AD converter using the output pulses (1024 pulses/rotation) from the optical rotary encoder that was built into the spindle as a trigger. Tshen, the average run-out wave pattern for 10 continuous rotations was processed by the 3-point method. The measurement results are the Fourier coefficients for the profile error of the target and for the run-out at the center of rotation. This evaluation used the absolute values of the Fourier coefficients for run-out to determine the actual run-out.

The 3-point method is known to include errors in the measured value of the order if the "scaling factor"<sup>2)</sup>, which is defined by the arrangement of the three displacement sensors (angle between the sensors) and the order of run-out, is small. Our evaluation calculated the "scaling factor" of each order at and below 32<sup>nd</sup>, and determined the sensor locations so that the minimum value would be the largest. Furthermore, after the measuring system was set up, the angle between the three sensors was measured by the rotary encoder that was built into the air spindle, and this value was used in the calculations.

### 3.2 Measurement results

Fig. 4 shows the measurement results of repetitive run-out of a magnetic disk air spindle (hereinafter referred to as "conventional spindle") that has been in production at NTN. The bearing is of the complex restriction type. The vertical axis represents the absolute values of the Fourier coefficients for run-out determined by the 3-point method, and the horizontal axis represents the order of run-out with respect to the shaft rotation, or the amplitude of run-out corresponding to each order. The peak of run-out are seen at the 3<sup>rd</sup>, 5<sup>th</sup>, 9<sup>th</sup>, and at the 17<sup>th</sup> orders. The maximum amplitude was recorded at the 5<sup>th</sup> order and was about 13nm. The measurement of another air spindle of the same design showed the peaks of

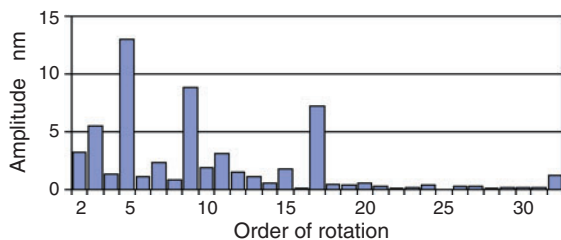


Fig.4 Radial runout of conventional spindle measured by the 3 point method

amplitude at the same orders except for the unique differences in the sample populations.

### 4. Staggered layout of feed holes

Calculations indicate that a journal bearing with feed holes laid out at an equal pitch on its circumference produces run-out of specific high orders depending on the profile error of the rotating shaft and the number of feed holes<sup>3)</sup>. The profile errors are represented by  $\delta \cos \{m (\theta - \alpha)\}$  having the m number of lobes on the circumference, where d is the differential of the average radius and the maximum radius of the shaft divided by the average radial clearance of the bearing. The profile in the axial direction is assumed constant. (See Fig. 7.)

Fig. 5 shows the position of the shaft center of a shaft having the m number of lobes rotating in a single-row feed inherent restrictor journal bearing with the k number of feed holes laid out on its circumference. The position was obtained by equilibrium of static force. The position of the shaft center in Fig. 5 assumes  $\delta = 0.1$  and shows the k number of feed holes on the horizontal axis and the m number of the lobes of roundness error on the vertical axis. It shows the position of the shaft center corresponding to each combination. Run-out occurred at  $m=nk \pm 1$  (n is a natural number) and it was particularly large at  $m=nk+1$ . During one shaft rotation, the shaft center rotates the m number of times around the center of the bearing and produces run-out of the m<sup>th</sup> order.

Unlike the configuration used in the reference<sup>3)</sup>, the journal bearing of the conventional spindle is a double-row feed type having four feed holes laid out on the circumference at an equal pitch at two axial locations, and a circumferential groove is installed to connect these feed holes. If this similar mechanism is to produce run-out of higher orders, it is possible that it will produce run-out of the 5<sup>th</sup>, 9<sup>th</sup>, 13<sup>th</sup>, and the 17<sup>th</sup> order, because  $k=4$ . This is in good approximation with the run-out measurement shown in Fig. 4, and therefore the repetitive run-out of higher order with conventional spindles may be produced by the profile

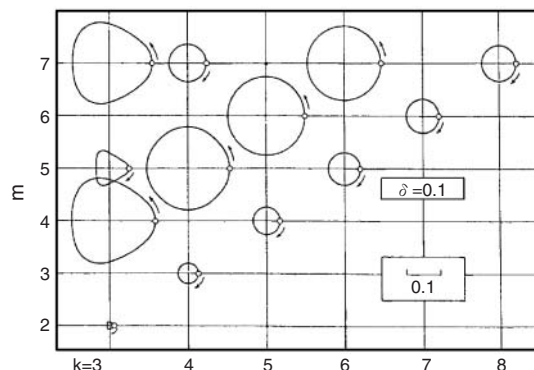


Fig.5 Effect of number of feed holes and lobes on radial runout



error of the shaft and the layout of the feed holes.

To reduce this run-out, it is effective to increase the number of feed holes on the circumference. However, if the feed holes are increased without careful consideration, it will reduce stiffness and the damping factor, making the bearing vulnerable to external disturbances.

The feed holes of a double-row feed journal bearing are typically laid out in the same phase as shown in Fig. 6 (a). On the other hand, the profile error of a spindle shaft is usually a copy of the run-out error of a grinder's work spindle during the finishing process, and it is considered consistent through the axial direction. If the profile of a rotating shaft is consistent in the axial direction, feed holes on each row in staggered layout as shown in Fig. 6 (b) should achieve the same effect as when the feed holes are doubled over the circumference. However, asymmetrical layout of the feed holes in the axial direction will produce the moment of force that works to tilt the shaft. In order to reduce this the moment of force, you may either layout the feed holes of the two journal bearings that support the rotating shaft in a

totally symmetrical order or, as shown in Fig. 6 (c), arrange the feed holes at more than two locations on the circumference and establish symmetry in each bearings.

### 5. Calculated bearing performance

To determine the specifications of a journal bearing for prototyping an air spindle, bearing performance was calculated. With a journal bearing for a conventional spindle as a basis (bearing a0: Shaft diameter 30mm, Bearing width 25mm), the prototype expanded the bearing width by 15mm to 40mm total, primarily to improve the damping characteristic. Performance was calculated for the three types of feed hole arrangements shown in Fig. 6. Table 1 summarizes the bearing specifications that were used for this calculation.

The method of calculation used was finite difference method using the DF method, which is generally used to calculate performance of grooved aerostatic bearings.

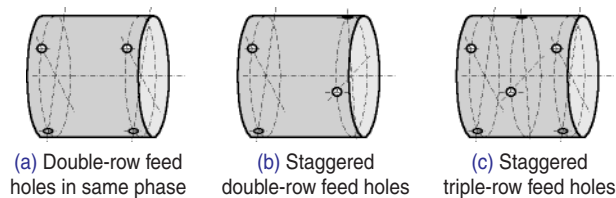


Fig.6 Feed hole arrangement of journal bearing

Table 1 Bearing specification

	Bearing width	Rows of feed holes	Number of feed holes per row	Arrangement
a0	25mm	2	4	Same phase
a	40mm	2	4	Same phase
b	40mm	2	4	Staggered
c	40mm	3	4	Staggered

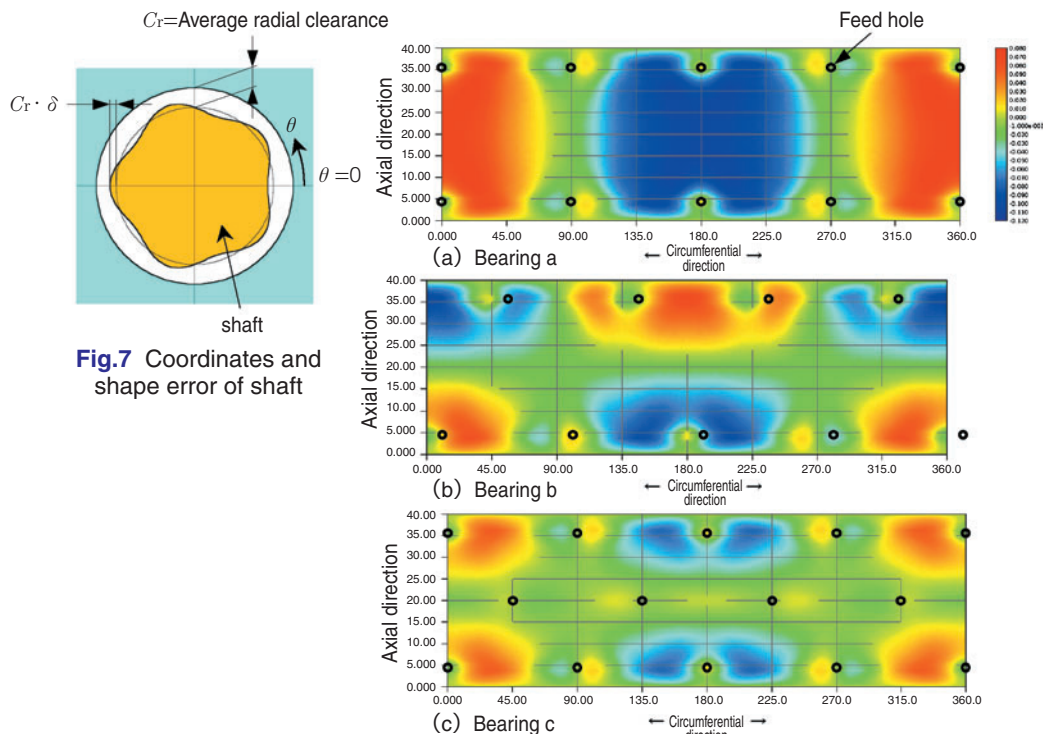


Fig.8 Calculated pressure variation induced by the shape error

### 5.1 Calculated pressure distribution at bearing clearance

Fig. 8 shows the effects of the shaft profile errors on pressure distribution in the bearing clearance about bearings a, b, and c. The contour lines represent the differences between the pressure distributions with and without profile errors.

The black dots indicate the feed holes. The red region indicates pressure rise due to the profile error, and the blue region indicates pressure drop. As shown in Fig. 7, the shaft center is assumed to match that of the bearing, the shaft's profile errors are given by the five peaks of the sinusoidal waves in the circumferential direction, and the profile is assumed consistent in the axial direction. The amplitude of the profile error is  $\delta = 0.1$ , a non-dimensional value normalized by the bearing clearance, which is supposed to be largest at  $0^\circ$  coordinate in the circumferential direction. A bearing which has two rows of feed holes arranged in the same phase shows high pressure at wide clearances or at  $0^\circ$  positions and low pressure on the opposite side. As a result, it produces a force that pushes the shaft in the  $180^\circ$  direction, causing run-out of the shaft with respect to the bearing. When the shaft rotates  $1/2$  turn ( $36^\circ$ ) on the lobe cycle, the bearing clearance widens in the  $180^\circ$  direction, which is reverse what is shown in Fig. 7. This increases the pressure, causing the shaft to run-out in the  $0^\circ$  direction. If the shaft turns another  $72^\circ$  from its original state, the clearance returns to the original amount. Thus, the profile errors of five peaks causes run-out of fifth orders.

With bearing b that has two rows of feed holes laid out in the staggered manner, regions of high and low pressures exist symmetrically with respect to the center line of the axial direction and cancel each other. As a result, this configuration does not produce force that caused the shaft to run-out in the radial direction. However, since there is force that pushes the shaft in the  $0^\circ$  direction in the top half of the figure and force that pushes the same in the  $180^\circ$  direction in the bottom half, a moment of force is present that tilts the shaft.

Bearing c has three rows of feed holes and the feed holes on the central row of which are staggered with respect to the rows on the both sides. With this bearing, the pressure distribution is the same as that of bearing a. However, the magnitude of pressure changes are much smaller than that of bearing a due to the staggered layout of the feed holes on the central row.

### 5.2 Run-out by profile errors

Fig. 9 shows the amplitude of high order run-out obtained by the simple method introduced in a reference<sup>3)</sup>. Force on the shaft is first obtained from the pressure distribution on the shaft when the centers of the shaft and the bearing match, and then it is divided by radial stiffness obtained by perturbation method assuming small displacement. The quotient is the approximate value of the radial displacement of the shaft center. As in the case of Fig. 7, the profile error that is consistent in the axial direction but varies in the sinusoidal wave pattern in the circumferential direction was calculated within the profile error range of 3~13 in the lobe number  $m$ .

The amplitude of the profile error was  $\delta = 0.1$ . The vertical axis is the nondimensional run-out amplitude  $\epsilon$  normalized by the bearing radial clearance. The number of peaks  $m$  of the profile error is also indicated in the figures.

Bearings a0, a, and c, with the feed holes of  $k=4$  on the same circumference, produce run-out when the profile error lobe number is  $m=nk \pm 1$ . The run-out magnitude of the  $\epsilon$  is about  $1/2$  of  $\delta$  at the largest and it is smaller than that of the single-row feed hole type with no circumferential groove as shown in Fig. 5. On bearing a which maintained the same phase arrangement of the feed holes but increased the bearing width,  $\epsilon$  is larger than that of the conventional spindle bearing a0. On the other hand, run-out is smaller on bearings b and c where the feed holes are staggered. Bearing b, in particular, shows no run-out when  $m=3, 5, 11$ , and  $13$ . The  $m$  value at which the shaft produces run-out is the same as when eight feed holes are laid out. However, as shown in Fig. 10, bearing b produces the moment of force that tilts the shaft when  $m=3, 5, 11$ , and  $13$ . On the other hand, bearings a0, a, and c do not produce the moment of force. Fig. 10 shows the nondimensional moment of force  $M$  normalized by the air supply pressure  $p_s$  and

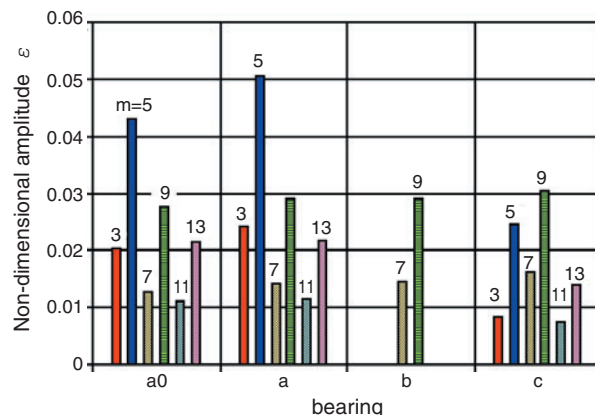


Fig.9 Calculated nondimensional amplitude of rotational error

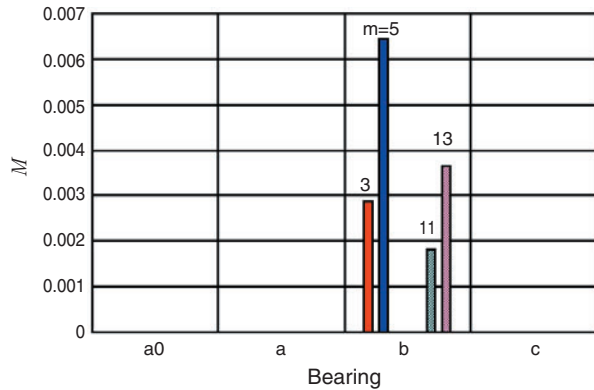


Fig.10 Calculated nondimensional moment

the bearing diameter  $D$ .

$$(M = m_f / p_s D^3, m_f: \text{Moment of force})$$

### 5.3 Radial stiffness and damping factor

Run-out accuracy is subject to a shaft's response to external disturbance. Damping characteristics near the natural frequencies of air spindle are particularly important. For this reason, stiffness and the damping factors of each bearing type were calculated and compared. In this calculation, it was assumed that a shaft would not rotate but produce fine translational motion near the center of a bearing, and then the perturbation method was used to obtain radial stiffness  $k$  and radial damping factor  $c$  with respect to a small displacement. The calculation did not consider the profile error. Fig. 11 and 12 show non-dimensional radial stiffness  $K$  and non-dimensional radial damping factor  $C$ , respectively, that were normalized by the air supply pressure  $p_s$ , bearing diameter  $D$ , average radial clearance  $C_r$ , and by the angular frequency  $\omega$  of translation frequency.

$$(K = k \cdot C_r / p_s D^2, C = c \cdot C_r \cdot \omega / p_s D^2)$$

The horizontal axis in both figures indicates the squeeze number  $\sigma$ .

$$\left( \sigma = \frac{12 \mu \omega R^2}{P_a C_r^2} \right)$$

Bearings a and b have the same layout of the feed holes and almost the same stiffness and the damping factors, and therefore they are represented by a single line in the figures.

Radial stiffness (Fig. 11) of bearings a, b, and c is about double that of bearing a0 of the conventional spindle in the  $50 < \sigma$  region due to large dynamic pressure caused by extended bearing width.

As to radial stiffness (static stiffness) at  $\sigma \doteq 0$ , bearings a and b are slightly greater than that of

bearing a0 and bearing c is about the equal to that of bearing a0.

Regarding the damping factor (Fig. 12), bearings a and b show the largest values in the region where  $\sigma$  is small (low frequencies), but when  $\sigma$  is at or above 50, the damping factor drops almost as low as that of bearing a0. If  $\sigma$  is at or above 20, the damping factor of bearing c is the largest or about three times that of bearing a0. In conclusion, bearing c can achieve the least run-out relative to external disturbance near the characteristic frequencies of the spindle.

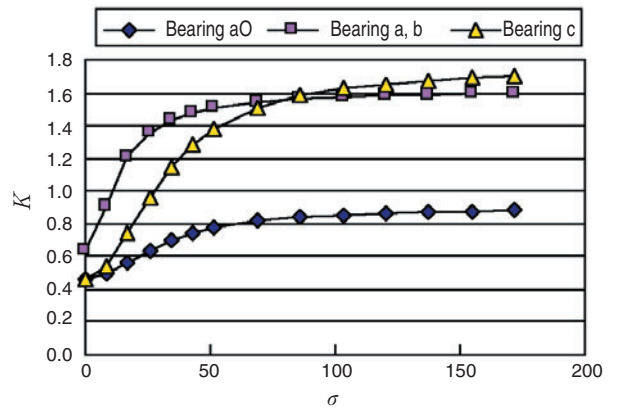


Fig.11 Calculated nondimensional radial stiffness

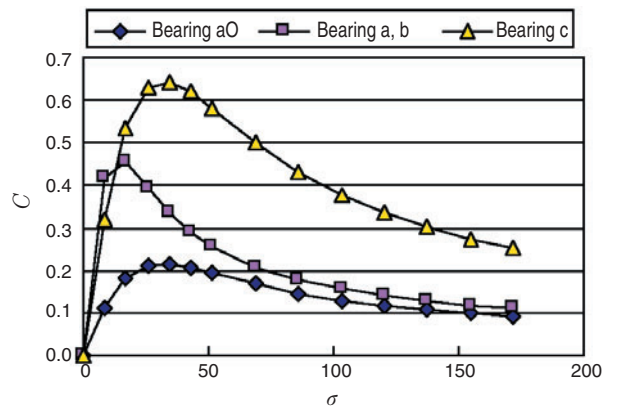


Fig.12 Calculated nondimensional damping factor

## 6. Measurement of run-out on a prototype spindle

Based on the above study results, bearing c was selected for prototype spindle, and repetitive run-out and non-repetitive run-out were measured and compared to those of the conventional spindle using bearing a0. The structure of the prototype is the same as one shown in Fig. 2 except that the total length of the spindle is longer than that of the conventional spindle by 30mm because the width of the journal bearing was extended by 15mm. The longer support portion of the journal bearing will increase the angular stiffness at the bearing. Except for the journal bearing, everything is the same between the prototype and the conventional spindle.

Fig. 13 shows the repetitive run-out of the prototype unit measured by the 3-point method. The conventional spindle (Fig. 4) showed the peaks at the 5<sup>th</sup>, 9<sup>th</sup>, and the 17<sup>th</sup> order, but the prototype unit does not exhibit any apparent peaks. The staggered feed holes on the prototype unit apparently reduced run-out of the 5<sup>th</sup> order that is caused by the profile error and the feed hole layout. Furthermore, since the triple row layout of the feed holes increased the damping factor, run-out at the 9<sup>th</sup> and the 17<sup>th</sup> orders apparently decreased.

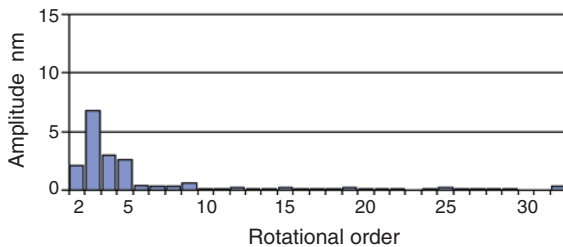


Fig.13 Measured repetitive radial runout of the improved spindle

Fig. 14 and 15 show the measurement results of non-repetitive run-out of the conventional spindle and the prototype unit, respectively. The measurement of non-repetitive run-out was carried out in the following method.

In the identical measuring system shown in Fig. 3, 3-point method, one capacitance type displacement sensor was used.

- Using the origin signals (once/rotation) from the rotary encoder as triggers, outputs of the capacitance type displacement meter for 2000 rotations were sampled and stored in the memory.
- For the 2000 data values, difference of two consecutive data values was calculated to produce 1,999 non-repetitive run-out data.

Non-repetitive run-out measured in this fashion of the air spindle unit was typically  $\pm$  several nm. In contrast, non-repetitive run-out of the conventional spindle shown in Fig. 14 was  $\pm$ 33nm. This is because the air spindle used for this study had a dummy clamp protruding significantly from the bearing and a steel ball was secured at the tip of this clamp.

As compared to the conventional spindle, non-repetitive run-out of the prototype unit (Fig. 15) was reduced to about 1/2 or  $\pm$ 17nm. This improvement is believed to have been made by the improvement in the damping factor of the journal bearing with the triple-row feed hole configuration.

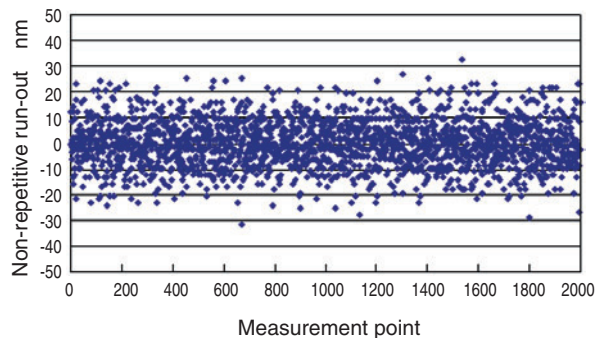


Fig.14 Measured non-repetitive runout of the conventional spindle

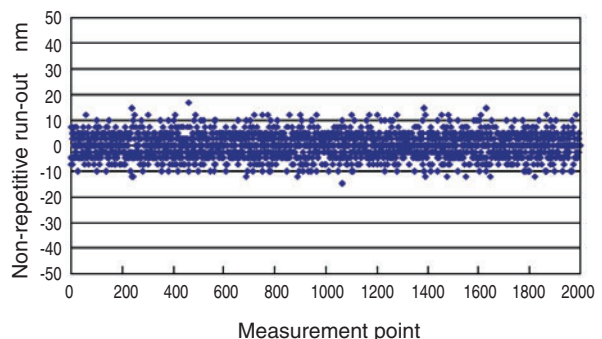


Fig.15 Measured non-repetitive runout of the improved spindle

## 7. Conclusion

Calculations and experiments have verified the effects of improvement in the run-out accuracy of a new aerostatic journal bearing that has adopted triple-row feed holes with a staggered layout.

Run-out accuracy of air spindles is subject to many other factors other than the bearing performance, which was the focus of this study. All other factors should be reviewed comprehensively. The accuracy in the rotating speed also needs to be further improved. NTN will continue to resolve these issues so that we may provide the market with higher level of precision to meet the market needs.

### Reference

- 1) Japanese Published Patent Application 2002-334498  
KAWAGUCHI, YAMAZAKI, KUSAKAYA
- 2) AOKI, OZONO, J\_JSPE, 32, 12 (1966), p831
- 3) YABE, Trans, JSME(c), 58, 548. (1992), p1177

### Photos of authors

---



Yoshio FUJIKAWA  
Precision Equipment Division  
Product Engineering Dept.



Tahashi HARAGUCHI  
Precision Equipment Division  
Product Engineering Dept.

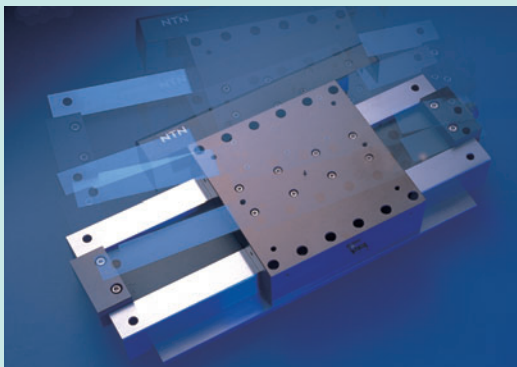


Kazuyuki AONO  
Precision Equipment Division  
Product Engineering Dept.



Teruyoshi HORIUCHI  
Precision Equipment Division  
Product Engineering Dept.

## Nanometer accuracy positioning system



Akio NAKAJIMA\*

This paper describes two types of very high precision positioning systems. One is the linear positioning stage that is capable of one nanometer accuracy. This stage consists of an Air Slide, Linear Motor, and Laserscale. The other is the rotational positioning Air Spindle that has a resolution of 151-million increments per revolution. We recently completed development of an exclusive controller system, the Nanoscale Controller.

### 1. Introduction

The production equipment for semiconductors, optical disks, hard disks, and other information devices requires highly accurate precision positioning technology. Lately, accuracy as little as a nanometer is required of such equipment. This report describes the development and commercialization of a precision positioning system that is capable of stopping at nanometer accuracy and has reduced speed fluctuation at low speed movement. The mechanism consists of an air slide that is driven by a voice coil type linear motor. The amplifier is a newly developed low-noise linear amplifier and the measurement section uses a glass scale. As a result, the system has exceeded the original expectations.

In the manufacture of optical disks and hard disks, not only linear positioning but also angular positioning may be required at times. NTN applied this positioning technology to an air spindle that utilized an aerostatic bearing to accomplish angular resolution of 151.2 million pulses per circumference or nanometer accuracy resolution. This paper also explains this product.

### 2. Higher precision in positioning technology

One of the applications of a high precision positioning system is the optical disk mastering device (L.B.R.).

**Photo 1** is the main portion of a L.B.R. This device uses a spindle equipped with a rotating glass plate and an optical head that moves in the radial direction of the glass plate, and sends short-wave laser to create spiral grooves.

For such a device, it is important for its positioning system to accurately determine not only the final target position, but also the positions in the path. Therefore, the device must have accurate dynamic performance. The accuracy requirements are determined by the track pitch or the movement of the optical head per rotation of the spindle. The track pitch of a CD is  $1.6 \mu\text{m}$  and that for a DVD is  $0.74 \mu\text{m}$ . However, the latest Blu-ray disk requires  $0.32 \mu\text{m}$ , 1/5 that of a CD.

One of the most important elements about the accuracy of positioning systems is a position measurement scale. L.B.R. typically requires 1~3%

\*Precision Equipment Division Product Engineering Department

normal track pitch.

Naturally, NTN's precision positioning systems have improved the position measuring resolution every year as shown in Fig. 1.

A laser interferometer is used for resolution of 10nm and a glass scale for all other resolutions.

Generally, laser interferometers and capacitance type sensors are often used for the measuring units of precision positioning systems. Presently at NTN, the glass scales are used more often. Capacitance type sensors have short range of measuring distance and exhibit big temperature drift, but they show excellent frequency response characteristics. Laser interferometers, on the other hand, are highly accurate, but vulnerable to air disturbances.

The glass scale, though its cumulative error at long distances is greater than that of a laser interferometer, is less prone to temperature changes and shows relatively good accuracy within the track pitch distance. The lattice pitch is typically the minimum of

about 1  $\mu$  m, and accuracy at the lower levels is obtained by electrically dividing the sin/cos signals produced by the scale. The division error is the interpolative error. The interpolative error of the scale occurs at about 1% the lattice pitch. With these issues taken into consideration, NTN engaged in a joint development of a high precision scale with a scale manufacturer. As a result, we learned that in order to increase accuracy and achieve it at or below 1nm within a narrow range, it was necessary to minimize the lattice pitch and select a smaller interpolative error with respect to the lattice pitch.<sup>1) 2)</sup>

### 3. Nanometer positioning system

Photo 2 and Fig. 2 show the positioning system, which is the mechanism for the nano-scale positioning system. The system specifications are as follows. This device is an application of optical heterodyne FFT<sup>3)</sup>. The performance requirements for this device is the same as those for L.B.R.

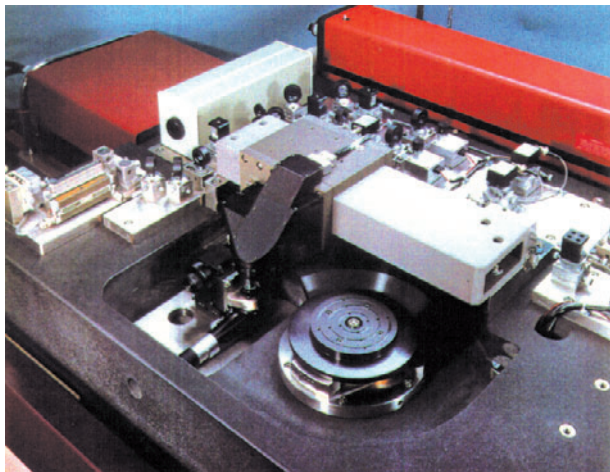


Photo 1 Main part of L.B.R.

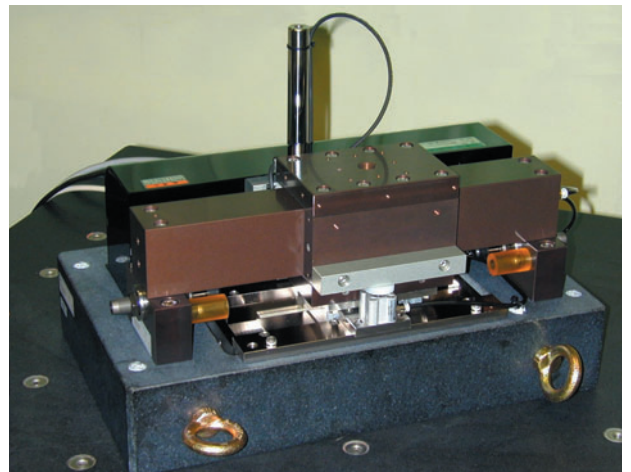


Photo 2 Photograph of the positioning system

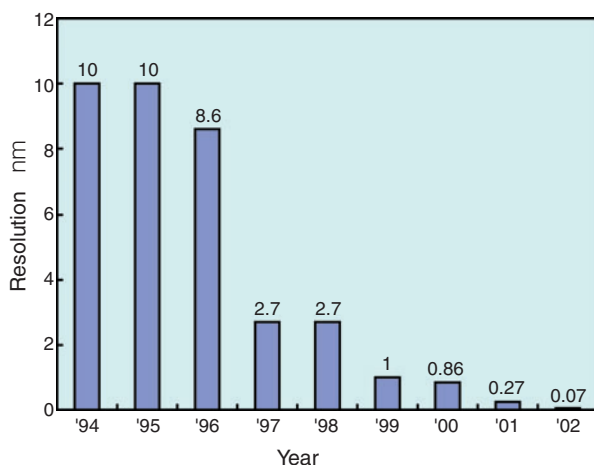


Fig.1 Trend of the positioning system resolution

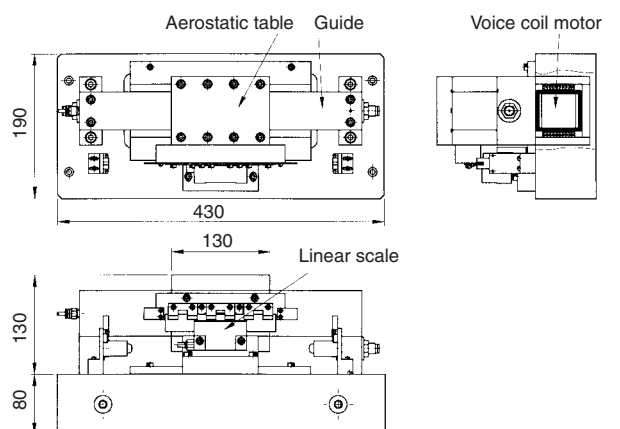


Fig.2 Schematic of the positioning system

The table specifications are as follows.

The slide stroke, resolution, etc. can be changed depending on applications.

<b>Guide</b> .....	Air slide
<b>Linear motor</b> .....	Voice coil type
<b>Materials</b> .....	Aluminum alloy
<b>Rated load</b> .....	30N
<b>Stroke</b> .....	100mm
<b>Resolution of scale</b> .....	About 0.2759nm
<b>Thrust constant</b> .....	5.7N/A
<b>Mass of moving portions</b> .....	4.02kg
<b>Maximum current</b> .....	4.0A
<b>Control type</b> .....	PID
<b>Servo sample</b> .....	50kHz
<b>Amplifier</b> .....	Linear amplifier

Actual measurement of straightness of the table under rated load was as follows.

<b>Up/down</b> .....	0.09 $\mu$ m/100mm
<b>Side to side</b> .....	0.01 $\mu$ m/100mm

The table and the scale are normally off position, causing Abbe's error. Therefore, it is extremely important for the table to possess straightness in the side to side direction.

As shown in Fig. 3, the speed fluctuation at or below 1mm/s turned out to be  $\pm 1$ nm or less in position conversion, which was good. Deviation in the stop positions was also within 1nm. Due to the absence of external means that can easily measure the table position by the units of 1nm or smaller, signals of deviation between the controlling scale signals and the command position signals are used instead. Thus, changes in the speed are indicated as changes in the positions (deviation from the ideal position). Accuracy of this system has been fully verified indirectly by actually producing products using this system.

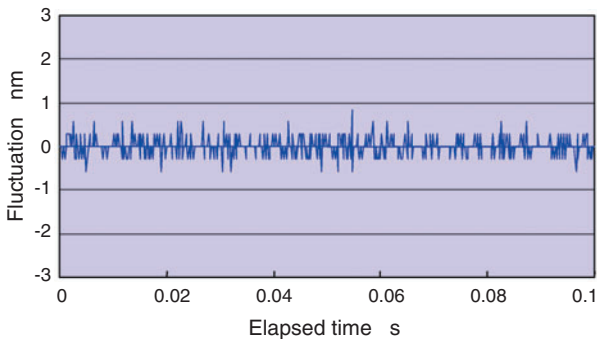


Fig.3 Positioning error while moving at 1mm/s

As shown in Fig. 4, transient movement accompanied by linear acceleration of about 0.04 second turned out well. If better acceleration method or control method is used, better characteristics should be achieved.

In order to maintain performance at the nano-scale level as one uses such a high precision positioning system, various precautions must be taken. A damper bench to eliminate impacts of floor vibration and stiffness of the components must be carefully evaluated. Lack of stiffness will cause unnecessary vibration which adversely affects the control system. Connecting cables and hoses to moving portions of the system must also be carefully installed to prevent them from interfering with the operation of the system.<sup>4)</sup>

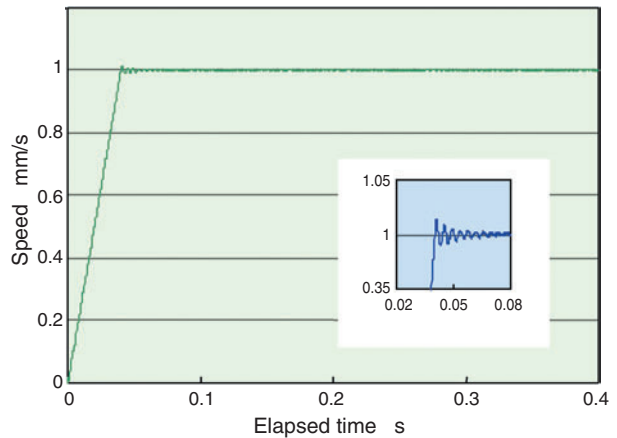


Fig.4 Transient response of speed



#### 4. Spindle unit for high-resolution positioning

An air spindle supports a rotating shaft by supplying air or other pressurized gases in between the rotating and fixed portions, thereby forming a non-contact structure.

**Fig. 5** shows NTN's standard air spindle. The structure of this air spindle consists of two journal bearings and two thrust bearings that support a rotating shaft, an AC servo motor, and a non-contact type optical rotary encoder directly connected to the shaft. Since the rotating portions are of a totally non-contact structure, there is very little friction. Also, the averaging effect of aerostatic bearings improves accuracy. For these characteristics, NTN's standard air spindles are used in broad applications, especially in high precision fabrication and inspection. <sup>5)</sup>

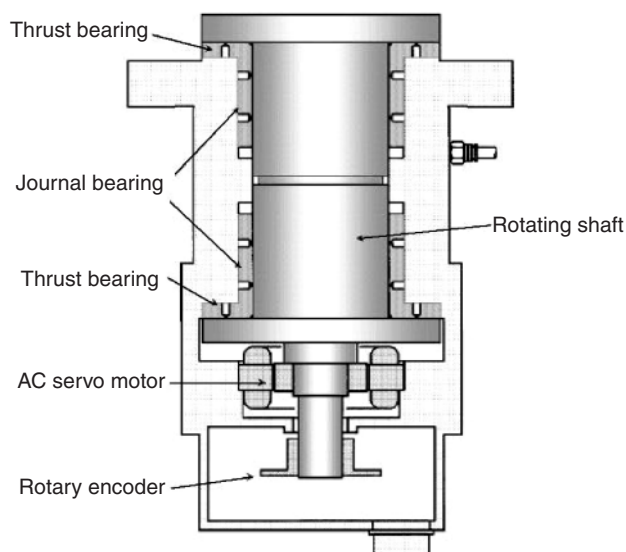


**Fig.5** Construction of air spindle

For continuous rotation, the PLL control method is suitable. Rotational fluctuation (deviation in the rotating frequency) can be controlled at or below 1PPM depending on the operating conditions. With the PLL control method, phase difference between the command and the feedback pulses determines deviation, and therefore it is possible to introduce small deviations of less than 1/2 pulse into the control system. On the contrary, deviation equal to or greater than 1/2 pulse can't be detected. Consequently, NTN primarily uses those air spindles of which the rotary encoders have low resolution of 1024 or 4096 pulses per turn. With this system, rotation can't be stopped.

The deviation pulse method is used to determine the stop position. This method can't detect deviation

until a minimum deviation of 1 pulse is produced. Consequently, high-resolution rotary encoders of 1 million pulses or greater per turn may be used. Under this method, accuracy of a rotary encoder is extremely critical and is most closely related to the stopping accuracy of the spindle. To increase the angular resolution, an appropriate rotary encoder must be selected. The rotary encoder<sup>6)</sup> developed for use on the hard disk servo track writer (STW), shown in **Fig. 6**, was used to develop a spindle unit that has resolution up to 151.2 million pulses. The spindle body is a standard spec unit of NTN. The encoder head uses a reflective type head for detection of the STW arm head position, and for a reflective type scale, an improved donut shape scale of 12.04mm in effective radius for detection of the STW clock is used. **Fig. 7** shows the schematic of the encoder. The spindle specifications are as follows.

Spindle	: NTN standard spindle (HRA3M equivalent 7)
Encoder	: SONY P.T. BH10
Multiplying Equipment	: SONY P.T. BB100
Pulse count	: 302,400 × 500 Multiplying
Total pulse count	: 151,200,000 pulses/turn
Resolution	: 0.00857 second
Cumulative accuracy	: ± 12 seconds (actual measurement for encoder)
Controller	: Nano-scale controller Made by NTN (linear drive)
Maximum rpm	: 300rpm (NTN controller)
Stopping accuracy	: ± 5~10 pulses (with NTN controller)

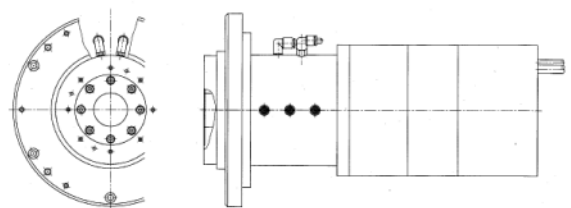


**Fig.6** Schematic of high resolution air spindle

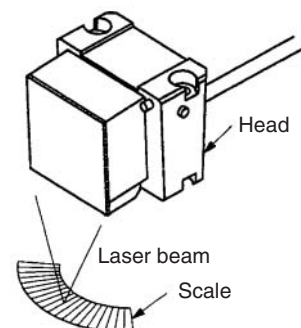


**Fig.7** Schematic of rotary encoder

The resolution at the outer most circumference,  $r=60\text{mm}$ , of a CD or a DVD, for example, is  $2.5\text{nm}$  in distance conversion. In reality, there is a positioning error on NTN's controller.

The positioning accuracy was  $\pm 40$  seconds. A 12-sided polygon mirror was used for the measurement and the expected measuring error is about  $\pm 1$  second. **Fig. 8** shows the measurement data.

The errors shown occurred in the form of a sinusoidal wave, and therefore the rotational synchronization was the main component. When this component was removed, the remaining 2nd order and higher were about  $\pm 5$  seconds. The primary cause of the 1st order of this error was believed to be misalignment of installation of the donut shaped scale. However, since repeatability was within  $\pm 1$  second, calibration should improve the absolute accuracy markedly.

Due to the absence of means that can dynamically measure fluctuation in the rotational speed, signals of deviation between the controlling scale signals and the command position signals are used instead. Thus, changes in the indexing speed are indicated as changes in the indexing positions (deviation from the ideal position). As shown in **Fig. 9**, deviation was more or less  $\pm 0.1$  second or less at low speeds.

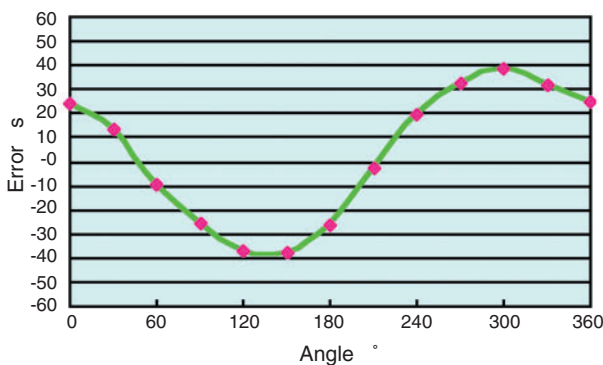


**Fig.8** Cumulative positioning error

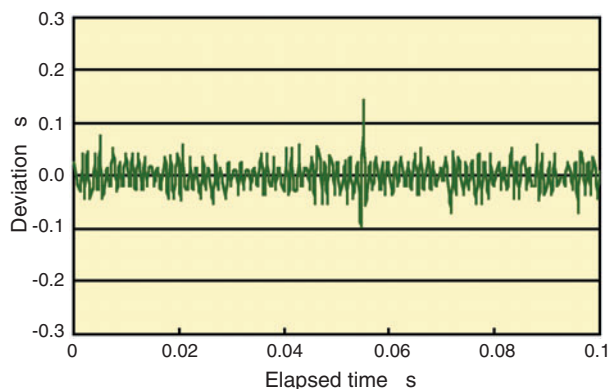


**Fig.9** Indexing error while rotating at 1 degree/s

## 6. Control method

The control method for the servo unit is the popular PID control for both the spindle and the slide. The controller uses the same specifications of the previously mentioned nano-scale controller for super precision positioning slides that is capable of stopping at  $1\text{nm}$ . Like the trends in the recent controllers, the scale directly receives the scale signals without multiplying equipment, hence achieving high-speed operation even though it accomplished high accuracy.

With switching elements becoming more popular in recent years, PWM (Pulse Width Modulation) amplifiers are often used to power motors. However, these amplifiers produce much noise and torque fluctuation among other issues. They also use constant voltage, and therefore they are not suitable for powering fine movement. The newly developed device uses a sinusoidal wave linear amplifier to avoid harming the hard disk head that handles very small signals, and it has proven to show good results. **Fig. 10** illustrates the main components of the amplifier.

In the positioning controller, the direction of micro current reverses at high speeds when the device is stationary. For this reason, the amplifier demands close attention to the crossover distortion, which, in continuous rotation, would not become an issue. **Fig. 11** shows an example of crossover. In general, occurrence of crossover distortion creates dead zones, affecting the servo unit and impairing accuracy. For this reason, proper bias voltage is applied to the FET drive or the final stage to prevent crossover distortion from occurring. **Photo 3** is the developed special controller and the driver.

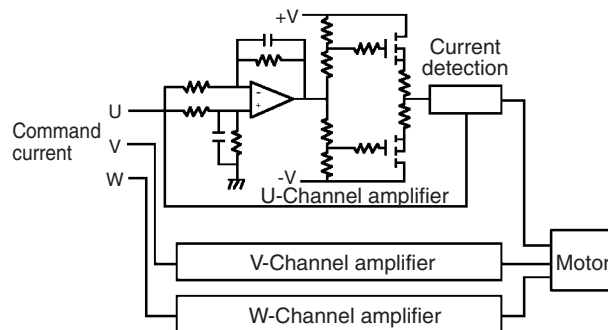


**Fig.10** Diagram of amplifier

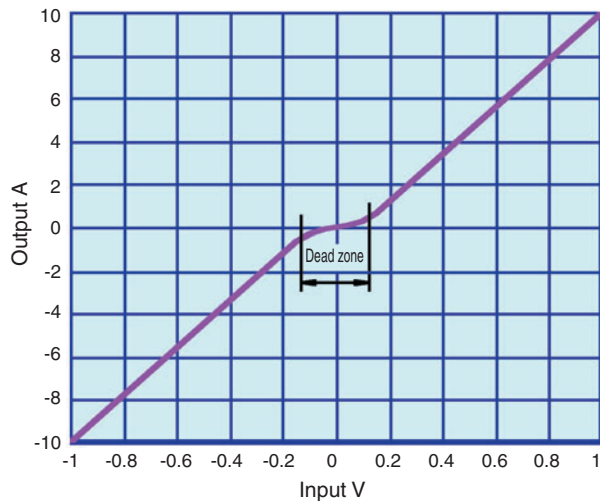


Fig.11 Example of crossover distortion



Photo 3 Nanoscale Controller and amplifier

## 7. Conclusion

A positioning system that can perform uniform motion within 1 nm deviation has been developed along with its evaluation method. This system has proven to be production-worthy. This paper also presented the structure of and the measurement results using a super precision positioning spindle based on the same technology. NTN will continue to research the technologies in an effort to develop positioning systems that meet the market demands for higher precision and accuracy.

## Reference

- 1) Motohiro Takaya, Kayoko Taniguchi and Tadahiko Shiman, Nanometetr Controlled Stage, digitalscale international workshop, Tsukuba, (2001-11)
- 2) Hiroshi Saitou, high precision , high resolution Linear encoder, Fuji, Technosystem, highly accuracy precision positioning technology, (2000) 419
- 3) Akiko Hirai, Lijiang ZENG and Hirokazu Matumoto, Heterogyne Fourier Transform Spectroscopy using Moving Diffraction Grating, Jpn. J. Appl. Phys. Vol.40 (2001) 6138 Part 1, No.10 Oct. 2001
- 4) Akio Nakajima, Nanometer accuracy positioning technology to practical, optical disk's meyor field at application, engineering society, high accuracy precision positioning special committees, No.2002-4 (4) 27 2002.11.15. NTN corp.
- 5) Yoshimi Fujikawa, The Tribology 3 (2003), 44
- 6) Yukihiro Uematu, Masanori Fukushi, and Kayoko Taniguchi, Development of the Pushpin free STW IEEE TRANSACTIONS ON MAGNETICS 37, NO.2, MARCH 200
- 7) Air Spindle Unit NTN Catalog No.5403-III/J

## Photos of author

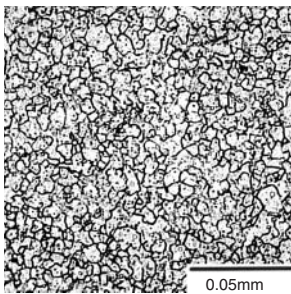


Akio NAKAJIMA

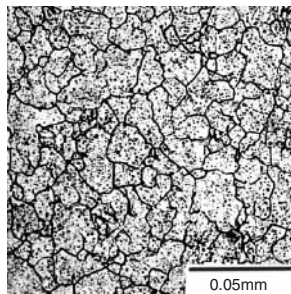
Precision Equipment Division  
Product Engineering Dept.

## FA Tapered Roller Bearings

Achieve long life through grain refinement and carbonitriding technologies for bearing steel  
**Fine Austenite Strengthening: Grain refining and carbonitriding technologies for bearing steel**

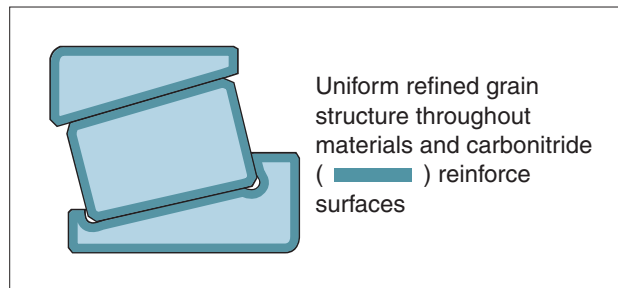


FA treated



Normal quenching

The prior austenite grain boundaries

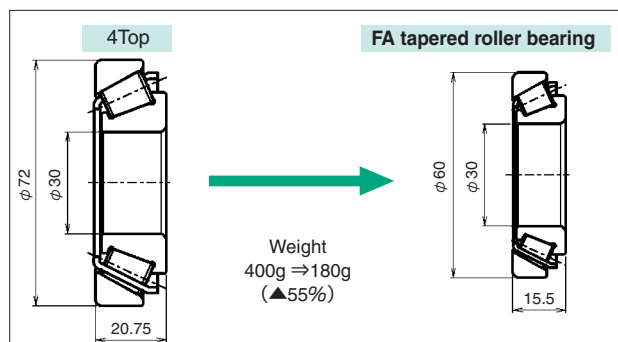


### Performance (compared to NTN's 4Top series)

- Nearly 3 times longer life under lubrication with clean oil
- Nearly 14 times longer life under lubrication with contaminated oil
- Lower torque by 10%, or greater, within normal rotational range
- Improved seizure resistance by 25% in rotating speed and 200% in surface pressure
- Reduced preload loss by half
- Reduced assembly width settling rpm by half
- Improved indentation resistance by about 1.5 times

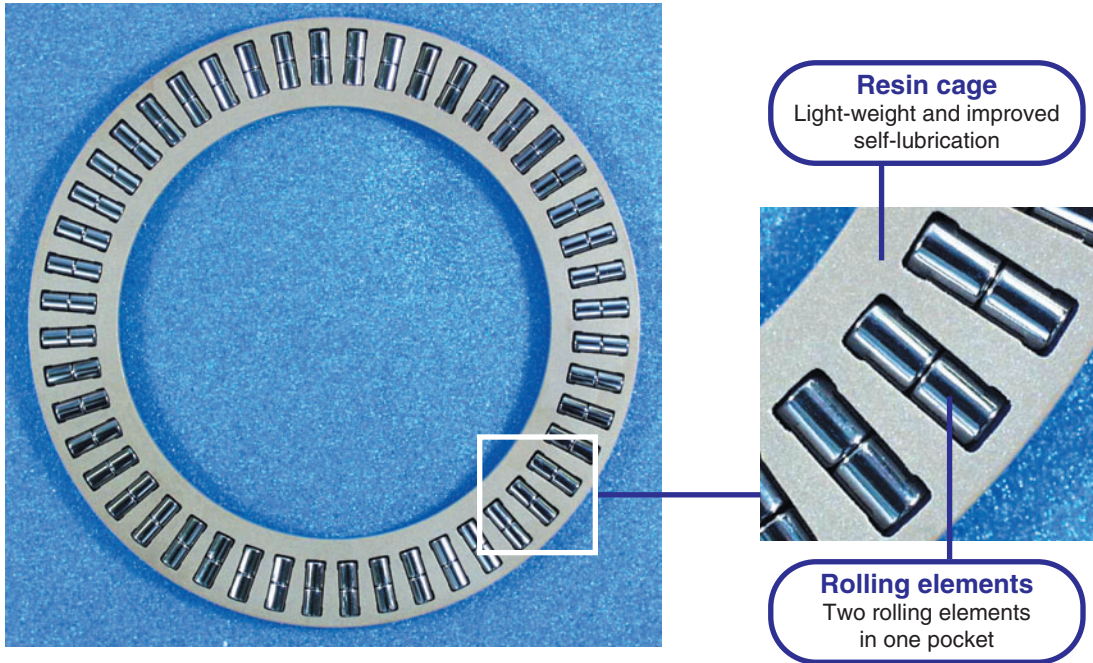
### Compact body

- Compact structure by FA treatment and design optimization



## Double-Row Thrust Needle Bearings for automobile air-conditioners and compressors

Achieve long life, low torque, and low noise through double-row rolling elements



### Features

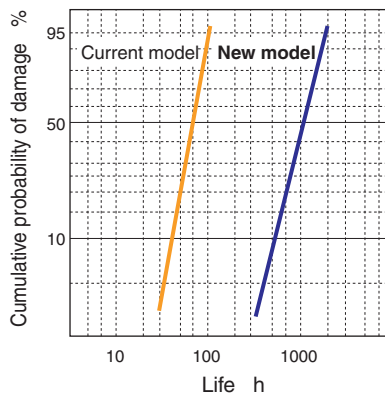
- 12 times longer life (from damage originating on surface)
- 50% reduced rotating torque
- 8dBA reduced noise
- Lightweight resin cage

### Applications

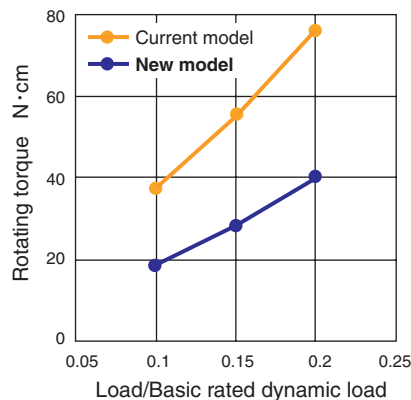
- Automobile air-conditioners and compressors

### Performance (compared to current models)

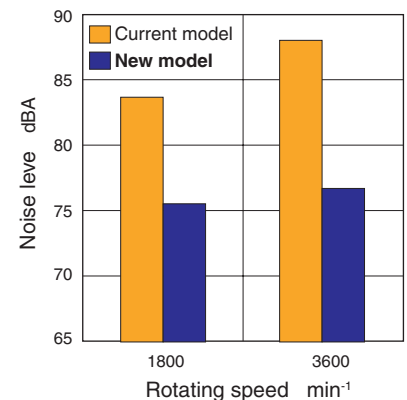
Life before damage on surface



Rotating torque



Noise



## FA Needle Bearings for rocker arms

Achieve longer life for rocker arm bearings through adoption of FA treatment  
 Fine Austenite Strengthening: Grain refining and carbonitriding technologies for bearing steel



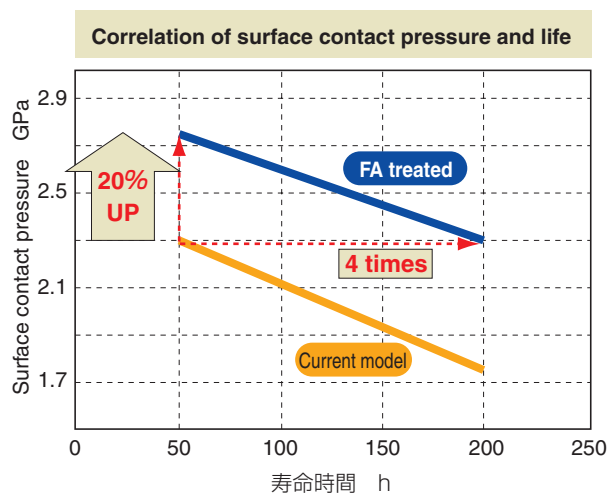
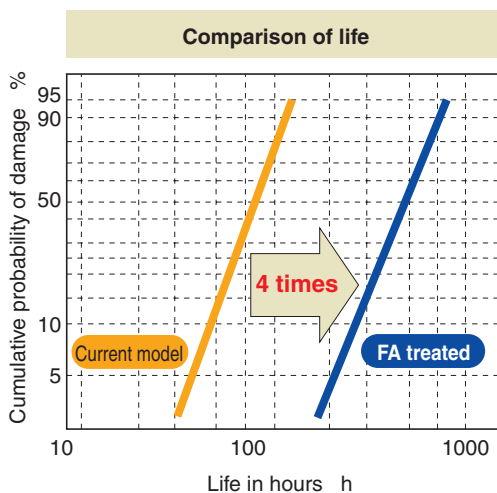
### Features

- 4 times longer life
- 20% lighter weight by size reduction (through improved allowable surface pressure)

### Applications

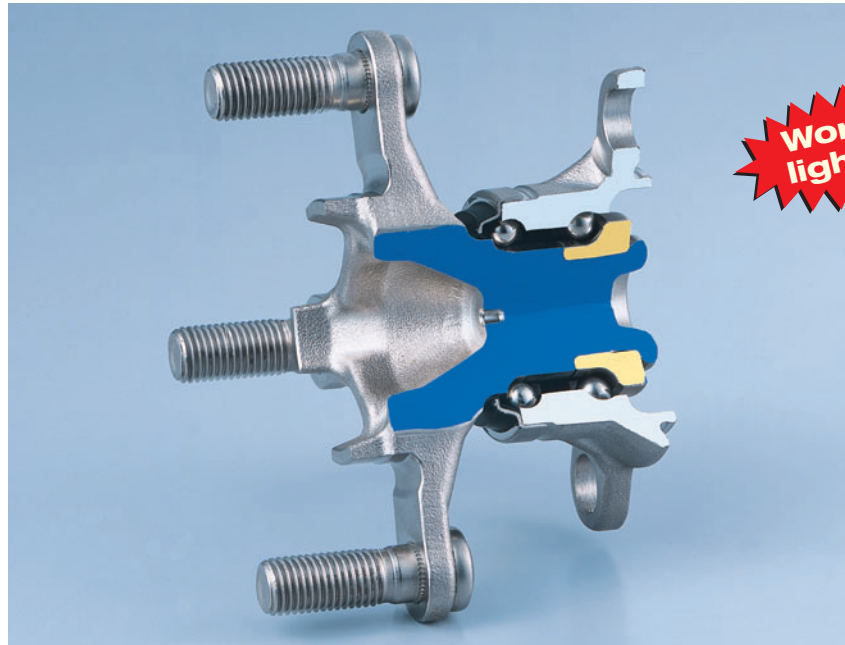
- Engines and rocker arms

### Performance



## Ultra-Light GEN3 Hub Bearings

Extremely light, “Mass weight of 1.0kg”, hub bearing for sub-compact automobiles



### Features

- Lightweight
- Compact design
- High-strength carbon steel (newly developed material)
- Long-life grease
- Long service life

### Applications

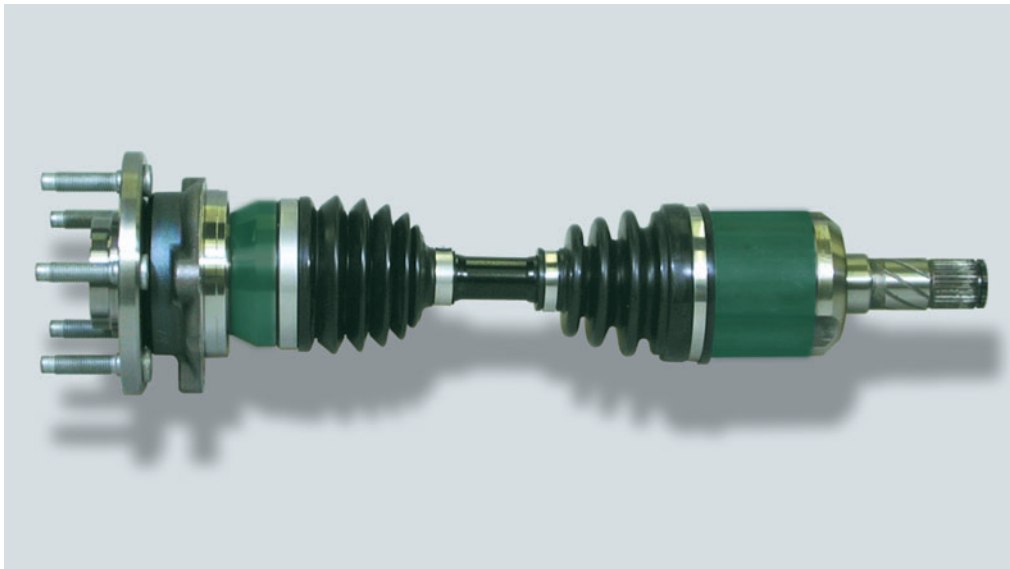
- Wheel bearings for sub-compact automobiles

**Improved performance and fuel consumption**

by reduced unsprung mass weight

## GEN4 Hub Joints

Integrated new constant-velocity joint and GEN3 hub bearing,  
Offering compact, lightweight, and easy-to-assemble GEN4 hub bearing with  
Unique expansion crimp



### Features

- **Lightweight**

Integration of the CVJ and bearing, adoption of a hollow joint shaft, and use of the new CVJ bearing tightening method reduces the weight by 10% or more.

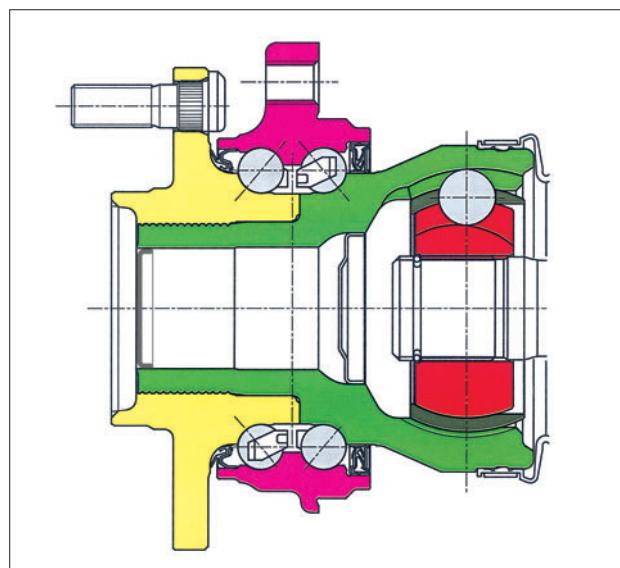
- **Smaller axial dimension**

Integration of the new constant-velocity joint and bearing reduces the axial dimension by 20% or more.

- **High efficiency and low heat generation**

Adoption of the new E-series constant-velocity joint reduces torque loss by 30% during power conveyance. Heat generation has also been reduced by 20°C compared to the conventional type.

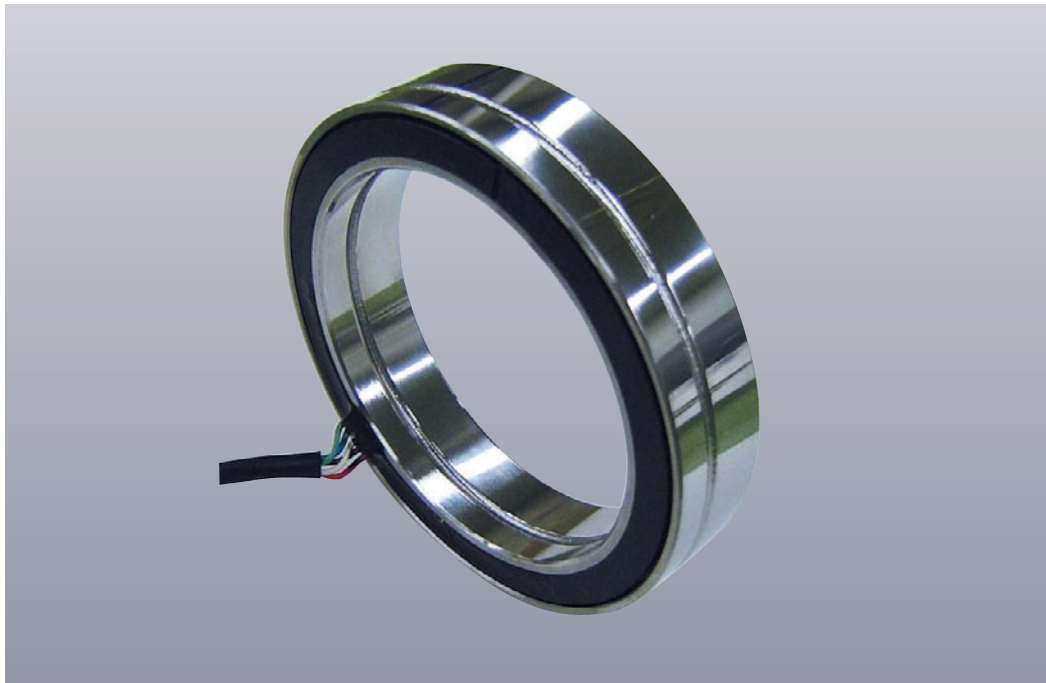
### Structure



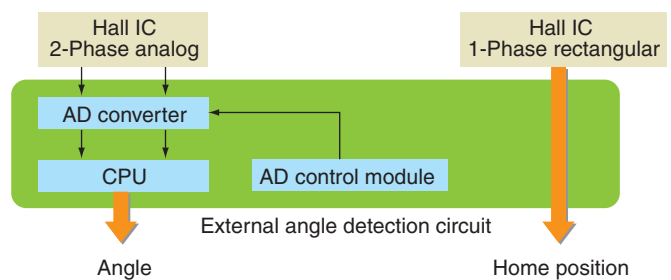
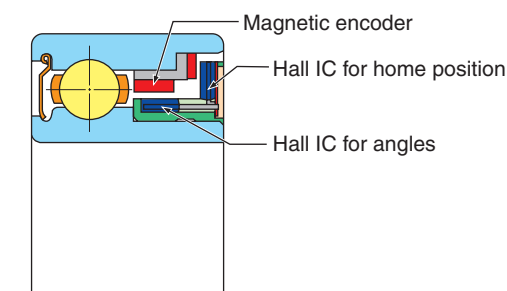


## Integrated Sensor Bearing with Absolute Encoder (Hall IC type)

Integrated sensor bearing with built-in absolute type encoder (hall IC type) and high precision home position



### Structure



### Features

- Detects absolute angles
- Detects home position with high accuracy
- Lightweight/Compact

### Applications

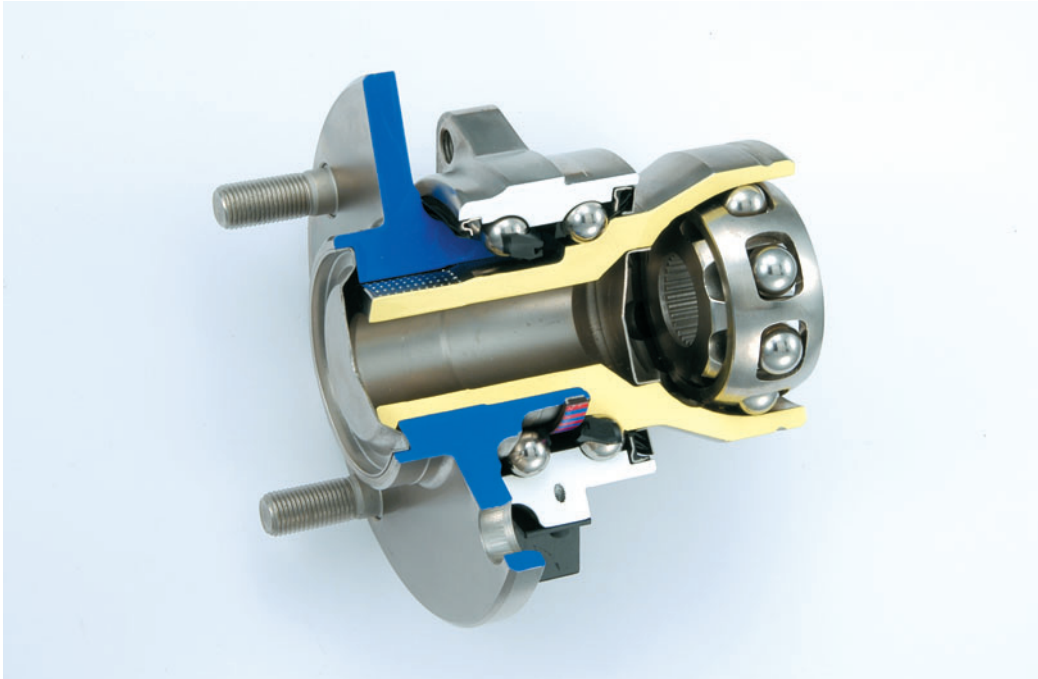
- Joints for robots
- Motors
- Locations of which absolute angles need detection

### Specifications

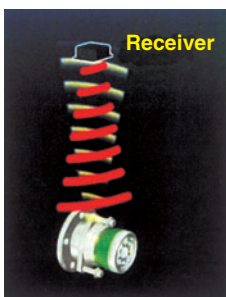
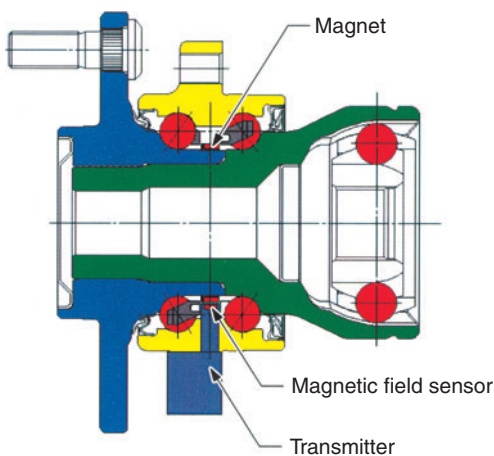
- Bearing number: #6811
- Sensor type: Magnetic encoder + Hall sensor
- Angular accuracy:  $\pm 6^\circ\text{C}$
- Home position repeatability:  $0.05^\circ$  or smaller
- Operating temperature range:  $0\sim 50^\circ\text{C}$

## Zero-Speed Compatible Active Type Wireless ABS Sensor Unit

The wireless ABS sensor unit detects zero-speed and the direction of rotation of wheels by transmitting wireless feed to the active magnetic sensor and the sensor signal transmitter that are built in the hub bearing.



### Structure



### Features

- **Wireless feed**
- **Detects rotating speed of ultra low speed (zero-speed compatible)**
- **Detects direction of rotation**  
Outputs rotating signals of different phases by 90° (A/B phases)
- **Lightweight/Compact**
- **Reduced assembly time**
- **Improved design flexibility**

### Applications

- **Automobile axle units**

**“The First Mono-Zukuri Product Creation Awards” Innovative Product Award**

## Fluid Dynamic Bearing Unit

Hydrodynamic pressure bearing utilizing oil-impregnated sintered alloy is unitized. “FDB Unit” realized low NRRO by radial/thrust hydrodynamic pressure effects.



### Features

- **Non-contact spindle rotation due to hydrodynamic pressure effects**  
**High running accuracy**  
**Extremely low noise**
- **Sintered alloy bearing sleeve with press-formed dynamic grooves**  
**Superior manufacturability**
- **Sintered alloy impregnated with lubrication oil**  
**Anti-seize features ensure long service life**
- **Lead-free brass housing thrust bushing**  
**Environmentally sound design**

### Applications

- **HDD spindle motors**  
(PC's, HDD video cameras, automotive navigation systems, etc.)
- **Spindle motors for high-density optical disks**
- **Polygon scanner motors, etc.**

Thanks to NTN's unique product concept and the motor technology of Nippon Densan Co., NTN's "FDB Unit" won the "Innovative Product Award" at the "The First Mono-Zukuri Product Creation Awards" (sponsored by Nikkan Kogyo Shimbun, Ltd.).



Winner of ADY2004 <Display Testing Equipment Category> Grand Prix Award!

## Multi-Repair System for LCD Color Filters

First in the industry, the Multi-Repair System consolidates all functions necessary to repair LCD color filters in one unit. This system dramatically improves productivity and quality in the manufacturing processes for LCD color filters.



Laser cutting to repair black defects

Ink coating to eliminated white defects

Tape polishing to fix particle defects

This system has been developed jointly with Takano Co., Ltd.

### Features

- Provides high quality repairs for a variety of color filter defects
- Greatly reduces equipment costs, required floor space, and overall repair time
- Can be built with an integrated inspection unit
- Can handle large glass color filter substrates up to seventh generation (1870 x 2200mm) display panels

### Main functions

- **Laser cutting function**  
Uses the second and third high-order YAG laser (equipped with the slit q function) to repair defects.
- **Ink coating function**  
Coats ink on white defects with the coating needle (patented) (needle tip diameter:  $\phi$  30,  $\phi$  50,  $\phi$  70  $\mu$  m).
- **Tape polishing function**  
Controls the polishing pressure while polishing particle defects to a uniform height (accuracy:  $\pm$ 0.5mm).
- **Height measurement function**  
Measures particle height, using probe pressure of 1mN max., 0.1mm resolution, and measuring range of  $\pm$ 35  $\mu$  m.
- **Review function**  
Uses a glass surface plate to emit reflected and transmitted light to make it possible to observe the state of defects.